DESIGN CONSIDERATIONS IN BROADBAND BEAMSTEERING WITH OPTICAL SPACE-FED ARRAYS

Thesis

Submitted To

Graduate Engineering & Research
School of Engineering

UNIVERSITY OF DAYTON

In Partial Fulfillment of the Requirements for

The Degree

Master of Science in Electro-Optics

by

Lawrence J. Barnes

UNIVERSITY OF DAYTON

Dayton, Ohio

December 1993

DESIGN CONSIDERATIONS IN BROADBAND BEAMSTEERING
WITH OPTICAL SPACE-FED ARRAYS

APPROVED BY:

Mohammad A. Karim, Ph.D.
Advisory Committee, Chairman

Edward A. Watson, Ph.D.
Advisory Committee, Member

Vincent G. Dominic, Ph.D.
Advisory Committee, Member

John S. Loomis, Ph.D.
Advisory Committee, Member

Donald L. Moon, Ph. D.
Interim Associate Dean/Director
Graduate Engineering & Research
School of Engineering

Joseph Lestingi, D.Eng., P.E.
Dean
School of Engineering

ABSTRACT

DESIGN CONSIDERATIONS IN BROADBAND BEAMSTEERING WITH OPTICAL SPACE-FED ARRAYS

Barnes, Lawrence, Joseph
University of Dayton, 1993

Advisor: Dr. M. A. Karim

Broadband beamsteering with optical space-fed arrays suffers from degradation due to the diffractive properties of the array. The optical arrays can be modeled as gratings and Fresnel zone plate lenses and are configured with single, dual, and three element systems incorporating both reflective and transmissive element configurations. The systems are evaluated using paraxial derivatives and a commercial ray trace program's spot diagram analysis. Results from paraxial analysis indicate that the basic limiting aberration can not be corrected using other diffractive elements without also removing the steering accomplished by the system. Paraxial analysis also indicates that it is possible to use optical arrays in a field of view selector system without severe degradation due to the chromatic aberrations. Spot diagram analysis of several systems indicate the efficacy of diffractive beamsteering of ladar beams with space-fed arrays. Several models of space-fed array systems perform theoretical diffraction limited monochromatic imaging indicative of an excellent laser radar beamsteering system. The utility of the devices in an uncorrected broadband imaging system that steers a field of view is hampered by the dispersive nature of the modeled device.

ACKNOWLEDGMENTS

I would like to thank my advisor Dr. Karim for his patience and understanding while coaxing me through to the conclusion of this work.

I would also like to thank Ed Watson for his guidance and many helpful suggestions and informative discussions, my other committee members Dr. John Loomis and Dr. Vince Dominic for their timely insights. Lawrence Meyers and Paul McMannamon for their enthusiasm and tutelage of the liquid crystal device and beamsteering systems. Bill Martin, Don Tomlinson, and WL/AARI-2 for their timely procurement of an optical ray tracing program and providing an encouraging environment. Arturo Serrano and Technology/Scientific Services Inc. for their moneys, guidance, and services. Wanda Vogler and South Western Ohio Council for Higher Education for providing my initial employment on this project. Rob Fetner, Wendy Shemano, Alan Carney and Mike Salisbury for making my time on this project more productive and less stressful. Ralph Oberly for stimulating my interest in electro-optics at Marshall University.

Finally, I would like to thank my family without whom I wouldn't have gotten the opportunity to perform this work.

TABLE OF CONTENTS

LIST OF ILLUSTRATIONS

LIST OF TABLES

CHAPTER I

INTRODUCTION

The use of shorter wavelengths in radio detection and ranging (radar) systems is a trend driven by the larger bandwidth of the shorter wavelength systems. The larger bandwidths allow for more accurate velocity resolution. The shorter wavelengths have smaller far field spot sizes, which allow increased angular resolution of objects.[1] With the advent of the maser it became possible to perform coherent radar at microwave wavelengths. Now laser radar (ladar) systems are operating at wavelengths from far infrared through the ultraviolet. Eyesafe ladar systems are being designed to operate at wavelengths greater than 1.54 μm for safe real world applications.[2]

Infrared imaging systems can rely on emitted radiation for source light and therefore can be operated in low visible light conditions without illumination. The amount of emitted radiation is proportional to the temperature with a peak emission for a blackbody object given by Wien's displacement law.[3] The infrared radiation emitted by the high temperature of most engines is difficult to conceal from infrared imaging systems. Passive acquisition sensors operating in the far infrared band, 8 μm to 12 μm, can optimally acquire images for room temperature blackbody objects (~16.5 °C).[4] While, passive acquisition sensors operating in the mid infrared band, 3 μm to 5 μm, can acquire images optimally for hotter blackbody objects (~451 °C), i.e., engine exhausts.[4]

Highly agile beam steerers are desired for use in pointing laser radar (ladar) beams to reduce the interrogation time of targets or angular switching time.[5] The large fields of regard for many military applications demand acquisition of targets passively with angular handover to the active ladar channel, as will be shown in **Chapter II**. The passive acquisition is desired to be broadband for greater sensitivity. It also needs to be capable of imaging an appreciable field of view for acceptable scan rates of the field of regard. The passive acquisition should possess a common optical path as the ladar channel for increased accuracy and precision in the angular handover.

There are a variety of ways to accomplish the beamsteering. Mirrors,[6, 7] microlens[8] and micromirror arrays,[9] prisms,[10, 11] and phased arrays[12] can be used to direct the pencil light beams to specified directions. Beamsteering using moving macroscopic optical elements in relationship to one another is mechanical beamsteering as mechanical actuators tilt, rotate, or otherwise displace an optical element in a beamsteering system effecting steering. Beamsteering with no moving parts is referred to as non-mechanical beamsteering and has advantages over its mechanical counterpart. Non-mechanical beamsteering employs the changing properties of materials by application of an external energy and can have faster switching times.

Mirrors possess no chromatic dispersion and the ladar channel can be introduced into the optical path of the passive channel with a dichroic mirror. Tilting aperture stop mirrors reduce the agility of the system as the aperture stop is the largest diameter optic of a converging system. While tilting a smaller internal field stop mirror requires the imaging system to possess a field of view equal to the field of regard for optics located on the object side of the field stop as the mirror acts as a field of view selector. The agility of the system is inversely proportional to the weight of the tilting components, while the power requirements and mirror stiffness are proportional to the weight for specific designs.[13]

Microlens arrays[8] can be used to steer a collimated ladar channel and dichroic mirrors could be used to separate the ladar beam path from the passive acquisition channel. The agility of microlens arrays depends on the weight of the arrays and the amount of decentering needed to steer the beam to output angles. The amount of decentering to effect steering to a specified angle is proportional to the *f#* of the individual sub-element lenses. Micro mirror arrays tilt sub-element mirrors to effect steering.

One type of beamsteerer[11] employs ferroelectric liquid crystal arrays and birefringent wedges. The birefringent wedges can be configured as Wollaston prisms. This type of beamsteerer utilizes switchable half-wave ($\lambda/2$) ferroelectric liquid crystal plates to alter the polarization of the beam between the birefringent plates to digitally steer the beam by selecting the polarization of the beam propagating through the birefringent prism. By cascading the individual beamsteering elements, the system can digitally steer to 2^n angles, where n is the number of individual beamsteerers.

Prism beamsteerers[10] use rotating prisms to deviate the light. The scan patterns for continuous scanners are dependent upon the powers of the prisms, the relative frequencies of rotation and the initial angle between the individual prism apex axes. Thus the switching speed between two angles will be dependent upon the fixed scan pattern. If the prisms are not continuously rotating and are allowed to be driven to specific angles then the speed in switching is dependent upon the mechanical rotator as is the number of angles the device is able to scan. This device can be operated using broadband radiation and the dispersive properties of the material comprising the prism dictate the color aberrations of this system. The use of the prisms in this type of system depends only on the angle of deviation of the prism. Thus the material comprising the prisms can be a low dispersion material.

The beamsteering of the radar beams has evolved from mechanical rotating antennas to non-mechanical phased arrays. Phased arrays[12] have been used since World War II to direct the energy of radar beams to specified angles. Because the phased array systems use time delay circuits to vary the amount of phase delay between individual elements of the array, the speed in switching for these arrays is fast compared to the mechanical systems. An optical phased array consists of an optical element composed of an array of sub-apertures each with a phase thickness or optical depth associated with it. To steer a single wavelength plane wave to a specific angle, a phase ramp is written across the aperture. The phase thickness or optical depth may be reset an integral number of wavelengths at any point across the phase ramp without changing the direction of the monochromatic output plane wave. There is dispersion associated with the phased arrays if there are phase resets between the sub-elements of the phase ramp array.

The non-mechanical beamsteering devices considered here employ nematic liquid crystals as the medium for writing dynamic phase shifts to the phased array beamsteerer.[14] The space-fed array arises due to the resetting of the phase retardation across the device, which is necessary to reduce the thickness of the liquid crystal layer. Agility or speed in switching between steering angles for this device is proportional to the square of the thickness of the liquid crystal layer.[1] The liquid crystal devices are often reflective to reduce the thickness of the layer necessary to impart a wavelength of phase retardation at the tuned or center wavelength. It is the reduced power requirements, reduced weight, and agility of this liquid crystal beamsteerer compared to tilted mirror steering systems that make it advantageous to use liquid crystal arrays for beamsteering elements.

It is possible to build these devices on a curved substrate allowing for the development of an imaging or concave beamsteerer. If the individual elements of the beamsteerer are independently addressable, then it is possible to write a dynamic

diffractive lens to a planar liquid crystal phased array device.[15] A diffractive Fresnel zone plate lens can be modeled as a radially symmetric phase grating with a period dependent upon the radial distance from the center of the grating. An imaging system, which consists entirely of transmissive diffractive Fresnel zone plate lenses,[16] has been theoretically developed to be achromatic to the first order about the design wavelength.

It is the purpose of this thesis to investigate theoretical aspects of diffractive broadband beamsteering to determine good system design constraints necessary for optimum performance and to model several baseline systems comparing and contrasting them for benefits and liabilities. The basic system considerations and definitions of a broadband beam steering system are given in **Chapter II**. An initial examination of the paraxial position and slope derivatives with respect to wavelength of particular systems is provided in **Chapter III.** The elements comprising these theoretical systems are gratings, Fresnel zone plate phase lenses,[17] concave mirrors, or lenses with arbitrary dependence on wavelength. This provides insight into the difficulties of designing a first order achromatic system and the conditions under which the systems are paraxially achromatic. A field of view beam selecting system is defined and investigated for utility in beamsteering systems.

In **Chapter IV**, specific single and dual element systems are analyzed using spot diagram analysis generated by OSLO,[18] a commercial ray tracing program. The diffraction limited bandwidth of an ideal thin lens and grating steering system defines the baseline diffractive imaging system. Single element diffractive (concave dynamic gratings) and single element reflective (concave tilting mirrors) steering systems are compared. Dual element reflective and diffractive (flat-concave) systems are also investigated. Finally, the diffractive lens system, which is achromatic to the first order, will be examined and evaluated as a steering system. **Chapter V** summarizes the results of the thesis and suggests future work areas for the problem.

CHAPTER II

BROADBAND BEAM STEERING CONSIDERATIONS

Broad spectral band (broadband) beamsteering is of interest as a passive acquisition channel for an active ladar (laser radar) channel. A passive acquisition channel for the ladar arises to reduce the search field for the ladar channel. The ladar channel can feature narrow transmitted beam solid angles given by[19]

$$\Omega_{XMIT} = \left(\frac{\lambda K_a}{D} \right)^2 . \tag{1}$$

Where Ω_{XMIT} is the solid angle field illuminated by the diffraction limited ladar channel. The wavelength of operation of the ladar is λ. K_a is the illumination constant for the output aperture incorporating the aperture shape and illumination beam profiles at the output aperture. D is the diameter of the output aperture. The area of the field of regard is given by[19]

$$\Omega_s = \frac{A_s}{R^2} . \tag{2}$$

Where Ω_s is the solid angle field to be searched. A_s is the area of the sphere to be searched and R is the range to target. The number of individual angles, N, required to search the field of regard is

$$N = \frac{\Omega_s}{\Omega_{XMIT}} . \tag{3}$$

As an example, the minimum number of angles to be searched for a 2 micron laser radar channel with a 4 cm aperture over a 10 degree squared solid angle is

$$N_{\text{LADAR}} = \frac{\Omega_s}{\Omega_{\text{XMIT}}} = \frac{\left(10^\circ \frac{\pi}{180^\circ}\right)^2}{\left(\frac{2\mu m}{4cm}\right)^2} = 1.218 \times 10^7. \tag{4}$$

Where it is assumed that the illumination constant for the aperture is unity and the diffraction limited divergence of the ladar beam is constant over the field of regard. It is the large number of angles to be searched that propels the effort into passive acquisition channels for angular handover to the ladar channel. If the passive acquisition channel possesses a 2 degree full field of view, the minimum number of steered angles to passively search the field of regard is

$$N_{\text{passive}} = \frac{\Omega_s}{\Omega_{\text{XMIT}}} = \frac{\left(10^\circ \frac{\pi}{180^\circ}\right)^2}{\left(2^\circ \frac{\pi}{180^\circ}\right)^2} = 25. \tag{5}$$

If the passive acquisition channel is imaged onto a 256 by 256 pixel array detector with accurate angular handover, the number of angles to be searched for interrogation of the object is

$$N_{\text{LADAR with handover}} = \frac{N_{\text{LADAR}}}{N_{\text{passive}} N_{\text{pixels}}} = 7.437 \ . \tag{6}$$

For the preceding assumptions such that the object occupies a single ladar angle and single pixel in the passive channel. It is this vast reduction in the number of angles to be actively searched by the ladar system that drives the research into a passive acquisition channel with good angular handover for the ladar beamsteering system.

The passive acquisition is desired to share as much of the optical components of the ladar transceiver as possible to reduce the cost, weight, and size of the system. Sharing the same optical path at the steering mechanism and output aperture yields better accuracy and precision in the angular handover through elimination of boresighting errors of the ladar channel. The passive acquisition channel is desired to be broadband to increase the signal to noise ratio of the passive channel.

Broad spectral band (broadband) refers to the wavelength content of the directed light. The bandwidth can be defined by the center wavelength and the two cutoff or edge wavelengths. The percent bandwidth is given by

$$\% \ \text{Bandwidth} = \frac{(\lambda_o - \lambda_{\min})}{\lambda_o} 100\% = \frac{(\lambda_{\max} - \lambda_o)}{\lambda_o} 100\%, \tag{7}$$

where λ_0 is the center wavelength, λ_{min} is the minimum wavelength in the band, and λ_{max} is the maximum wavelength in the band and the band is symmetrical about the center wavelength. Because most diffractive and refractive optical components have properties, which vary nonlinearly with respect to wavelength, the two edge band wavelengths will not produce symmetric angular deviations about the tuned wavelength. Thus the edge band wavelengths possess rays that are distinct and not symmetric about the center wavelength ray in symmetric steering systems.

2.1 : Baseline System Bandwidths

Broadband beamsteering with optical phased arrays is the steering of polychromatic light based on the diffractive properties of the phased space array. The liquid crystal device is assumed to be operated in the regime of many resets, which can be

modeled accurately by diffraction gratings. The device is operated in this regime because the switching speed is proportional to the square of the thickness of the device, which dictates a thin device for agility. A phase ramp must be written across the device for high efficiency at the steer angles. The number of resets necessary to build a folded phase wedge with modulo 2 π resetting at the design wavelength for the thin device dictates the operation of the device in the regime of many resets.

The maximum angular extents of the steered base ray from the reference ray of the system define the field of regard. The field of regard is not necessarily symmetric about the normal to the surface or optical axis as shown in Fig. 1. A reference ray is defined to be the ray passing through the angular center of the field of regard and is also shown in Fig. 2. The steer angle is defined to be the angular deviation between this reference ray and the steered base ray. The base ray is a ray of the center wavelength from the center of the field of view passing through the center of the steering element to the center of the image plane, shown in Fig. 1 and Fig. 2. The angular extent of the image at any steered base ray is the full field of view, which is symmetric in angular extent about the steered base ray. The amount of diffractive deviation is defined to be the angular deviation of a base ray caused by the diffractive properties of the optical phase space-fed array. It is important to note that the steer angle and the amount of diffractive steering are equal only when no diffractive deviation of the reference ray takes place.

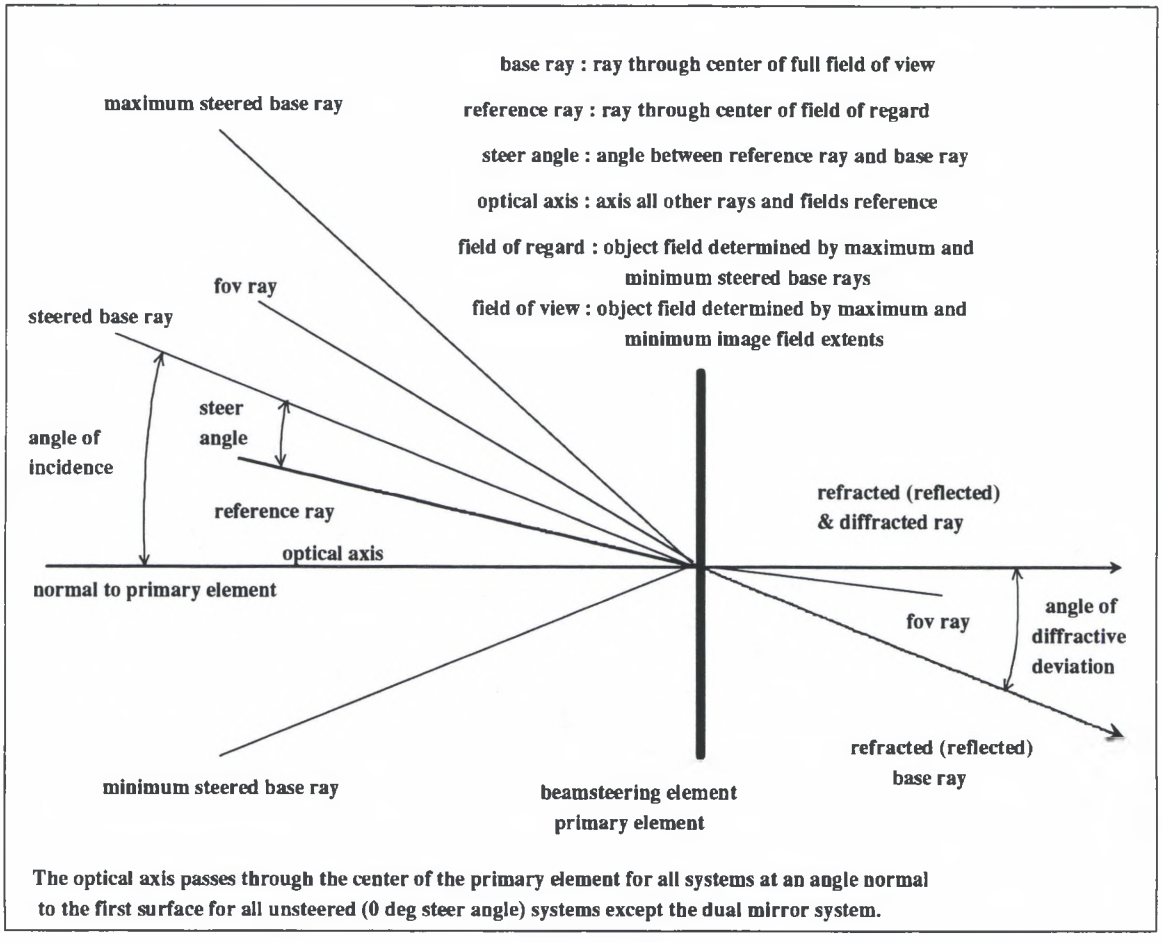

Figure 1 Basic System Drawing with Rays and Angles Labeled

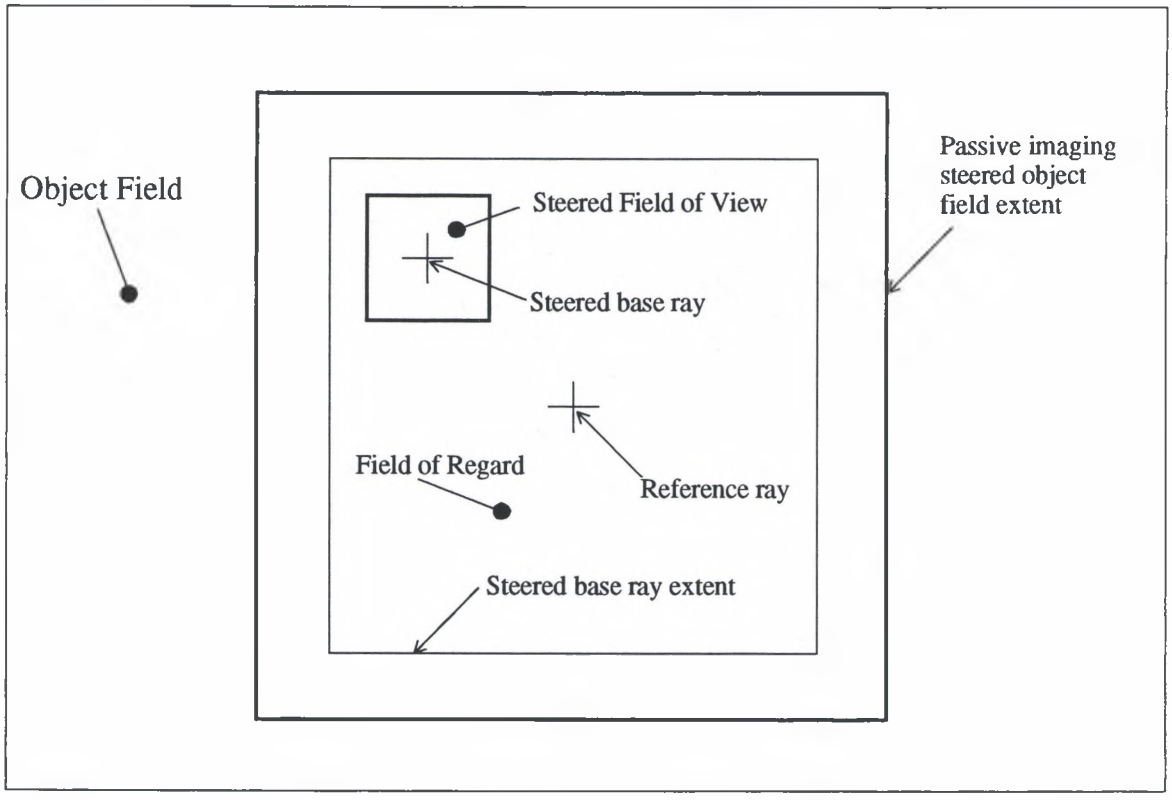

Figure 2 Object Field with Rays and Fields Labeled

An ideal imaging system consisting of an ideal thin lens and a coincident grating element is shown in Fig. 3. The ideal thin lens has ideal imaging properties while the ideal grating diffracts all of the incident light into one specified order. The reference ray for this system is coincident with the optical axis. This causes no angular deviation by the diffractive properties of the grating when the steered base ray is coincident with it, i.e., 0 degree steer angle. The steer angle is the angular deviation between this reference ray and the steered base ray, which for this system is equal to the amount of diffractive angular deviation of the steered base ray.

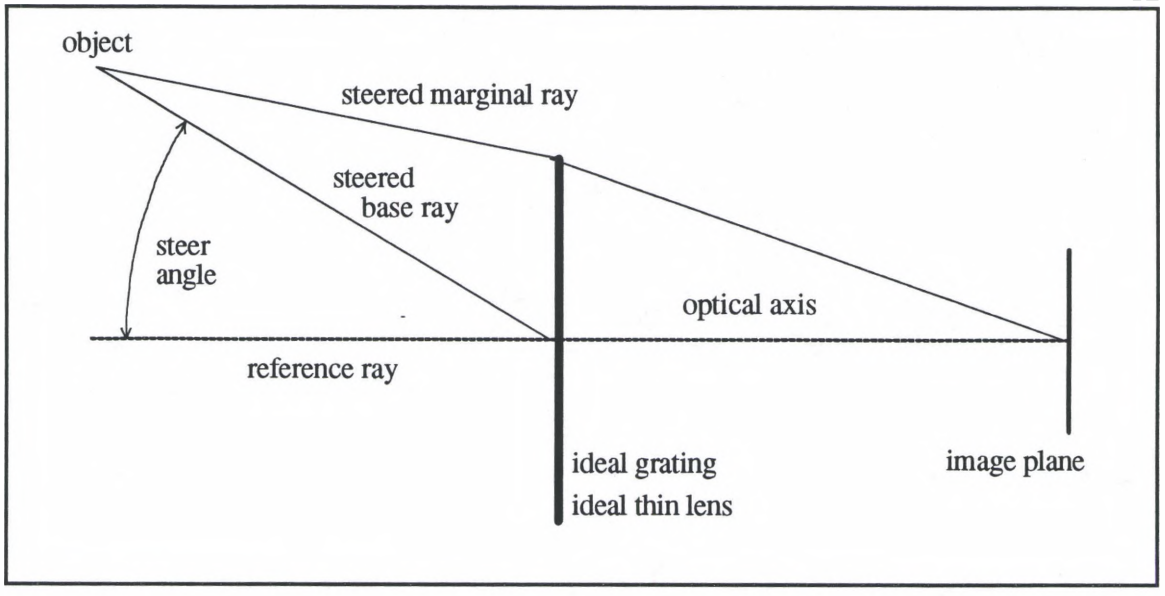

Figure 3 Ideal Beamsteerer System Drawing

The maximum diffraction limited bandwidth is defined to be the bandwidth for which the geometric spot size of the imaging system is equal to the diffraction limited spot size for the center wavelength. A plot of the diffraction limited spot size versus the *f*# for the system in Fig. 3 is shown in Fig. 4. The bandwidths, as defined by Eq. 7, are plotted for given steer angles versus the *f*# of the system, where the *f*# is defined by the marginal ray in image space of the system shown in Fig. 3. The diffraction limited bandwidth is the percentage change in wavelength necessary for the difference in angular deviation caused by the difference in wavelength between the center wavelength and maximum wavelength diffractive properties of the space-fed array to yield a geometric spot size radius equal to the Airy radius caused by the diffractive properties of a finite circular aperture. The calculations are carried out only on the longer wavelength side of the incident light for the diffractive deviation and are compared to the Airy radius calculated at the center wavelength.

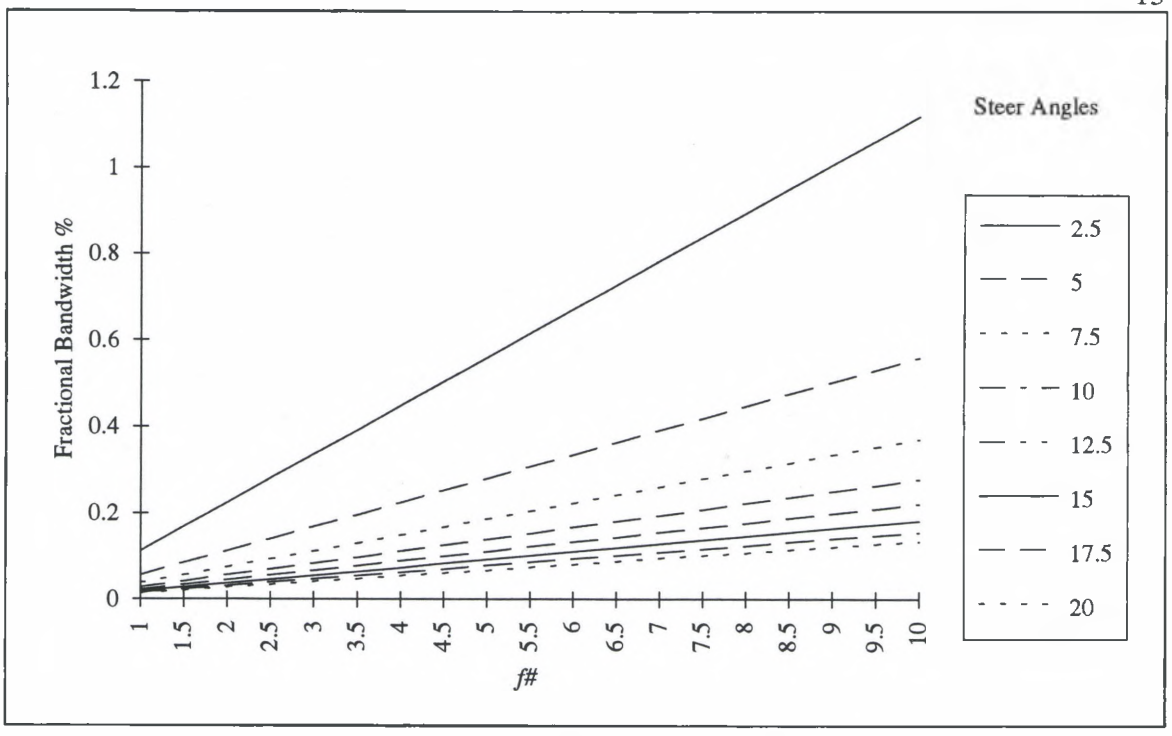

Figure 4 Diffraction Limited Bandwidths versus *f#* for Ideal Beamsteerer

From Fig. 4, the diffraction limited bandwidths for the indicated steer angles are small compared to the desired bandwidth for a passive acquisition system, which can be as large as 50% for broadband detection. It is evident from Fig. 4 that there are two ways to increase the diffraction limited bandwidth of this system. The first is to increase the *f#* of the system, but this decreases the light gathering capacity of a system with a fixed focal length (size). Decreasing the angle of diffractive steering or the amount of diffractive deviation of the light by the grating of the device also increases the diffraction limited bandwidth.

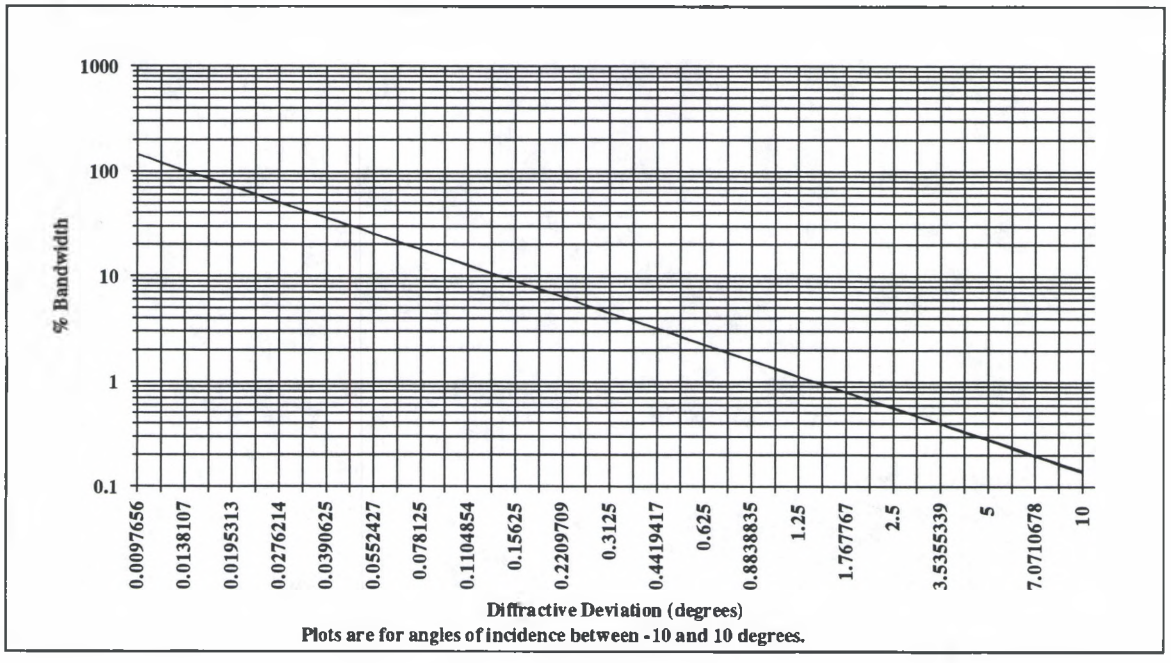

Figure 5 Diffraction Limited % Bandwidth versus Diffractive Deviation for a *f*/5 System

The diffraction limited bandwidth versus diffractive deviation angle for angles of diffractive deviation between 0 and 10 degrees is shown in Fig. 5 for an ideal system having its *f*/5 system as described for Fig. 3. The angles of incidence, which are diffractively deviated, are between -10 and 10 degrees (~-0.2 and 0.2 radians). Angles of incidence are not labeled in the plot due to the small magnitude of the dependence of the diffraction limited bandwidth on the angle of incidence for the given diffractive deviation angles. The dependence of the angle of incidence on the diffraction limited bandwidth is such that the line widens for large angles of diffractive deviation. The results presented in Fig. 5 are plotted with logarithmic axes to show the nonlinear dependence of the diffraction limited bandwidth on the diffractive deviation angle.

2.2 : Diffraction Limited Imaging Considerations

A system composed of a single ideal thin lens and a single ideal thin grating is shown in Fig. 6. The system steers, via diffraction, the tuned wavelength from an object point located on the axis to an off-axis image point, This system exhibits an interesting phenomenon in that the locations of the entrance and exit pupils can cause conflicting interpretations of the system from a linear systems viewpoint. This system is defined as a *f*/5 system using the Rayleigh convention[20] of calculating the *f*# for an on-axis image point in image space, when the grating does no steering. However, when the grating steers, the reduced exit pupil from the Rayleigh convention of calculating the *f*# in image space actually increases the *f*#. It is the limiting ray bundle in object space that determines the diffraction limit. The method of intercepting the spatial frequencies in object space, Abbe's convention,[20] accurately describes the system because the aperture limiting the spatial frequencies transmitted through the system is the entrance pupil. Thus diffractive elements can distort the effective exit pupil of the system as shown in Fig. 6.

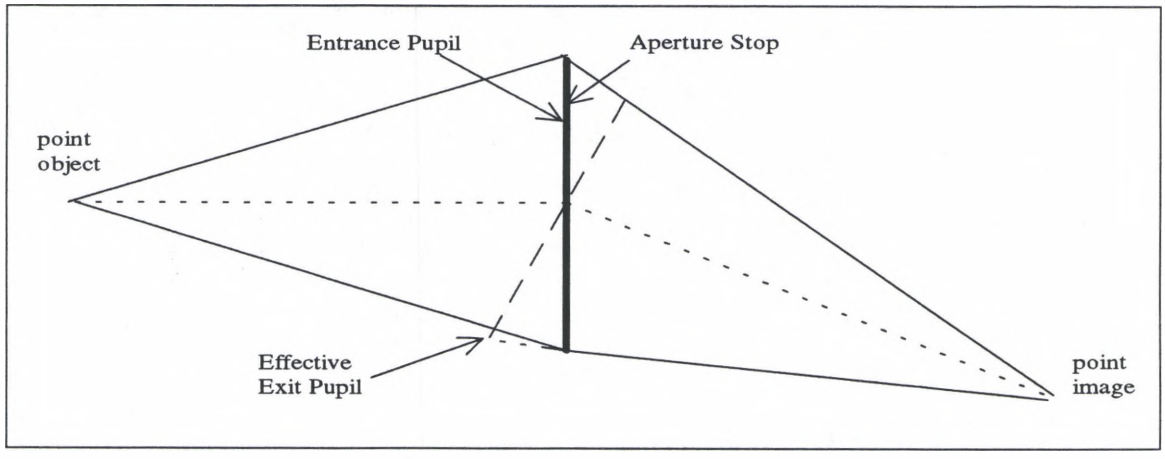

Figure 6 Distortion of Exit Pupil in a Diffractive Steering System

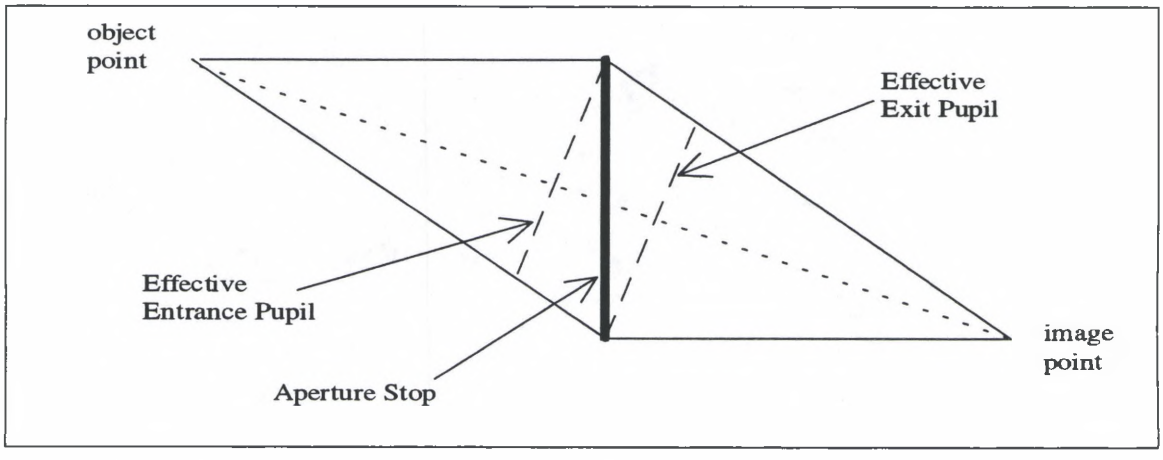

Figure 7 Exit Pupil in Non Diffractive Systems

Mirror and refractive systems do not possess these phenomena because the reduction in both the entrance and exit pupils are equal when considering off-axis points as shown in Fig. 7. This monochromatic pupil distortion affects all diffractive imaging elements when they are steering. This indicates that a steering system with the object normal to or centered about the steering aperture stop is advantageous.

The basic system in Fig. 3 would possess a *f*# that would vary as the reciprocal of the cosine of the angle of the steered base ray as shown by the plot in Fig. 8. The *f*# plot in Fig. 8 can be scaled to any value *f*# system by multiplying *f*# axis of the plot by the *f*# of the system. Because the plots shown in Fig. 4 demonstrate the dependence of the diffraction limited bandwidth with respect to *f*#, the variance in the *f*# with respect to the object (steer) angle will affect the diffraction limited bandwidth at the steer angle. The plots in both Fig. 4 and Fig. 5 neglect the effect of the change in *f*# with respect to steer angle.

This phenomenon is noted here, but does not affect the geometric ray tracing analysis. It does indicate that systems with off-axis object angles possess a degradation in the diffraction limited spot size. Systems with off-axis unsteered (diffractively deviated) objects possess a larger diffraction limited bandwidth than indicated by this analysis, which neglects this effect.

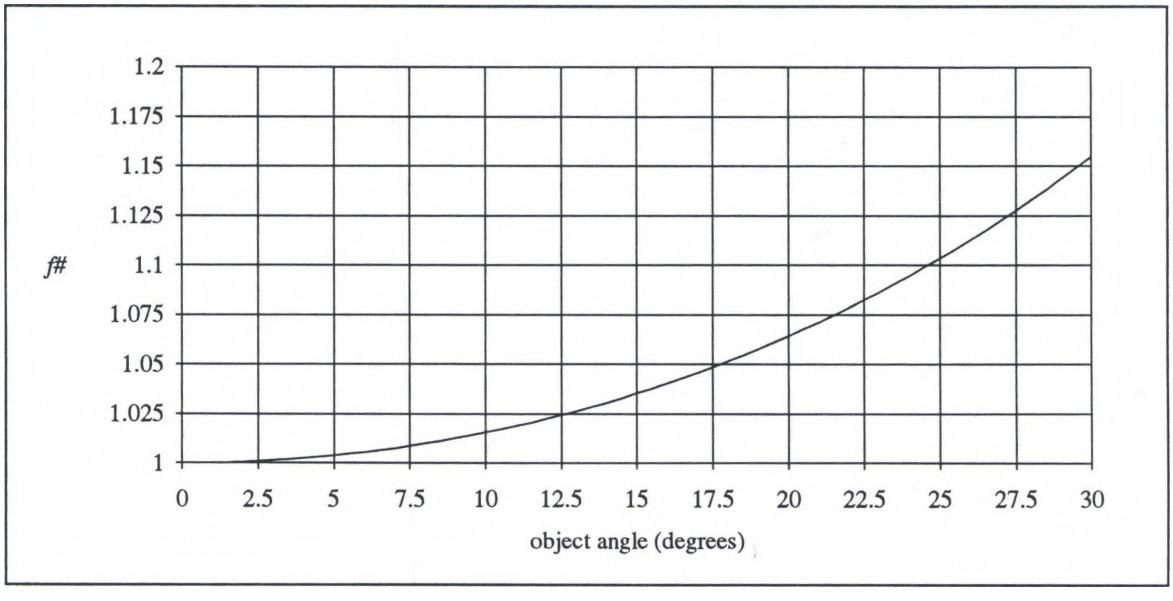

Figure 8 *f*# versus Off-Axis Angle for *f*/1 System

CHAPTER III

PARAXIAL ANALYSIS

In this chapter, a first order analysis of color aberrations of specific systems consisting of two and three elements is performed. The systems evaluated are a single grating system, a dual grating system, a Fresnel zone plate lens system, a three grating system, and a dual grating followed by an arbitrary single lens. The paraxial analysis of these systems consists of evaluating the paraxial ray trace derivatives for the various systems consisting of gratings, lenses, and Fresnel zone plate lenses. The single element in Section 3.2, dual element in Section 3.3, and three Fresnel zone plate systems in Section 3.4 will be evaluated in the ray trace analysis in **Chapter IV**.

3.1 : Paraxial Definitions and Conventions

Paraxial analysis is a first order analysis of the properties of an optical system. From a first order analysis, equations can be generated defining the conditions that must be met for a particular system to posses no chromatic aberrations while steering a field of view.

The sine function of an angle θ can be expanded as a series

$$\sin\theta = \theta - \frac{\theta^3}{3!} + \frac{\theta^5}{5!} - \frac{\theta^7}{7!} + \ldots \quad . \tag{8}$$

The corresponding expansion for the cosine function is

$$\cos\theta = 1 - \frac{\theta^2}{2!} + \frac{\theta^4}{4!} - \frac{\theta^6}{6!} + \ldots \quad . \tag{9}$$

First order analysis is obtained by approximating the series expansions of Eq. 8 and Eq. 9 by dropping all the higher order terms (terms with exponential powers greater than one) yielding

$$\sin\theta \cong \theta \tag{10}$$

and

$$\cos\theta \cong 1. \tag{11}$$

The paraxial ray slope for the i^{th} surface is defined as

$$u_i = \tan(\theta_i) = \frac{\sin(\theta_i)}{\cos(\theta_i)} \cong \sin(\theta_i) \cong \theta_i. \tag{12}$$

Where θ_i is small and expressed in radians[21]. The percentage error of the approximation in Eq. 12 is shown in Fig. 9. We find that the percentage error for the approximation at 0.175 radians (~10 degrees) is about 1%. The paraxial approximation is valid for a grating, lens, or Fresnel zone plate (diffractive) optical element as long as the angles with respect to the optic axis or base ray are small.[22]

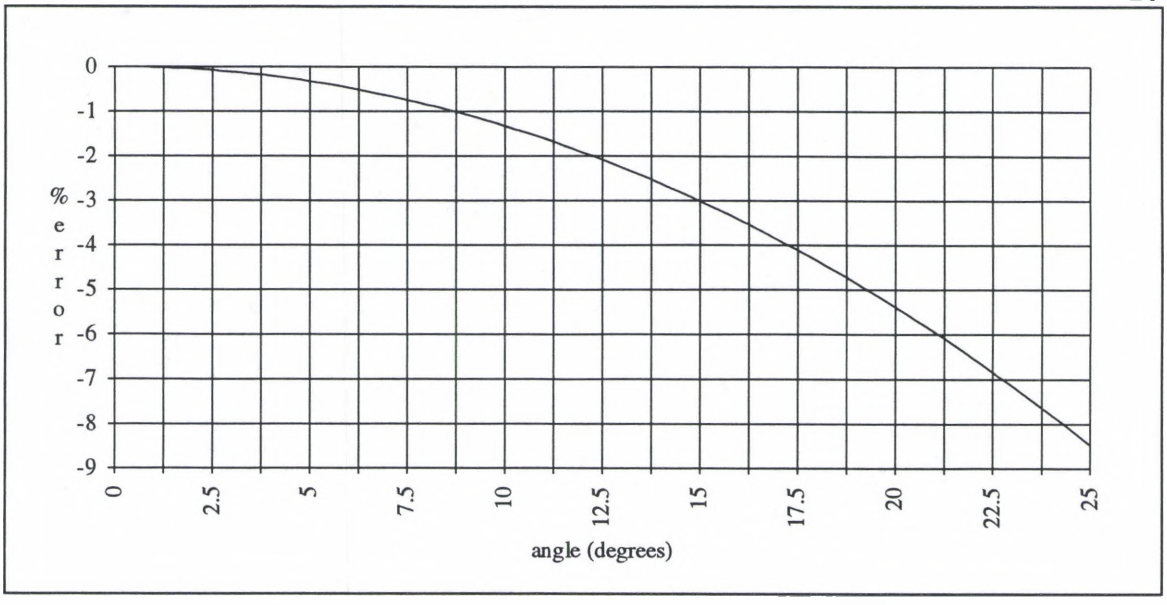

Figure 9 Paraxial Angle % Error versus Angle of Propagation

The paraxial ray position for the $(i+1)^{th}$ surface is given by

$$y_{i+1} = y_i - u_i \cdot x_i. \tag{13}$$

Where y_i is the ray height for the i^{th} surface, x_i is the distance between the i^{th} and the $(i+1)^{th}$ surface and u_i is the paraxial slope of the ray between the i^{th} and the $(i+1)^{th}$ surfaces. The sign convention used here for the paraxial angles is down positive.[16] The pertinent variables are shown in Fig. 10.

The corresponding equation for the paraxial ray slope is dependent upon the type of element involved. The general analysis will consider three types of elements. Ideal gratings of perfect efficiency and diffracting light into the single diffraction order of choice will be the first type of element investigated. Ideal thin lenses with an optical power calculated using a formula approximation of the index of refraction variation with wavelength (dispersion) will be the second element considered. The last element considered will be ideal Fresnel zone plate lenses modeled as radially symmetric gratings

with a period dependent upon the distance from the radial center and with perfect efficiency into the desired order.

These three elements can either be transmissive or reflective. Transmissive elements will have their angles of incidence, refraction, and transmitted diffraction measured from the normal to the ideal surface with a clockwise or down positive convention. Reflective surfaces will have their angle of incidence measured from the normal to the ideal surface with a clockwise positive convention while the angles of reflection or reflected diffraction will be measured from the normal to the ideal surface with a counter-clockwise or down positive convention.

The angular deviations caused by an ideal grating is given by the grating equation,[21]

$$n \cdot \lambda = \rho[\sin\theta - \sin\alpha]. \tag{14}$$

Where λ is the wavelength of the ray, ρ is the grating period, α is the angle of incidence, θ is the angle of diffraction, and n is the order of diffraction. This becomes under paraxial approximations,

$$u_{i+1} = \frac{n_i \lambda}{\rho_i} + u_i. \tag{15}$$

Where u_i is the incident paraxial ray slope, u_{i+1} is the diffracted paraxial ray slope, and the grating period, ρ_i, has been divided by the specific grating order investigated, n_i. For an active beamsteerer the grating period is dynamic to enable steering. The amount of diffractive steering being accomplished by the grating is defined to be the difference between the initial axial ray paraxial slope and the output axial ray slope, which is a function of the grating period.

For transmission through a lens, the paraxial ray slope is

$$u_{i+1} = u_i + y_{i+1}\Phi_{i+1}. \tag{16}$$

The optical power of the $(i+1)^{th}$ element, Φ_{i+1}, is a function of wavelength for nearly all elements except mirrors. The derivative of the power with respect to wavelength, $\partial\Phi_{i+1}/\partial\lambda$, for a lens constructed from a homogeneous material with concave, planar, and/or convex surfaces is dependent upon the dispersion of the material. The dispersion formula,[23] which approximates the dispersion curve for materials, in the infrared region of the electromagnetic spectrum is

$$N^2 = a + b\lambda^2 + \frac{c}{\lambda^2} + \frac{d}{\lambda^4} + \frac{e}{\lambda^6} + \frac{f}{\lambda^8} + \frac{g}{\lambda^{10}}. \tag{17}$$

Where N is the index of refraction of the material, λ is the wavelength, and a, b, c, d, e, f, and g are constants. The constants, a through g, are derived for each material utilizing known index of refraction values for specific wavelengths and solving a set of simultaneous equations.

The power of a single lens surface is

$$\Phi_{i+1} = \frac{(N_{i+1} - N_i)}{R_{i+1}} \tag{18}$$

Where N_{i+1} is the index of refraction of the material comprising the lens. N_i is the index of refraction preceding the lens surface and R_{i+1} is the radius of curvature of the lens surface. Taking the derivative of the power yields

$$\frac{\partial\Phi}{\partial\lambda} = \frac{\left(2b\lambda - \frac{2c}{\lambda^3} - \frac{4d}{\lambda^5} - \frac{6e}{\lambda^7} - \frac{8f}{\lambda^9} - \frac{10g}{\lambda^{11}}\right)}{2R\sqrt{a + b\lambda^2 + \frac{c}{\lambda^2} + \frac{d}{\lambda^4} + \frac{e}{\lambda^6} + \frac{f}{\lambda^8} + \frac{g}{\lambda^{10}}}} \tag{19}$$

Where N_i is assumed to be constant and the i+1 subscript is removed for simplicity. This derivative is a function with a trivial solution when b, c, d, e, f, and g all equal zero indicating a material with no wavelength dependence.

The power of an ideal mirror is

$$\Phi_i = \frac{2}{R_i}, \tag{20}$$

which is independent of wavelength. The derivative of the optical power of a mirror with respect to wavelength is zero. Thus the mirror generates no chromatic angular error.

The power of a Fresnel zone plate type lens[16] as a function of wavelength is

$$\Phi_i(\lambda) = \frac{\Phi_i(\lambda_0)\lambda}{\lambda_0} \tag{21}$$

and the derivative of the power of the lens is

$$\frac{\partial \Phi_i}{\partial \lambda} = \frac{\Phi_i(\lambda_0)}{\lambda_0}. \tag{22}$$

Where $\Phi_i(\lambda_0)$ is the power of the element at the tuned wavelength, λ_0. The paraxial ray slope for transmission through a Fresnel zone plate type lens evaluated in the first order is given by

$$u_{i+1} = \frac{\Phi_i(\lambda_0)\lambda}{\lambda_0}(y_i - \delta y_i) + u_i. \tag{23}$$

Where y_i is the ray height incidence to the grating, δy_i is the decentering of the diffractive element's optical axis from the optical axis of the system, and u_i is the incident ray slope.[14]

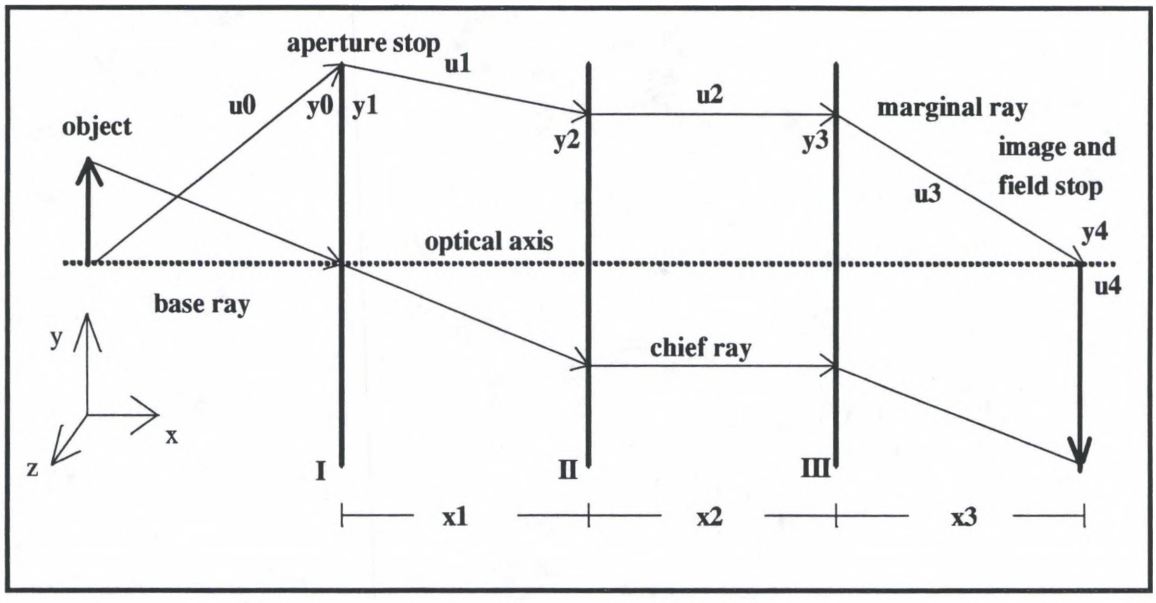

Figure 10 General System Drawing for Paraxial Analysis

The convention[23] in lens design for quantifying color aberrations is to measure the change in focal length for the longitudinal color or the change in image size for lateral color at specific wavelengths. The change in focal length is the longitudinal color and is found theoretically by tracing marginal rays through the system and calculating the distance between the intersection of the two marginal rays and the optical axis at the two wavelengths of interest. By similar calculation of chief rays intersecting an image plane the lateral color can be found. Thus the longitudinal color is the distance between image planes and the lateral color is the difference in transverse magnification at an image plane. These color metrics are defined when the powers of the elements comprising the system are a function of wavelength and the system is symmetric i.e., the reference ray possesses no color aberrations. Some of the systems to be considered in this analysis have no longitudinal or lateral color, but possess an image location that is a function of wavelength. This analysis will use other metrics for the color aberration, the angular and position errors in the rays traced. The longitudinal color can be represented as an angular

error in the marginal ray in the absence of positional errors in the ray at the surface preceding the image plane. The lateral color can likewise be represented as a position error in the chief ray in the absence of angular errors in the ray at the surface prior to the image plane.

An image is free of paraxial color aberration if the paraxial derivatives of the ray slope (u) and position (y) with respect to wavelength (λ) at the image or output plane are equal to zero. For simplicity only a two dimensional (x,y) system with $z = 0$ as shown in Fig. 10 will be considered. The derivative of ray slope at the image plane with respect to wavelength, $\partial u_4 / \partial \lambda$, is a metric of the angular color aberration. The derivative of ray position with respect to wavelength, $\partial y_4 / \partial \lambda$, is a metric of the position color aberration. For an afocal system the metrics of the angular and position error in the rays will be used as the longitudinal and lateral color aberrations are defined only for focal systems. From the analysis of the paraxial rays a determination of the conditions necessary for eliminating the paraxial color aberrations of the system can be discerned.

A system will have no paraxial color aberrations if the derivatives with respect to wavelength for the slope and position of the paraxial rays at the image plane vanish. The slope and position of a paraxial ray at the image or output plane are dependent upon the position and slope of the ray exiting the surface preceding the image plane, which can be expressed in terms of the prior surface's slope and position. This recursive relationship can be used to suitably express the slope and position of the ray at the output or image plane as a function of the initial slope and position. The slope and position of the rays at the output or image plane can be expressed solely as a function of the initial slope, initial position and variables describing the surfaces between the initial and output plane.

The output ray slope, u_4, for a system consisting of three elements is equal to the ray slope exiting the last element, u_3, of the system because the output plane is an evaluation plane in image space and the rays are unaffected by it. Thus the angular aberration metric of the system is

$$\frac{\partial u_4}{\partial \lambda} = \frac{\partial u_3}{\partial \lambda}. \tag{24}$$

The output ray position, y_4, is

$$y_4 = y_3 - u_3 x_3 \tag{25}$$

and the position aberration metric is

$$\frac{\partial y_4}{\partial \lambda} = \frac{\partial y_3}{\partial \lambda} - \frac{\partial u_3}{\partial \lambda} x_3. \tag{26}$$

Where it is assumed that x_3 is independent of wavelength, which is a good assumption given first order analysis in air media. If the angular aberration metric is zero, then

$$\frac{\partial u_4}{\partial \lambda} = 0 = \frac{\partial u_3}{\partial \lambda} \tag{27}$$

and the position aberration metric in the absence of angular aberration then becomes

$$\frac{\partial y_4}{\partial \lambda} = \frac{\partial y_3}{\partial \lambda}. \tag{28}$$

Therefore if a system is to be free of both angular and position errors, then the derivatives of ray slope and position at the last element must vanish. If the angular and position aberrations are zero then the longitudinal and lateral color aberrations are also zero. The following analysis of particular and general systems will investigate the conditions under which the derivatives of slope and position with respect to wavelength at the final element can be forced to vanish.

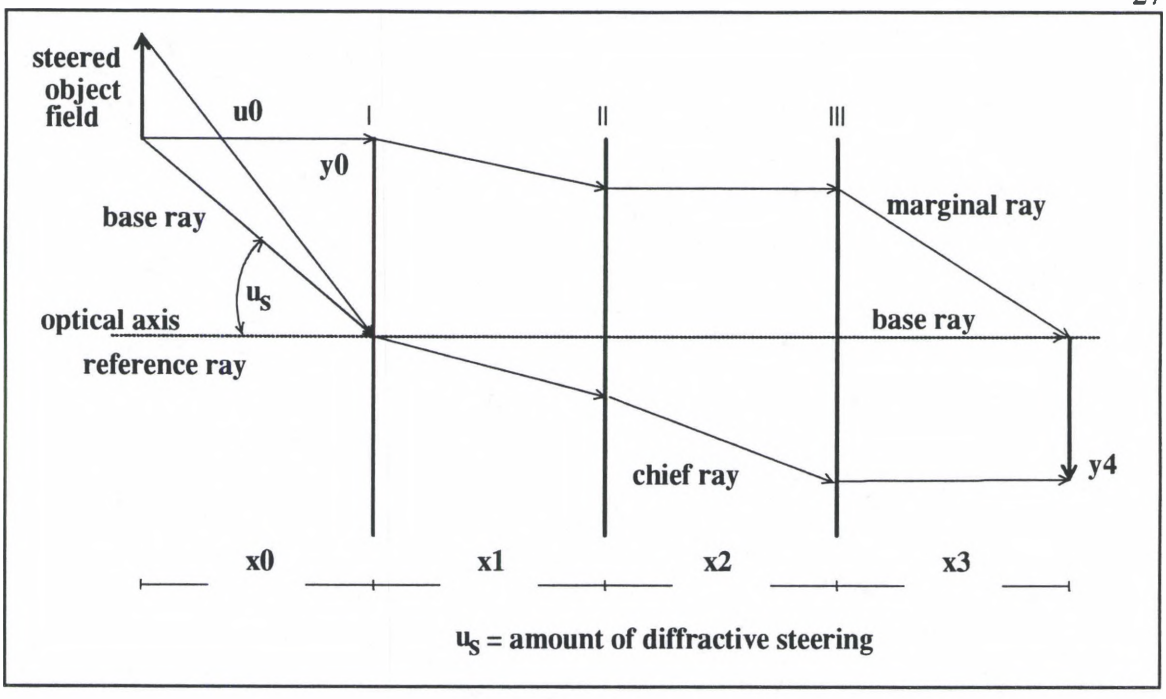

Figure 11 System Drawing Illustrating Diffractive Steering

The amount of deviation for a base ray in these systems is the change of the base ray slope entering the system to the base ray slope exiting the system as shown in Fig. 11. This allows for off-axis object or image location. The amount of diffractive deviation of the base ray is equal to the amount of diffractive deviation or steering for the system.

3.2 : Single Element System

The single dynamic grating with optical power is the most basic beamsteering system. It consists of a single dynamic transmission grating written onto a transmissive surface with optical power. This system is advantageous due to the simplicity of the system and the placement of the steering element coincident with the entrance pupil of the system as shown in Fig. 12. The single element system consists of two paraxial surfaces.

The first surface is the ideal grating, which diffracts the light into the single grating order of interest. The light is then focused by an ideal thin lens.

Placing the diffractive steering element coincident with the imaging element allows for the modeling of a dynamic concave grating. If the grating element is not coincident with and is located after the imaging element, then the amount of diffractive deviation required to steer the base ray to a common image point increases or the light gathering ability of the system diminishes depending on the sign of the optical power of the transmissive surface. A positive powered surface will cause the light to converge, but will not steer the light. The location of the steering element before the focus is desired as it will steer the image to the single image point location for all steered angles. Because the light is unsteered by the imaging element, the base ray of the light will propagate through the center of the imaging element and continue to propagate unsteered. The angle of diffractive deviation required for the dynamic grating to steer the light to the image point is greater than the amount of effective steering. This is because the grating will be required to direct the base ray to the same image point for all steer angles and the base ray propagation between the imaging element and the grating yields a positional error which the steering element must compensate. Correction for the positional error requires greater diffractive deviation by the dynamic grating.

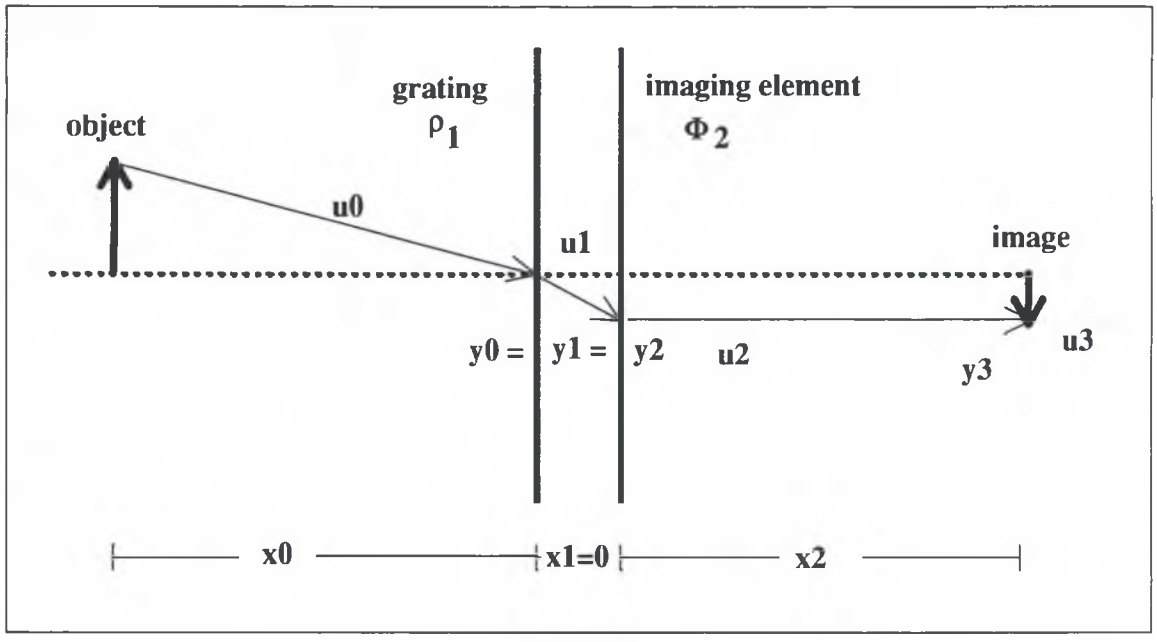

Figure 12 Single Element System Drawing

The ray position for all paraxial rays at the image plane is

$$y_3 = y_0 - \left(u_0 + \frac{n_1 \lambda}{\rho_1} + y_0 \Phi_2 \right) x_2. \tag{29}$$

Where y_0 is the input paraxial ray position, u_0 is the input paraxial ray slope, n_1 is the grating order, ρ_1 is the grating period, and Φ_2 is the optical power of the transmissive surface and constant with respect to wavelength. The derivative of the paraxial ray position with respect to wavelength of this system is given by

$$\frac{\partial y_3}{\partial \lambda} = \frac{n_1 x_2}{\rho_1}. \tag{30}$$

Due to the lack of dependence of the derivative on the input ray slope, u_0, and position, y_0 the derivative is identical for all paraxial rays. The paraxial ray slope at the image plane is

$$u_3 = \left(u_0 + \frac{n_1 \lambda}{\rho_1} + y_0 \Phi_2 \right). \tag{31}$$

The derivative of the paraxial ray slope with respect to wavelength is

$$\frac{\partial u_3}{\partial \lambda} = \frac{n_1}{\rho_1}. \tag{32}$$

The amount of diffractive deviation performed by this system is

$$u_3 - u_0 = \frac{n_1 \lambda}{\rho_1}, \tag{33}$$

where the term $u_3 - u_0$ yields the amount of deviation between the input and output paraxial rays and is evaluated with $y_0 = 0$ to null the amount of deviation from the powered imaging surface. From Eq. 30, Eq. 32, and Eq. 33, the amount of diffractive deviation is proportional to the amount of angular and position errors of the system. Thus the color aberrations of this system are a function of the amount of steering being performed by the system.

For a single reflective element system with the largest clear aperture, the image would be located off-axis, where it would not obscure the entrance pupil, while the object is located on-axis for the largest entrance pupil. The field of regard would be centered about the axis of the concave grating. This would require diffractive deviation to deflect the image rays to an off-axis location resulting in diffractive deviation of the ray in the center of the field of regard, which is the reference ray. This would cause color aberrations to be present in the reference ray of the system. Because the amount of diffractive deviation is directly proportional to the amount of color aberrations in the system, it is desired to minimize the amount of diffractive deviation throughout the field of regard. This is accomplished by requiring that the reference ray not be diffractively deviated. Thus a single on-axis reflective element beamsteering system cannot posses both an unobscured maximum entrance pupil and no diffractive deviation of the reference ray.

3.3 : Dual Element System

The dual element system evaluated here is a dual grating system consisting of a flat reflective steering grating and a concave transmissive imaging grating. The advantage gained from using two gratings is that the image plane can be centered on the axis of symmetry of the imaging element, while the reference ray of the field of regard is normal to the flat beamsteerer. This allows for on-axis imaging at the tuned wavelength and an unobscured entrance pupil shown in Fig. 13.

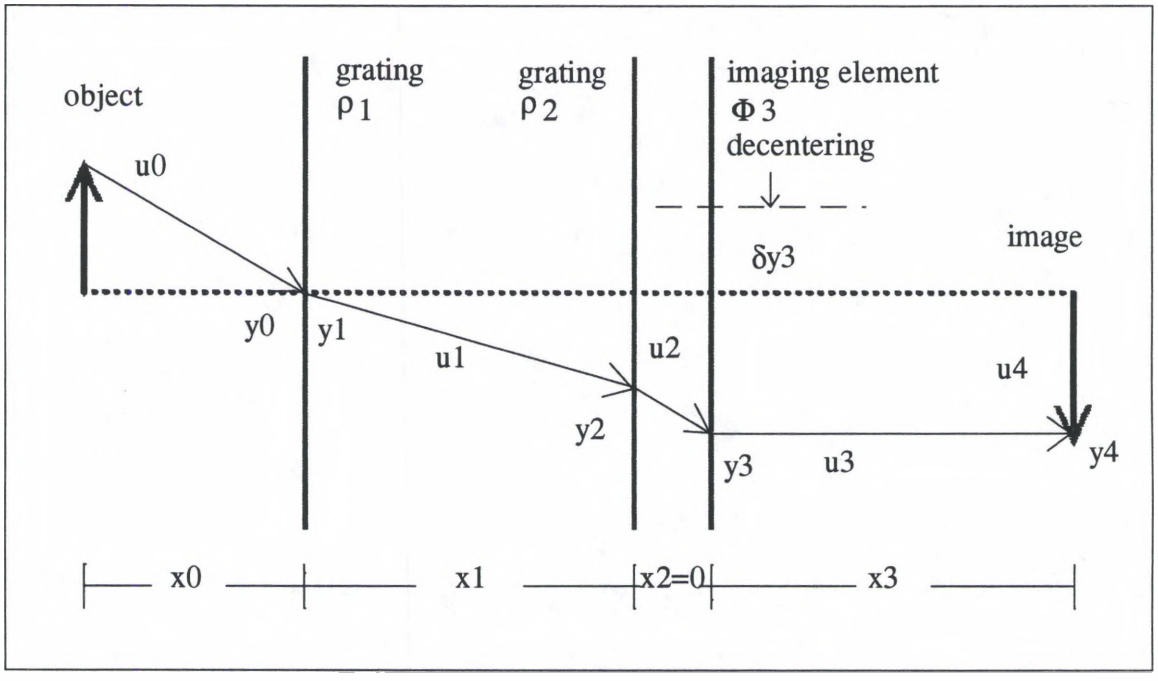

Figure 13 Dual Element System Drawing

The paraxial ray position at the image plane for the dual grating system is

$$y_4 = y_0 - \left(u_0 + \frac{n_1\lambda}{\rho_1}\right)x_1 - \left(u_0 + \frac{n_1\lambda}{\rho_1} + \frac{n_2\lambda}{\rho_2} + \left(y_0 - \left(u_0 + \frac{n_1\lambda}{\rho_1}\right)x_1 - \delta y_3\right)\Phi_3\right)x_3. \tag{34}$$

The derivative of the paraxial ray position with respect to wavelength is

$$\frac{\partial y_4}{\partial\lambda} = -\frac{n_1 x_1}{\rho_1} - \left(\frac{n_1}{\rho_1} + \frac{n_2}{\rho_2} - \frac{n_1 x_1}{\rho_1}\Phi_3\right)x_3 \tag{35}$$

and because this derivative is independent of the input paraxial ray slope and position, Eq. 35 is constant for all paraxial rays in the system. The positional aberration metric of the system can be simplified. If the object is near infinity, the back focal distance, x_3, becomes approximately equal to the focal length,

$$x_3 \cong \frac{1}{\Phi_3}. \tag{36}$$

The position aberration metric for the system under the condition of a near infinite object becomes

$$\frac{\partial y_4}{\partial\lambda} = -\left(\frac{n_1}{\rho_1} + \frac{n_2}{\rho_2}\right)x_3. \tag{37}$$

The paraxial ray slope at the image plane for the dual grating system is

$$u_4 = u_0 + \frac{n_1\lambda}{\rho_1} + \frac{n_2\lambda}{\rho_2} + \left(y_0 - \left(u_0 + \frac{n_1\lambda}{\rho_1}\right)x_1 - \delta y_3\right)\Phi_3. \tag{38}$$

The derivative of the paraxial ray slope with respect to wavelength is

$$\frac{\partial u_4}{\partial\lambda} = \frac{n_1}{\rho_1} + \frac{n_2}{\rho_2} - \frac{n_1 x_1 \Phi_3}{\rho_1}, \tag{39}$$

where the derivative of the optical power, Φ_3, is not a function of wavelength. Because this derivative is independent of the input paraxial ray position and slope, Eq. 39 is valid

for all paraxial rays of the dual grating system. The amount of diffractive deviation performed by the system is given by

$$(u_4 - u_0)_{diffractive} = \frac{n_1\lambda}{\rho_1} + \frac{n_2\lambda}{\rho_2}, \tag{40}$$

where $y_0 = 0$ and δy_3 is chosen to center the imaging elements axis of symmetry with the steered base ray and is given by

$$\delta y_3 = \left(u_0 + \frac{n_1\lambda}{\rho_1} \right) x_1, \tag{41}$$

From Eq. 40 and Eq. 37, the positional aberration metric of the system is directly proportional to the amount of diffractive deviation performed by the system.

It is possible to remove the position aberration metric in the dual element steering system. This requires that the back focal distance is equal (or nearly equal) to the focal length of the imaging element of the system. There can be diffractive deviation by the individual elements, provided that there be an equal and opposite amount of deviation by another element. This requires that there be no net diffractive deviation of the rays by the system and that there can be no steering of a field of view by the system if no position aberration is desired.

The conditions necessary for the elimination of angular error require that no diffractive deviations take place within the system, i.e. $n_1 = n_2 = 0$, or that the power of the imaging element is 0 and there is no net diffractive deviation by the system. This condition is caused by the position dependence of the amount of deviation of the light at the imaging element. These conditions restrict the utility of the dual element system as a field of view beamsteering system.

3.4 : Fresnel Zone Plate Lens System

The system consisting of three Fresnel zone plate lenses is a system of three lenses, whose focal lengths are linearly proportional to the wavelength of light transmitted through them. This system, shown in Fig. 14, can steer by decentering the lenses with respect to each other. To accomplish steering, the i^{th} lens is decentered by δy_i, which equals zero for an on axis element.

Because this system possesses elements whose optical power varies with wavelength, longitudinal and lateral color aberrations are present. The angular and position error metrics will be used as the aberration metric of the system. When the angular and position error metrics vanish, there is no longitudinal and lateral color aberration.

The paraxial ray position at the image plane is

$$y_4 = y_0 - \left[u_0 + (y_0 - \delta y_1)\frac{\Phi_1\lambda}{\lambda_0}\right]x_1 -$$

$$\left(\left[u_0 + (y_0 - \delta y_1)\frac{\Phi_1\lambda}{\lambda_0}\right] + \left[y_0 - \left[u_0 + (y_0 - \delta y_1)\frac{\Phi_1\lambda}{\lambda_0}\right]x_1 - \delta y_2\right]\frac{\Phi_2\lambda}{\lambda_0}\right)x_2 -$$

$$\left[u_0 + (y_0 - \delta y_1)\frac{\Phi_1\lambda}{\lambda_0}\right]x_3 - \left[\left(y_0 - \left[u_0 + (y_0 - \delta y_1)\frac{\Phi_1\lambda}{\lambda_0}\right]x_1 - \delta y_2\right)\frac{\Phi_2\lambda}{\lambda_0}\right]x_3 -$$

$$\left[\left(\left[y_0 - \left[u_0 + (y_0 - \delta y_1)\frac{\Phi_1\lambda}{\lambda_0}\right]x_1 - \delta y_2\right]\frac{\Phi_2\lambda}{\lambda_0}\right)x_2 - \delta y_3\right]\frac{\Phi_3\lambda}{\lambda_0}x_3$$

(42)

where u_0 is the input ray slope and y_0 is the input ray position. The derivative of the ray position at the image plane is

$$\frac{\partial y_4}{\partial \lambda} = \frac{\partial y_3}{\partial \lambda} - \frac{\partial u_3}{\partial \lambda} x_3 = -(y_0 - \delta y_1)\frac{\Phi_1}{\lambda_0} x_1 - (y_0 - \delta y_1)\frac{\Phi_1}{\lambda_0} x_2 -$$

$$\left(\left[y_0 - \left[u_0 + (y_0 - \delta y_1)\frac{\Phi_1 \lambda}{\lambda_0}\right] x_1 - \delta y_2\right]\frac{\Phi_2}{\lambda_0} - (y_0 - \delta y_1)\frac{\Phi_1}{\lambda_0} x_1 \frac{\Phi_2 \lambda}{\lambda_0}\right) x_2 -$$

$$(y_0 - \delta y_1)\frac{\Phi_1}{\lambda_0} x_3 - \left[\left(y_0 - \left[u_0 + (y_0 - \delta y_1)\frac{\Phi_1 \lambda}{\lambda_0}\right] x_1 - \delta y_2\right)\frac{\Phi_2}{\lambda_0}\right] x_3 +$$

$$\left[(y_0 - \delta y_1)\frac{\Phi_1}{\lambda_0} x_1 \frac{\Phi_2 \lambda}{\lambda_0}\right] x_3 -$$

$$\left(\left[y_0 - \left[u_0 + (y_0 - \delta y_1)\frac{\Phi_1 \lambda}{\lambda_0}\right] x_1 - \delta y_2\right]\frac{\Phi_2 \lambda}{\lambda_0} - \delta y_3\right) x_2 \frac{\Phi_3}{\lambda_0} x_3 -$$

$$\left[\left[y_0 - \left[u_0 + (y_0 - \delta y_1)\frac{\Phi_1 \lambda}{\lambda_0}\right] x_1 - \delta y_2\right]\frac{\Phi_2}{\lambda_0} x_2\right]\frac{\Phi_3 \lambda}{\lambda_0} x_3 +$$

$$\left[(y_0 - \delta y_1)\frac{\Phi_1}{\lambda_0} x_1 \frac{\Phi_2 \lambda}{\lambda_0} x_2\right]\frac{\Phi_3 \lambda}{\lambda_0} x_3 \qquad (43)$$

where x_3 is the back focal distance. The lateral color is given by substituting the input parameters for the chief ray into Eq. 42 and evaluating for the wavelengths of interest. If

the position error metric is equal to zero for the chief ray, then there is no lateral color. Removing lateral color from the Fresnel zone plate lens system is nontrivial as the derivative contains terms of wavelength squared, wavelength, and constants containing the decentering variables (δy_1, δy_2, and δy_3) which are varied to affect steering of the field of view.

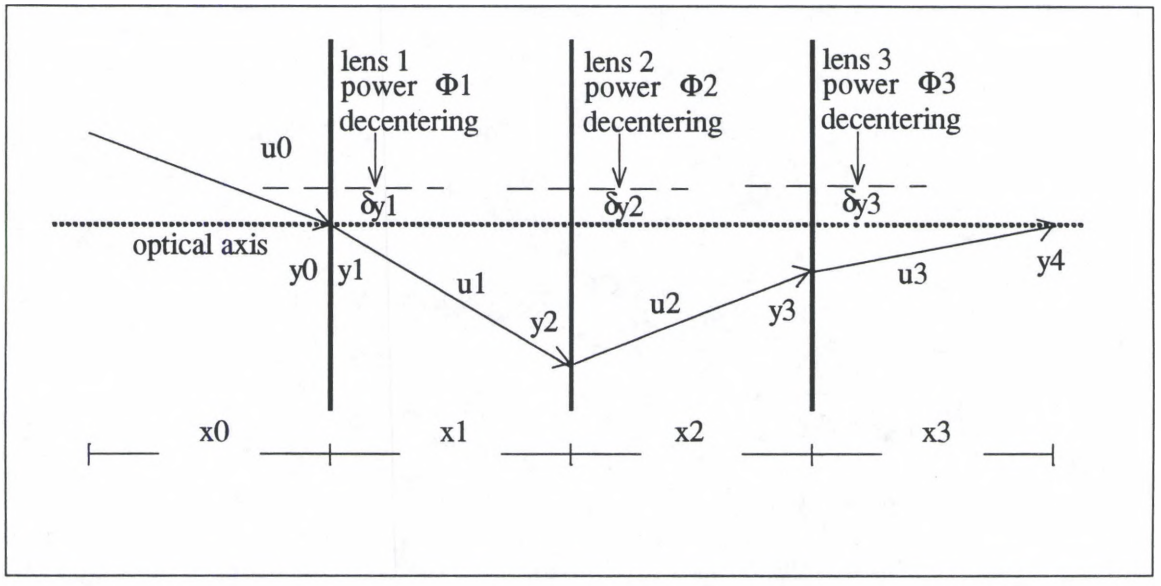

Figure 14 Fresnel Zone Plate Lens System Drawing

The paraxial ray slope at the image plane for this system is

$$u_4 = u_3 = u_0 + (y_0 - \delta y_1)\frac{\Phi_1\lambda}{\lambda_0} + \left(y_0 - \left[u_0 + (y_0 - \delta y_1)\frac{\Phi_1\lambda}{\lambda_0} \right] x_1 - \delta y_2 \right) \frac{\Phi_2\lambda}{\lambda_0} + \tag{44}$$

$$\left[\left(\left[y_0 - \left[u_0 + (y_0 - \delta y_1)\frac{\Phi_1\lambda}{\lambda_0} \right] x_1 - \delta y_2 \right] \frac{\Phi_2\lambda}{\lambda_0} \right) x_2 - \delta y_3 \right] \frac{\Phi_3\lambda}{\lambda_0}$$

where the slope at the image plane, u_4 is equal to the slope of the ray exiting the last surface, u_3. The derivative of the slope at the image plane yields the angular error in the rays and is

$$\frac{\partial u_4}{\partial \lambda} = \frac{\partial u_3}{\partial \lambda} = -(y_0 - \delta y_1)\frac{\Phi_1}{\lambda_0} + \left[\left(y_0 - \left[u_0 + (y_0 - \delta y_1)\frac{\Phi_1 \lambda}{\lambda_0} \right] x_1 - \delta y_2 \right)\frac{\Phi_2}{\lambda_0}\right] -$$

$$\left[(y_0 - \delta y_1)\frac{\Phi_1}{\lambda_0} x_1 \frac{\Phi_2 \lambda}{\lambda_0}\right] + \left(\left[y_0 - \left[u_0 + (y_0 - \delta y_1)\frac{\Phi_1 \lambda}{\lambda_0} \right] x_1 - \delta y_2 \right]\frac{\Phi_2 \lambda}{\lambda_0} - \delta y_3 \right) x_2 \frac{\Phi_3}{\lambda_0} +$$

$$\left[\left[y_0 - \left[u_0 + (y_0 - \delta y_1)\frac{\Phi_1 \lambda}{\lambda_0} \right] x_1 - \delta y_2 \right]\frac{\Phi_2}{\lambda_0} x_2 \right]\frac{\Phi_3 \lambda}{\lambda_0} - \left[(y_0 - \delta y_1)\frac{\Phi_1}{\lambda_0} x_1 \frac{\Phi_2 \lambda}{\lambda_0} x_2\right]\frac{\Phi_3 \lambda}{\lambda_0}. \quad (45)$$

Where the longitudinal color for the system in the absence of lateral color can be obtained by using the expression resulting from substituting the paraxial input parameters for the marginal ray for the particular steered field of view into Eq. 44 and evaluating for the wavelengths of interest. If the angular error metric, Eq. 45, is zero for the marginal ray, then there is no longitudinal color in the image.

It is possible to remove the longitudinal and lateral color from the Fresnel zone plate lens system for a single value of wavelength, λ.[16] The conditions necessary for no longitudinal or lateral color aberration restrict the system to possess negative power.[24] An additional condition required for no angular or position error dictates collinear centers of the lenses while steering.

The constraint regarding steering is brought about by the symmetry of the system. The Fresnel zone plate lenses can be modeled as radially symmetric gratings with a period

that is a function of the radial distance from the optical axis of the individual element. The optical axis passes through the center of all elements in a symmetric system. If the system steers through decentering, it is no longer a symmetric system and a ray can pass through the center of the first two elements. If this ray does not pass through the center of the third element, it will possess an angular error. It is possible for the three elements to be displaced with respect to each other and still possess colinear centers, a base ray could pass through the symmetrical center of all three elements. This is equivalent to tilting each of the surfaces of a symmetric system to the same angle. This system could steer without paraxial color aberrations as the constant tilt could be added or removed from the paraxial angles without affecting the amount of dispersion or diffractive deviation imparted by the Fresnel zone plate lens.

3.5 : Grating-Grating-Grating System

A system consisting of three plane gratings as shown in Fig. 15 will be afocal, but can steer a beam of light. The paraxial ray position for this system is

$$y_4 = y_0 - \left(\frac{n_1\lambda}{\rho_1} + u_0\right)x_1 - \left[\frac{n_2\lambda}{\rho_2} + \left(\frac{n_1\lambda}{\rho_1} + u_0\right)\right]x_2 - \left[\frac{n_2\lambda}{\rho_3} + \frac{n_2\lambda}{\rho_2} + \frac{n_1\lambda}{\rho_1} + u_0\right]x_3 \tag{46}$$

where x_3 is the distance to the evaluation plane as the system is afocal. The derivative of the paraxial ray position is

$$\frac{\partial y_4}{\partial\lambda} = -\frac{n_1 x_1}{\rho_1} - \left(\frac{n_2}{\rho_2} + \frac{n_1}{\rho_1}\right)x_2 - \left(\frac{n_3}{\rho_3} + \frac{n_2}{\rho_2} + \frac{n_1}{\rho_1}\right)x_3, \tag{47}$$

which is equal to the position aberration for all paraxial rays of the system as the derivative is independent of the paraxial input.

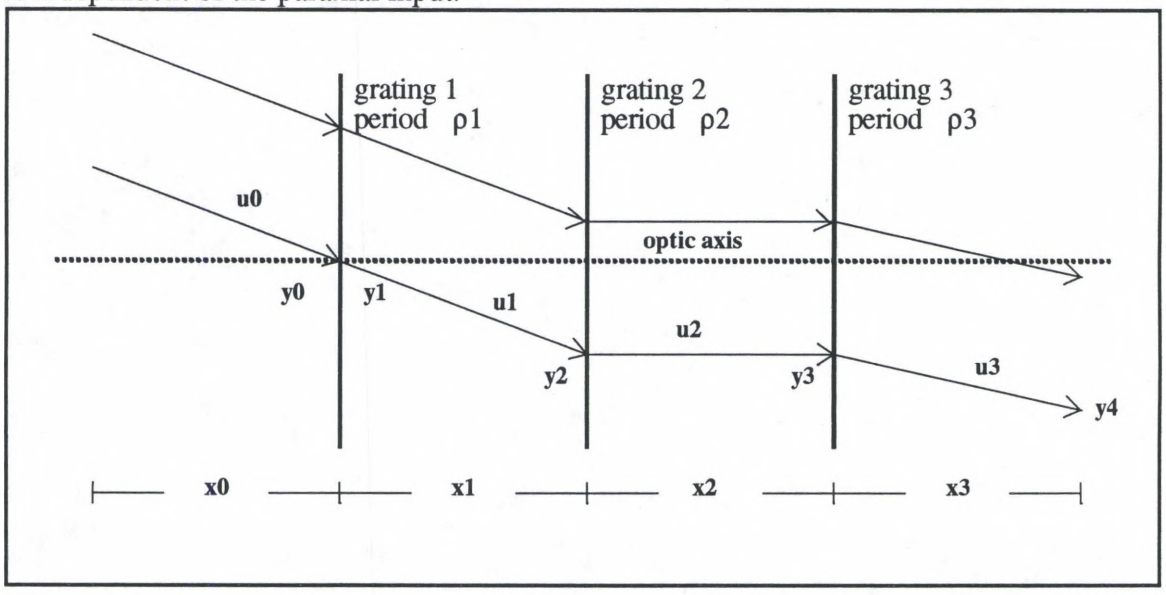

Figure 15 Grating-Grating-Grating System Drawing

The paraxial ray slope at the evaluation plane for the three grating system is

$$u_4 = \frac{n_3 \lambda}{\rho_3} + \frac{n_2 \lambda}{\rho_2} + \frac{n_1 \lambda}{\rho_1} + u_0 \tag{48}$$

and derivative with respect to wavelength of the paraxial ray slope is

$$\frac{\partial u_4}{\partial \lambda} = \frac{n_3}{\rho_3} + \frac{n_2}{\rho_2} + \frac{n_1}{\rho_1}. \tag{49}$$

The derivative is equal to the angular aberration for all paraxial rays of the system as the derivative is independent of the paraxial input slope and position. To remove the angular aberration, there can be no steering in this system as the constraints placed on the grating periods to eliminate the angular errors also eliminate the contributions to the angular deviation of the ray.

The condition for eliminating the ray position aberration metric, Eq. 47, places additional constraints on the separation distances between the gratings and the grating periods of the first two gratings. These constraints can be determined by evaluating Eq. 47 with the condition that Eq. 49 equal zero. This yields

$$0 = \frac{n_2 \rho_1}{n_1 \rho_2} - \frac{x_1 - x_2}{x_2}. \tag{50}$$

Thus the separations between the elements become a function of the periods of the first two elements. It is desired that the separations between the elements are constant for a non-mechanical beamsteering system. The three grating system will possess chromatic aberrations unless it doesn't steer and the separation between the first two elements is a function of the diffractive deviation of the first two gratings. The effect of the second and third grating is to null the effect of the first grating. The position of the rays exiting the third grating is equal to the position the rays would have intercepted the plane of the second grating with the first grating removed.

The system is afocal and would require additional optics for practical implementation as a passive acquisition sensor system. If each of the additional optics did not possess color aberrations and the gratings were operated under the conditions dictated by Eq. 50 and Eq. 49, then the addition of the optics to the system would not affect the paraxial analysis of the color derivatives of the system. Thus it is possible to build a focal system with gratings that does not possess color aberrations, but the system cannot steer fields of view due to the constraint imposed by Eq. 50.

3.6 : Grating-Grating-Lens System

A system consisting of two plane gratings followed by a lens as shown in Fig. 16 can both steer and image. This system is equivalent to a dual grating (flat-concave) imaging system if $x_2 = 0$, $\Phi_3 > 0$, and $\partial\Phi_3/\partial\lambda = 0$. The optical powers of the elements are considered to have an arbitrary dependence on the wavelength and therefore the elements could be any type of powered element, i.e. diffractive optical element, glass lens, concave, or convex reflective surface.

If there is no angular color aberration, the position aberration metric is dependent upon the position of the ray at the third element and all the elements are thin elements. The ray position at the third element is dependent only upon the first two elements and is independent of the third element. The ray position is

$$y_4 = y_0 - \left[\frac{n_2\lambda}{\rho_2} + \left(\frac{n_1\lambda}{\rho_1} + u_0\right)\right]x_2 - \left(\frac{n_1\lambda}{\rho_1} + u_0\right)x_1 -$$

$$\left(\left[\frac{n_2\lambda}{\rho_2} + \frac{n_1\lambda}{\rho_1} + u_0\right] + \left[y_0 - \left(\frac{n_1\lambda}{\rho_1} + u_0\right)x_1 - \left[\frac{n_2\lambda}{\rho_2} + \frac{n_1\lambda}{\rho_1} + u_0\right]x_2 - \delta y_3\right]\Phi_3\right)x_3 \tag{51}$$

where the variables are shown in Fig. 16. The derivative of the ray position at the image plane is

$$\frac{\partial y_4}{\partial \lambda} = -\left(\frac{n_2}{\rho_2} + \frac{n_1}{\rho_1}\right)x_2 - \frac{n_1 x_1}{\rho_1} - \frac{n_2 x_3}{\rho_2} + \frac{n_1 x_3}{\rho_1} - \left(x_2\left(\frac{n_2}{\rho_2} + \frac{n_1}{\rho_1}\right) + \frac{n_1 x_1}{\rho_1}\right)\Phi_3 x_3 -$$

$$\left[y_0 - \left(\frac{n_1 \lambda}{\rho_1} + u_0\right)x_1 - \left[\frac{n_2 \lambda}{\rho_2} + \frac{n_1 \lambda}{\rho_1} + u_0\right]x_2 - \delta y_3\right]\frac{\partial \Phi_3}{\partial \lambda} x_3$$

(52)

which is equal to the position error of the system. The paraxial ray slope for this system is

$$u_4 = \left[\frac{n_2 \lambda}{\rho_2} + \frac{n_1 \lambda}{\rho_1} + u_0\right] + \left[y_0 - \left(\frac{n_1 \lambda}{\rho_1} + u_0\right)x_1 - \left[\frac{n_2 \lambda}{\rho_2} + \frac{n_1 \lambda}{\rho_1} + u_0\right]x_2 - \delta y_3\right]\Phi_3$$

(53)

where the variables are again shown in Fig. 16.

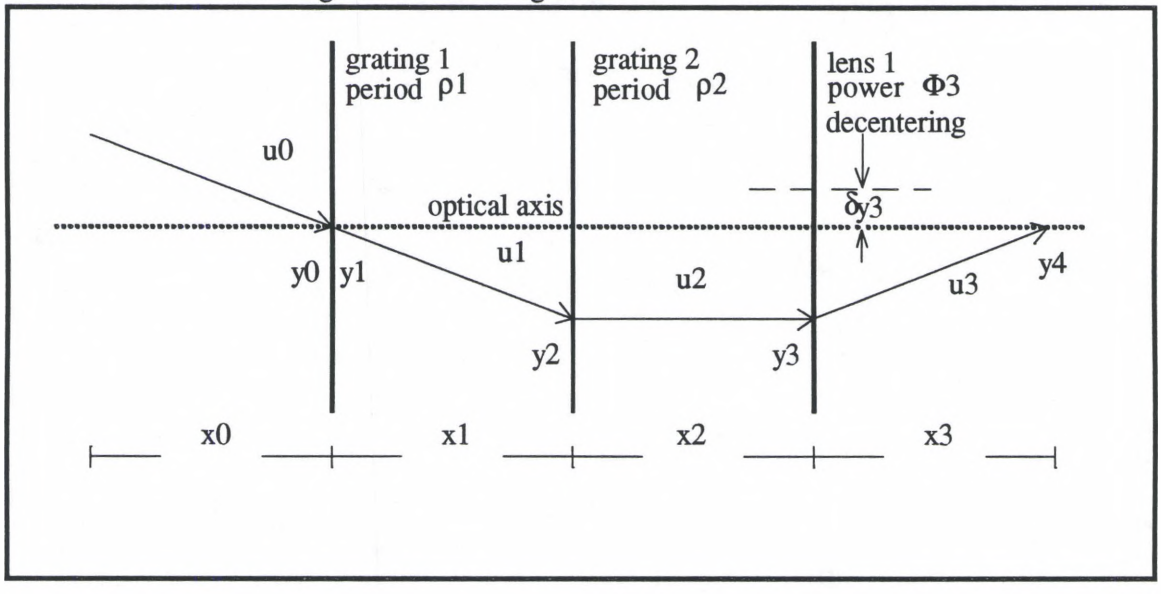

Figure 16 Grating-Grating-Lens System Drawing

The angular color aberration for the system of two gratings followed by a lens is

$$\frac{\partial u_4}{\partial \lambda} = \frac{n_2}{\rho_2} + \frac{n_1}{\rho_1} - \left(x_2 \left(\frac{n_2}{\rho_2} + \frac{n_1}{\rho_1} \right) + \frac{n_1 x_1}{\rho_1} \right) \Phi_3 +$$

$$\left[y_0 - \left(\frac{n_1 \lambda}{\rho_1} + u_0 \right) x_1 - \left[\frac{n_2 \lambda}{\rho_2} + \frac{n_1 \lambda}{\rho_1} + u_0 \right] x_2 - \delta y_3 \right] \frac{\partial \Phi_3}{\partial \lambda} \tag{54}$$

where δy_3 is the decentering of the third element and $\partial\Phi_3/\partial\lambda$ is the derivative of the optical power of the third element with respect to wavelength, which is dependent upon the type of element.

Because continuous reflective surfaces produce the same amount of optical path difference for all wavelengths the power of reflecting surfaces is not a function of the wavelength, i.e., $\partial\Phi_3/\partial\lambda = 0$. Accordingly, there is no dispersion introduced by purely reflective elements. Other materials exist for which there is only slight dependence of the refractive index upon the wavelength. For two gratings followed by a dispersionless powered surface Eq. 54 becomes

$$\frac{\partial u_4}{\partial \lambda} = \frac{n_2}{\rho_2} + \frac{n_1}{\rho_1} - \left(x_2 \left(\frac{n_2}{\rho_2} + \frac{n_1}{\rho_1} \right) + \frac{n_1 x_1}{\rho_1} \right) \Phi_3 . \tag{55}$$

The derivative of the optical power of the third element with respect to wavelength, $\partial\Phi_3/\partial\lambda$, for a lens constructed from a material with concave and/or convex surfaces is dependent upon the dispersion of the material. The derivative of the power of the third lens in this case is given by Eq. 19. When Eq. 19 is substituted into Eq. 54, the result is

$$\frac{\partial u_4}{\partial \lambda} = \frac{n_2}{\rho_2} + \frac{n_1}{\rho_1} - \left(x_2 \left(\frac{n_2}{\rho_2} + \frac{n_1}{\rho_1} \right) + \frac{n_1 x_1}{\rho_1} \right) \frac{\left(\sqrt{a + b\lambda^2 + \frac{c}{\lambda^2} + \frac{d}{\lambda^4} + \frac{e}{\lambda^6} + \frac{f}{\lambda^8} + \frac{g}{\lambda^{10}}} - 1 \right)}{2R} +$$

$$\left[y_0 - \left(\frac{n_1 \lambda}{\rho_1} + u_0 \right) x_1 - \left[\frac{n_2 \lambda}{\rho_2} + \frac{n_1 \lambda}{\rho_1} + u_0 \right] x_2 - \delta y_3 \right] \times$$

$$\frac{\left(2b\lambda - \frac{2c}{\lambda^3} - \frac{4d}{\lambda^5} - \frac{6e}{\lambda^7} - \frac{8f}{\lambda^9} - \frac{10g}{\lambda^{11}} \right)}{2R\sqrt{a + b\lambda^2 + \frac{c}{\lambda^2} + \frac{d}{\lambda^4} + \frac{e}{\lambda^6} + \frac{f}{\lambda^8} + \frac{g}{\lambda^{10}}}}$$

(56)

where an index of refraction of 1 (for air) is assumed for the media surrounding the lens. This equation is not a trivial equation to solve for the roots. The constants *a* through *g* must correspond to those of a real media for the solution to be realizable and δy_3 must also be fixed. The variables ρ_1 and ρ_2 must vary to affect non-mechanical beamsteering.

The power of a Fresnel zone plate lens as a function of wavelength is given by Eq. 21,

$$\Phi_3(\lambda) = \frac{\Phi_3 \lambda}{\lambda_0} \tag{21}$$

and the derivative of the power of the Fresnel zone plate lens is

$$\frac{\partial \Phi_3}{\partial \lambda} = \frac{\Phi_3}{\lambda_0}. \tag{57}$$

Where Φ_3 is the power of the element at the tuned wavelength, λ_0. Substituting Eq. 21 and Eq. 57 into Eq. 54 yields

$$\frac{\partial u_4}{\partial \lambda} = \frac{n_2}{\rho_2} + \frac{n_1}{\rho_1} - \left(x_2 \left(\frac{n_2}{\rho_2} + \frac{n_1}{\rho_1} \right) + \frac{n_1 x_1}{\rho_1} \right) \frac{\Phi_3 \lambda}{\lambda_0} +$$

$$\left[y_0 - \left(\frac{n_1 \lambda}{\rho_1} + u_0 \right) x_1 - \left[\frac{n_2 \lambda}{\rho_2} + \frac{n_1 \lambda}{\rho_1} + u_0 \right] x_2 - \delta y_3 \right] \frac{\Phi_3}{\lambda_0}$$

(58)

where again the solution of the roots of this equation must allow the variables ρ_1 and ρ_2 to vary to affect non-mechanical beamsteering.

3.7 : Field of View Selector System

A field of view selector system requires optics which could image the entire field of regard, but possesses a dynamic field stop which limits the illumination at the image plane to the selected field of view. This system could provide the broadband acquisition of images and achieve the accurate angular handover to the active channel, but the system would require enough pixels at the detector plane to image the entire field of regard at the resolution desired for the individual fields of view. If the field stop were implemented using non mechanical beamsteerers, then the system could possess the required agility of the broadband passive acquisition sensor desired for a ladar system. The three grating system, analyzed in Section 3.5, could be utilized in a field of view selector system, such a system is shown in Fig. 17.

The field stop of the system could be located coincident with the second grating of the three grating system discussed in Section 3.5, selecting the field of view. It would be necessary to place imaging optics before the first grating with a focal plane at the field stop and this is shown in Fig. 17 to be located coincident with the second grating. The

ladar channel could be introduced with a dichroic mirror between the first grating and the field stop for accurate steering of the active channel. The optics following the last grating would be required to relay the image of the entire field of regard with the desired resolution. The field stop limits the field imaged at any particular steer angle to be the angular size of the field stop. A field lens could be introduced to compress the size of the detector needed to image the entire field of regard, but the number of pixels necessary would remain constant.

If the optics introduced to the system possess no paraxial color aberrations, then the paraxial color analysis for the system is identical to that of the three grating analysis considered in Section 3.5. The system would be paraxially achromatic if the conditions for eliminating the angular and position color aberrations, Eq. 49 and Eq. 50, are met. These conditions only constrain the grating periods and grating separations and dictate that there is no overall diffractive deviation of the rays by the system.

To achieve high speed switching between angles we choose to keep the distances between the gratings fixed and we vary the grating periods in accordance with Eq. 49 and Eq. 50. This field of view selector system requires three active beamsteerers for each field of view selector system, which increases the weight and complexity of the system. The beamsteerers could be driven by the same drive electronics with proper choice of grating separations and construction of the dynamic gratings. If the separation between the steer grating and first correction grating is twice the separation between the first and second correction gratings, then the grating period of both correction gratings will be twice that of the steer grating. We could be construct our system with the correction gratings identical to each other but at twice the scale of the steer grating. This allows the same addressing electronics to be used for all the gratings. The correction gratings would have

to be operated at the order of opposite sign of the steer grating's order to null the effects of the first grating on the paraxial derivatives.

As the first grating, labeled the steer grating in Fig.17, steers incident light through the field stop, it introduces dispersion. The field stop is fixed and centered about the optic axis of the imaging optics. Thus for different angles of incidence, different wavelengths (colors) will pass through the center of the field stop. But, due to the special nature of the three grating system (see Eq. 49 & Eq. 50), all the spectral components from a single object point that pass through the field stop get mapped to a single spot in the image plane. An object, such as a airplane, imaged through the system will still be imaged to the same shape of the airplane, but the spectral content of the image will vary along the direction of steering by the steer grating. This is equivalent to replacing the gratings and field stop with a special field stop, which has transmission properties of a spectral filter where the center wavelength and bandwidth are functions of position. Thus an airplane next to the airplane considered above will also be imaged at the image plane accurately in position beside the other airplane, but the spectral content of the second airplane image will be different than that of the first, if the system is selecting an off axis image point. On axis image points would be imaged as though the grating system was removed and the image will be the angular extent of the field stop and will be free of spectral dispersion and color.

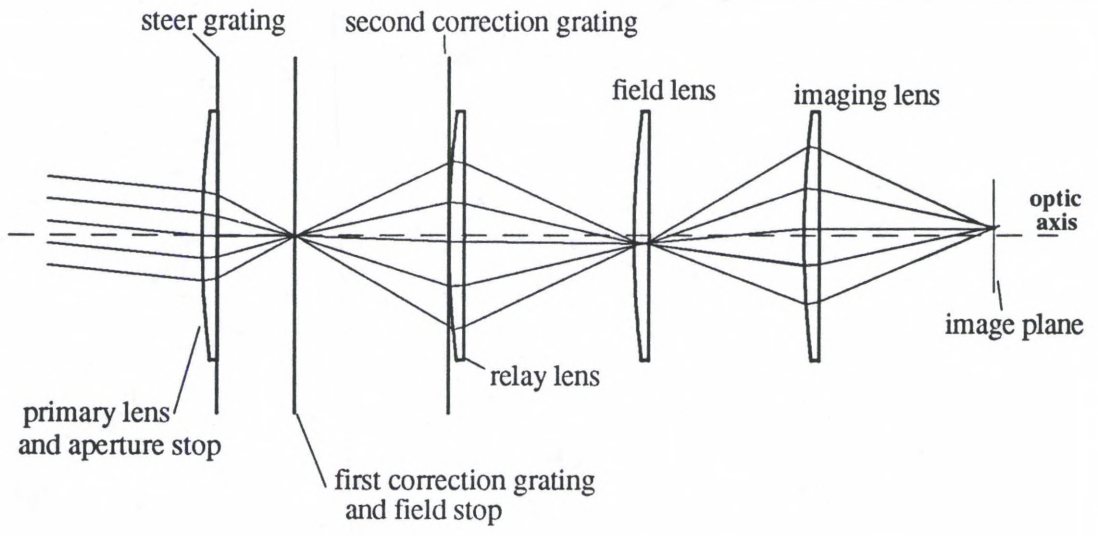

System shown steers objects rays from 2 degree steer angle to image plane.

Figure 17 Field of View Selector System Drawing

The field of view steering system maps a single object point to multiple image points depending on wavelength and this causes spectral blurring of the image, as shown in Fig 18. The field of view selecting system essentially is a field of view steering system followed with a field stop, gratings, and lenses to undo the steering and chromatic aberrations introduced by the steer grating and relay the image to another image plane. Because the light is uncorrected when it passes through the field stop, the field stop vignettes the light dependent upon the steer angle and the bandwidth of light incident and the spectral content of the corrected image is a function of position. This causes the spectral content of the image at the edges to not contain the same spectral content as the image on axis for a broadband object field, as shown in Fig. 18. Thus in a field of view selector system the object and image field are larger than the field stop and the object field is mapped accurately to the image field where the spectral content of the image is a function of position.

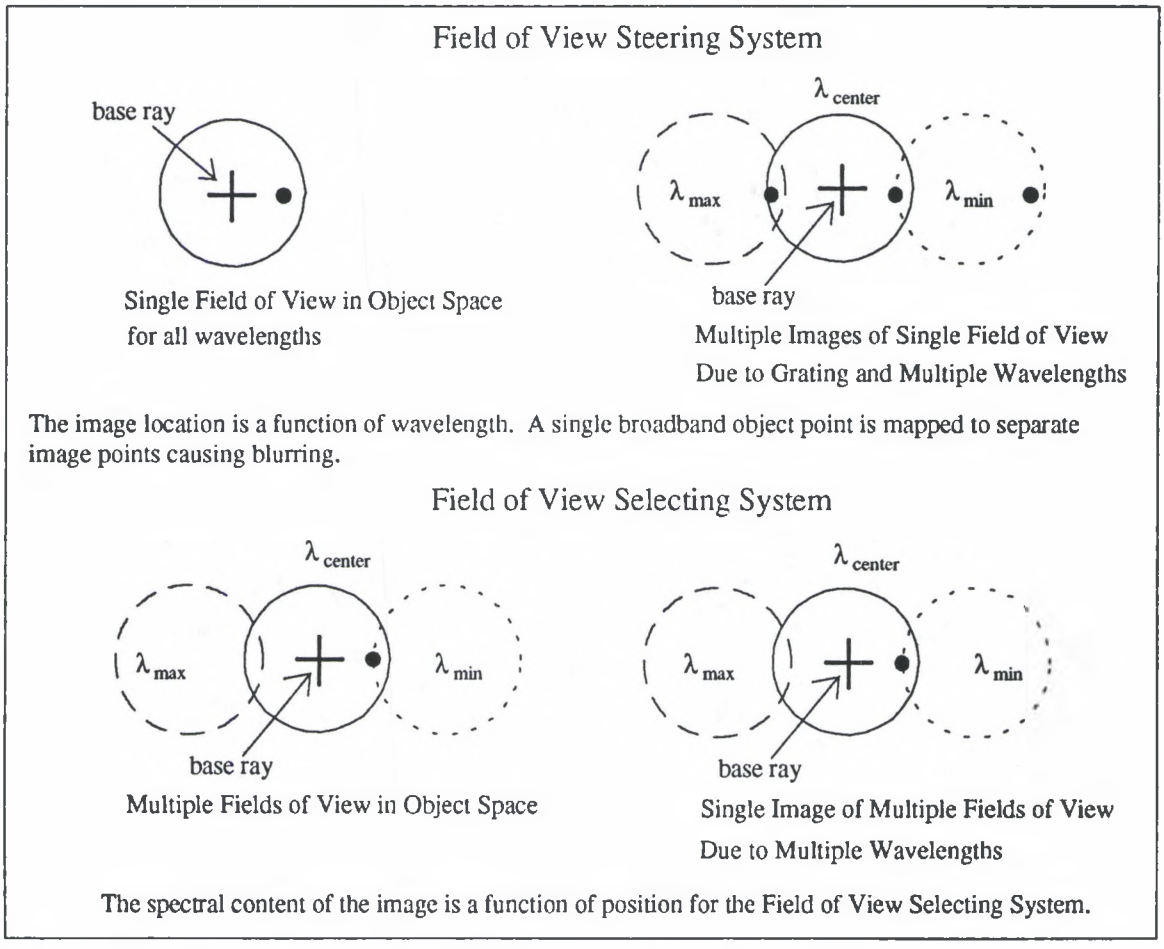

Figure 18 Field of View Mapping at Image Plane for Field of View Selecting and Steering Systems

This field of view selector system cannot steer fields of view to the same image plane locations. This is due to off axis image locations at intermediate planes within the symmetrical optical system. As shown in Fig. 19, a zero degree selected angle possesses an on-axis image location for all the internal image planes. Whereas a 5 degree selected angle possesses an off-axis image location for the field lens plane as shown in Fig.19.

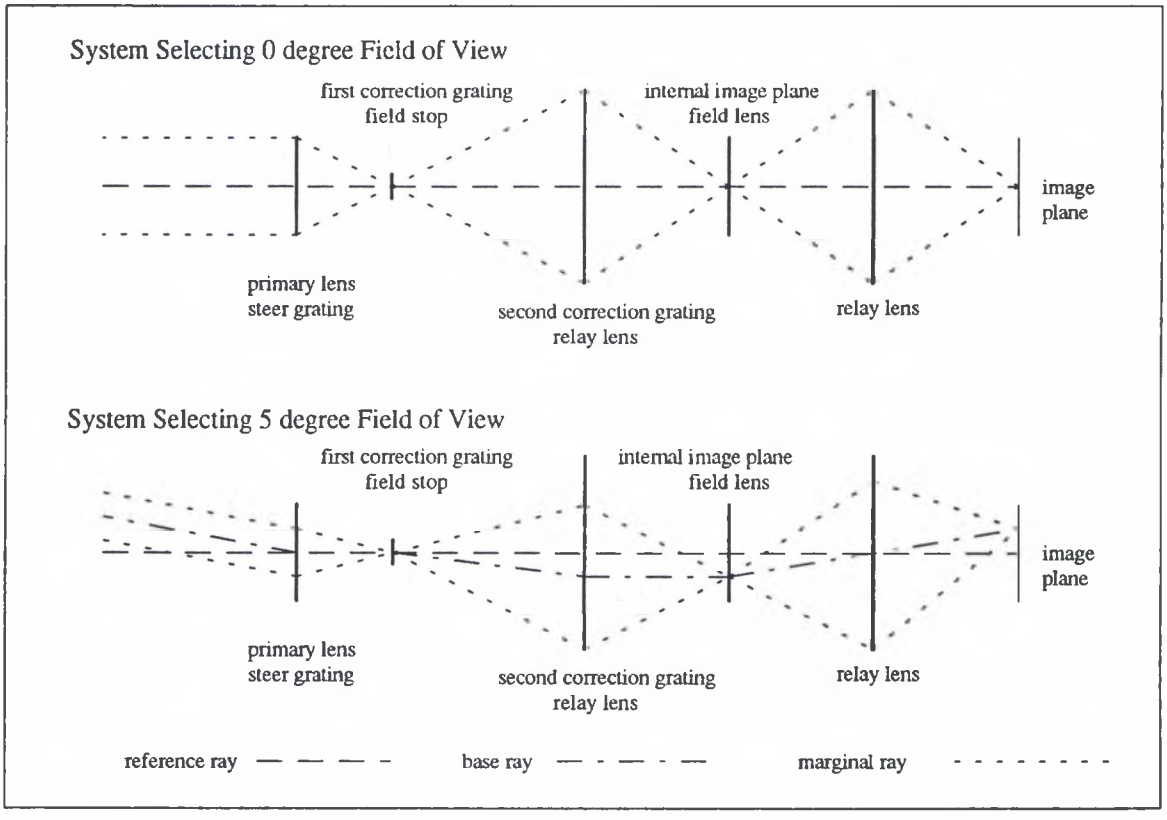

Figure 19 Field of View Selector System Selecting 0 and 5 degree Fields of View

The optical layout of the system selecting a 5 degree angle with the gratings removed and the effects of the gratings included is shown in Fig. 20. The off axis location of the field stop with respect to the relay lens dictates off axis image location, which causes the off axis image location at the field lens plane. Thus the system cannot possess a common image location for different selected fields. The locations of the selected base rays at the field lens for different selected fields of view are different and the field lens cannot force the base rays to intercept the image plane with zero height if they don't possess zero height at the field lens, which is proven paraxially in Appendix A.

The system drawing with the gratings removed, Fig. 20, shows a dynamic field stop and primary lens simulating the effects of the grating. The field stop would be a chromatic filter the transmitted wavelengths are a function of wavelength, as shown in Fig.

18, to accurately model the systems broadband performance. The amount of dispersion in the fields of view in Fig. 18 is a function of the amount of diffractive deviation of the steer grating. This system illustrates the off-axis image locations for the field of view selecting system.

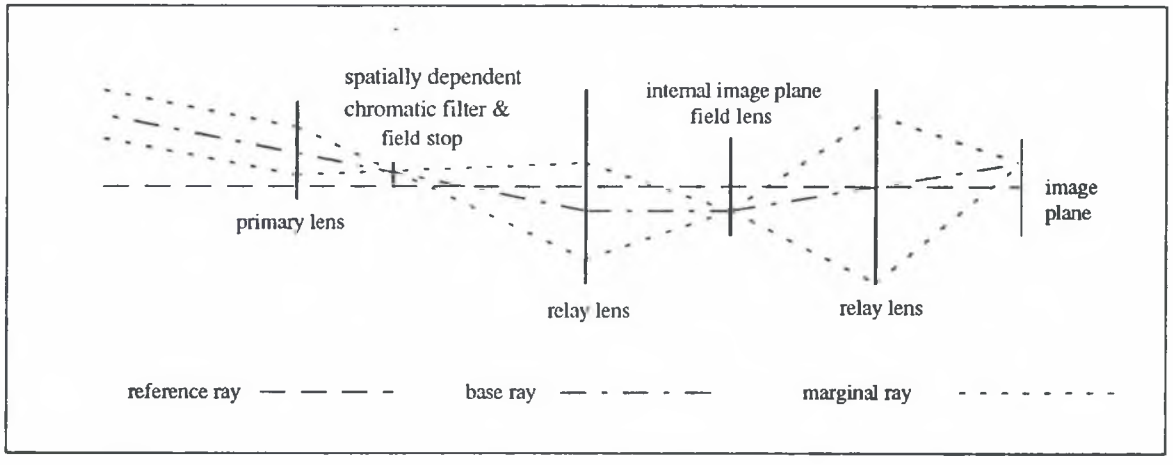

Figure 20 Selector System Selecting 5 degree Field of View without Gratings

Because this system does not steer the fields to the same image plane locations, it would require a large detector at the image plane, which possesses enough pixels to image the entire field of regard at the desired resolution of each field of view. The system could be used in a multispectral imaging system as indicated by Fig. 18. Each steered field of view's base ray would map to a unique position in the image plane depending on wavelength and the selected angle. The field of view selector system is limited in usefulness in a beamsteering system as the beamsteering system is desired to steer all fields of view to the same detector array, which is the field stop of the system.

3.8 : Discussion

From the examination of the paraxial derivatives it is apparent that the longitudinal and lateral color cannot be removed from a steering system that diffractively deviates the rays passing through the system if it is comprised solely of gratings, diffractive Fresnel zone plate phase lenses, and reflective optically powered surfaces. This is due to the diffractive surfaces possessing the same amount of dispersion for the same amount of diffractive deviation and only holds for the paraxial regime where the models of the elements as gratings is also valid. Removing the dispersion from the system also removes any overall steering performed by the system.

It is not possible to remove the longitudinal and lateral color aberrations from a single element system that diffractively deviates the base ray under any conditions while the system diffractively deviates a base ray. This system possesses dispersion proportional to the amount of diffractive deviation performed by the system. Therefore the single element system is not a good candidate for a ladar transceiver with a common passive acquisition channel.

A dual element system can be corrected for lateral color if no overall diffractive deviation of the base ray takes place, this condition determines that there can be no steering of a field of view by the system. It requires that the back focal distance is equal (or nearly equal) to the focal length of the imaging element of the system or the object distance is approximately infinity. The conditions necessary for the elimination of longitudinal color for the dual element system require that no diffractive deviation take place within the system, i.e., $n_1 = n_2 = 0$, or that the power of the imaging element is 0 and no overall diffractive deviation by the individual elements of the system takes place. This condition is brought about by the position dependence of the amount of deviation of the

longitudinal color for the dual element system require that no diffractive deviation take place within the system, i.e., $n_1 = n_2 = 0$, or that the power of the imaging element is 0 and no overall diffractive deviation by the individual elements of the system takes place. This condition is brought about by the position dependence of the amount of deviation of the light at the imaging element. These conditions restrict the utility of the dual element system as a field of view beamsteering system. This system could possibly be used as a field of view selector if additional imaging optics are incorporated into the system, but the ladar channel would have to be introduced into the system between the diffractive gratings.

The Fresnel zone plate lens system can image without lateral and longitudinal color at a single wavelength, but if the elements are displaced with respect to each other to affect steering and the centers of the elements are not colinear, the color aberrations are present. The Fresnel zone plate lens system also possesses negative power requiring an additional positive powered element for the formation of a real image. The dimensions of the system are dictated by the solutions to the longitudinal and lateral color equations, Eq. 43 and Eq. 45, which may require dimensions greater than those desired for the system.

The three grating system is an afocal system requiring additional powered imaging elements for utilization. This system can be corrected for longitudinal color only if there is no diffractive deviation (steering) of the paraxial rays by the system. The removal of lateral color restricts the values of the separations of the elements as a function of the individual grating periods and orders given by Eq. 50. This system is limited in its utility as a field of view steerer, but could be used as a field of view selector for an imaging system. The use of this system in a field of view selector system would have the effect of a field stop being moved about an intermediate image plane. The detector plane must be able to image the entire field of regard. Thus the field of view selector system would only

reduce the number of pixels illuminated, not the number of pixels necessary to image the field of regard.

The dual grating and single lens system could be corrected as a diffractive/refractive steering imaging system provided a material could be found with the proper material dispersion. The system would require a different material dispersion value for each diffractive steer angle. That requires each diffractive angle possess a different refractive optical path resulting in a nontrivial design task.

The systems examined paraxially could not be corrected for both longitudinal and lateral color aberrations if the system is required to steer a field of view diffractively. If this constraint is relaxed and the system is allowed to be used as a field of view selector, then the three grating and dual grating systems could be utilized with no longitudinal or lateral color aberrations. This could allow the system to provide the broadband acquisition of images to achieve the angular handover to the active channel, but the system would be required to possess enough pixels at the detector plane to image the entire field of regard at the resolution desired for the individual fields of view.

CHAPTER IV

SPOT DIAGRAM ANALYSIS

In this chapter specific single, dual, and triple element systems will be evaluated both monochromatically and polychromatically to determine the efficacy of the various designs of ladar transceiver with passive acquisition. This is accomplished using OSLO,[18] a commercial ray trace program, to trace grids of rays through the system for radial energy spot diagram analysis. The radial energy analysis is performed for the systems at various steer angles and bandwidths. Because the ray trace program can trace only three different wavelengths for spot diagram analysis, the radial energy plots may show a discontinuity, which would not be present if the analysis were evaluated with a continuous spectrum broadband light. The radial energy plots for a continuous spectrum would be bounded by the three wavelength radial energy plots evaluated at the fractional energy value of 1 if the centroid is the same for both spot diagrams. The centroid of the spot diagrams would be the same if all the wavelengths in the continuous spectrum were equally weighted, i.e. each wavelength possesses the same amount of energy or number of rays traced.

Each system has a system drawing showing the optical layout of the system. The system drawings are for a zero degree steer angle and 12.5% bandwidth. As the zero degree steer angle corresponds to the reference ray when it passes through the center of the aperture stop, the diffractive deviation of the reference ray is evident from the system drawings. If the drawing has three point images the reference ray is diffractively deviated.

4.1 : Definitions and Conventions

Broad spectral band (broadband) refers to the wavelength content of the directed light and is defined in terms of a percentage change from the center band wavelength to the edge band wavelengths. The bandwidth can be defined by the center wavelength and the two cutoff or edge wavelengths. The percentage bandwidth is given by Eq. 7.

Optical phased arrays steer light by diffraction and can be accurately modeled as blazed gratings, when the number of elements in the array is large.[5,25] Gratings will diffract light according to the grating equation, Eq. 14. From Eq. 14, the dependence of the amount of diffractive deviation on the wavelength is evident. The period of a grating is determined by evaluating the grating equation. Angular errors occur when light of wavelength other than the center wavelength is incident on the grating.

The amount of diffractive deviation is also a function of the order of diffraction, n. The different orders arise from the Fourier transform of the periodic object, which is periodic. The order selects which periodic image is being considered. All the energy from the first array is directed into all of the orders of the second array. The efficiency into any order of the transformed array is determined by the size, spatial shape, and phase shape of the elements of the initial array (grating elements). This analysis considers only one order of the diffracted light for each diffractive surface (n = 1 or -1) and assumes 100% of the incident light is diffracted into that order.

Optimum performance is determined by the maximum diffraction limited bandwidth with the least number of elements. The metric used in this analysis is the radial energy distribution of the polychromatic (three wavelengths) spot diagram about the centroid of the spot. The geometric radial energy plot is used because the diffraction limited spot size is a function of the field angle and wavelength and thus the ratio of the

spot radius to the diffraction limited spot size is also a function of the field angle and bandwidth. Thus the Airy radius of a circular aperture stop in this imaging system is not constant over a field of regard and is a function of the spectral content of the light.

The radial energy distribution is calculated by tracing a grid of 716 rays[23] as shown in Fig. 21 from specific object point, which is given by the field of view point, through the circular entrance pupil, which is defined here as the primary element. The fraction of the total rays that fall within a given radius measured from the centroid of finishing rays in the image plane define the radial energy distribution. Where the centroid is the mean location of the rays in the image plane that is determined by the least squares method.

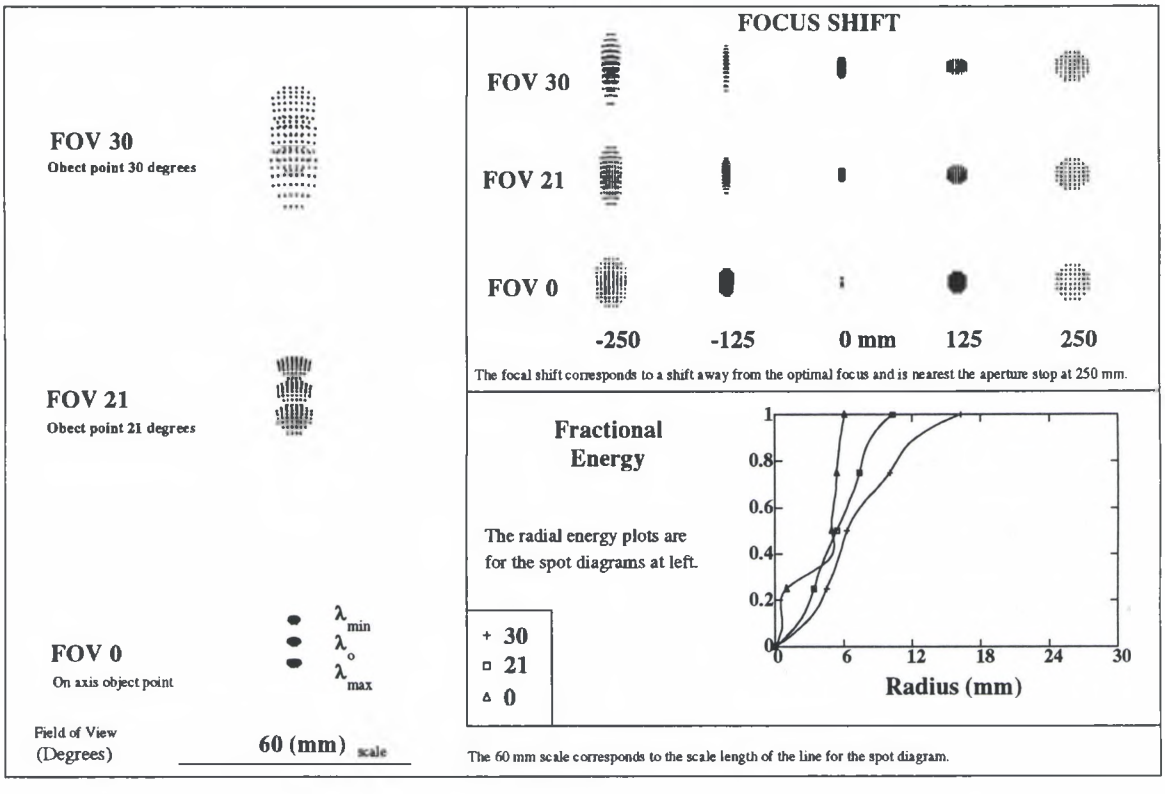

Figure 21 Spot Diagram Analysis with Radial Energy Plot

The radial energy plots for each system are calculated for three bandwidths at three points within the field of view for each of the steer angles. The steer angles are all positive and

equal to 0, 5, and 10 degrees. The bandwidths are 0% (monochromatic 10 μm), 6.25% (9.375, 10, 10.625 μm), and 12.5% (8.75, 10, 11.25 μm). The field of view points are 0, 1.7, and 2.5 degrees. Spot diagram analysis plots are shown in Fig. 21 for a single bandwidth (12.5%) and single steer angle (0 degrees) with 20 degrees diffractive deviation, for a 30 degree field of view. Field aberrations degrade the system's performance to the point where the three separate images arising from the three wavelengths defining the bandwidth and shown in the 0 degree FOV plot blur into a continuous spread of energy in the FOV 30 plot. The curve fitting routine of the ray tracing program causes the overshoot in fitting the discontinuity of the 0 degree FOV radial energy plot. Because the mean location is near the center of the center wavelength's (λ_0) spot and the band is nearly symmetric, the radial energy plot has only one discontinuity large enough to cause noticeable overshoot. as a radial area about the center wavelength is increased in area.

The systems are defocused for optimized monochromatic imaging before the polychromatic spot diagrams are analyzed and the vignetting or stopping of the rays transmitted through the systems is also measured and all systems except for the dual grating system in Section 4.5 have 100 % transmission. Each system is allowed to defocus from a reference plane, located at the on axis focal point for an infinite object, to minimize the monochromatic spot size at each steer angle's 0 degree field of view.

The system requirements considered here are a 20 degree field of regard, with a 5 degree instantaneous full field of view, and broadband imaging about the tuned (10 micron) wavelength. All the systems will be *f*/5 systems with 25 cm focal lengths. The systems will have a diffraction limited spot radius given by

$$r = 1.22\lambda f\# \tag{59}$$

where the aperture stop is circular. The value of the Airy radius is 0.062 mm for the tuned wavelength ($\lambda=\lambda_0=10\mu m$) and a $f\#=5$ system.

Because the system must be able to steer over the field of regard, classical reflective telescope designs such as the Cassegrainian are not advantageous when the primary mirror steers (tilts or diffracts). This is due to obstruction of the entrance pupil by the location of the secondary optic and the field aberrations inherent to these types of systems. The designs considered in the analysis will have an off optical axis image or object location to avoid obstruction of the entrance pupil by the detector or image plane in single element reflective designs and the secondary optic in dual element reflective designs.

Systems incorporating a steering optical phased array possess chromatic aberrations due to the diffractive nature of the steering device. Because of size and weight considerations the grating and imaging element are collocated on the same surface at the aperture stop (and entrance pupil) as is shown in Fig. 22. To minimize the diffractive steering required the beamsteering element is located at the aperture stop in front of the imaging element. On the basis of the Lagrange invariant, location of the beamsteering element at any smaller surface in the system would require greater diffractive deviation of the steered light.

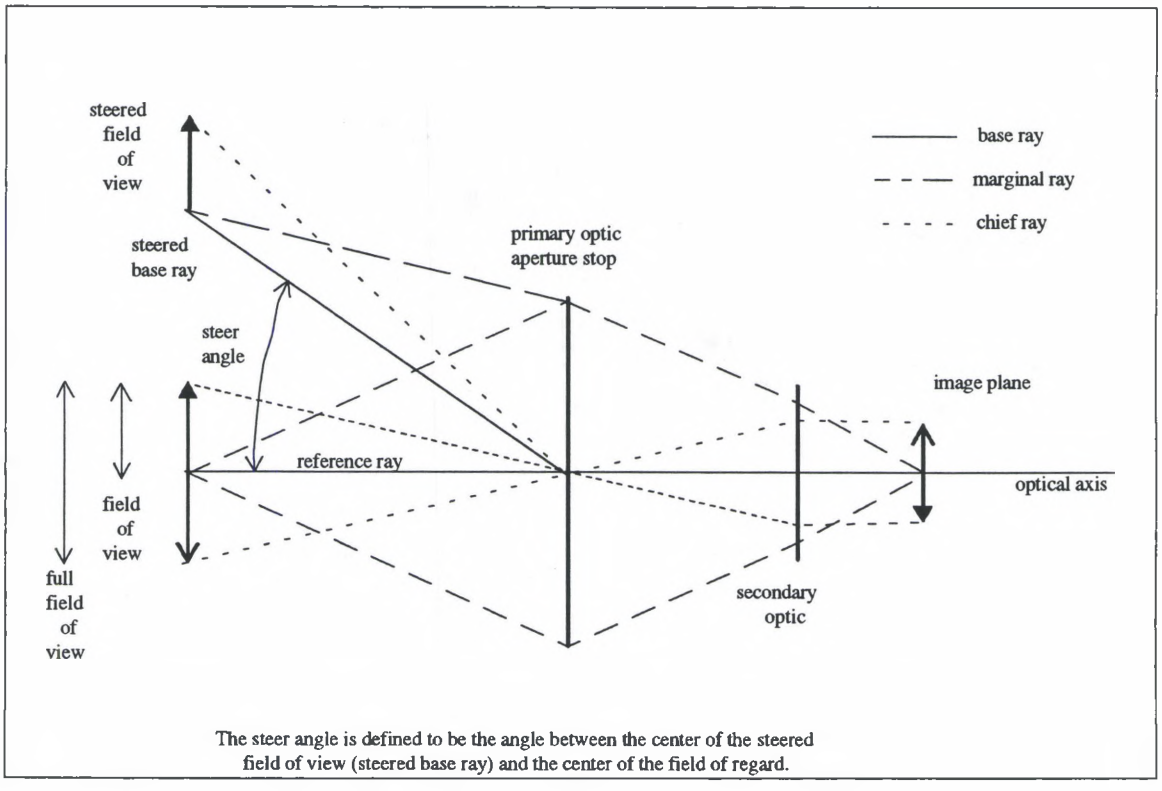

Figure 22 Basic System Diagram with Steered Field of View

Various systems shown in Table 1 with their respective acronyms will now be evaluated beginning with the single tilted mirror system (STM) in Section 4.2. Mirror systems do not deviate rays diffractively nor refractively. Thus the reflective systems have no color aberrations. This allows the mirror systems to provide a baseline for the diffractive beamsteering systems. A single element diffractive steering system (basic single dynamic grating system, SGR20) is the second system evaluated in Section 4.3.A. Then an improved monochromatic grating system (SGR0) will be evaluated in Section 4.3.B. Followed by an improved broadband grating system (SGR10) in Section 4.3.C. A dual mirror system (BSO) is evaluated in Section 4.4 and its corresponding dual grating system (BBBS) is evaluated in Section 4.5. Then a diffractive lens system (DFY) is evaluated as a steering system in Section 4.6. The diffractive systems are then discussed in Section 4.7.

Table 1

System Descriptions with Acronyms and Section Numbers

Section	Appendix	System Description	Acronym
Section 4.2	B.1	Single Tilted Mirror System	STM
Section 4.3.A	B.2	Basic Single Dynamic Grating System	SGR20
Section 4.3.B	B.3	Improved Monochromatic Grating System	SGR0
Section 4.3.C	B.4	Improved Broadband Grating System	SGR10
Section 4.4	B.5	Dual Mirror System	BSO
Section 4.5	B.6	Dual Grating System	BBBS
Section 4.6	B.7	Diffractive Lens System	DFY

4.2 : Single Tilted Mirror System

The first system (STM) considered is a single parabolic mirror, which is tilted to allow for an off-axis image location and described in Appendix B.1. The performance of this system provides a baseline to which the other systems can be compared. The image point (detector) is fixed and steering is accomplished reflectively by tilting the mirror with respect to the reference ray as shown in Fig. 23. Radial energy plots for the system are presented in Fig. 24. The mirror system steers an object point located in the center of the field of regard (10 degrees above the optical axis) to an image point located 10 degrees below the optical axis. This allows the system to steer a 5 degree full field of view over the field of regard (± 10 degrees) with no obstruction of the rays traveling from the object to the image by the detector.

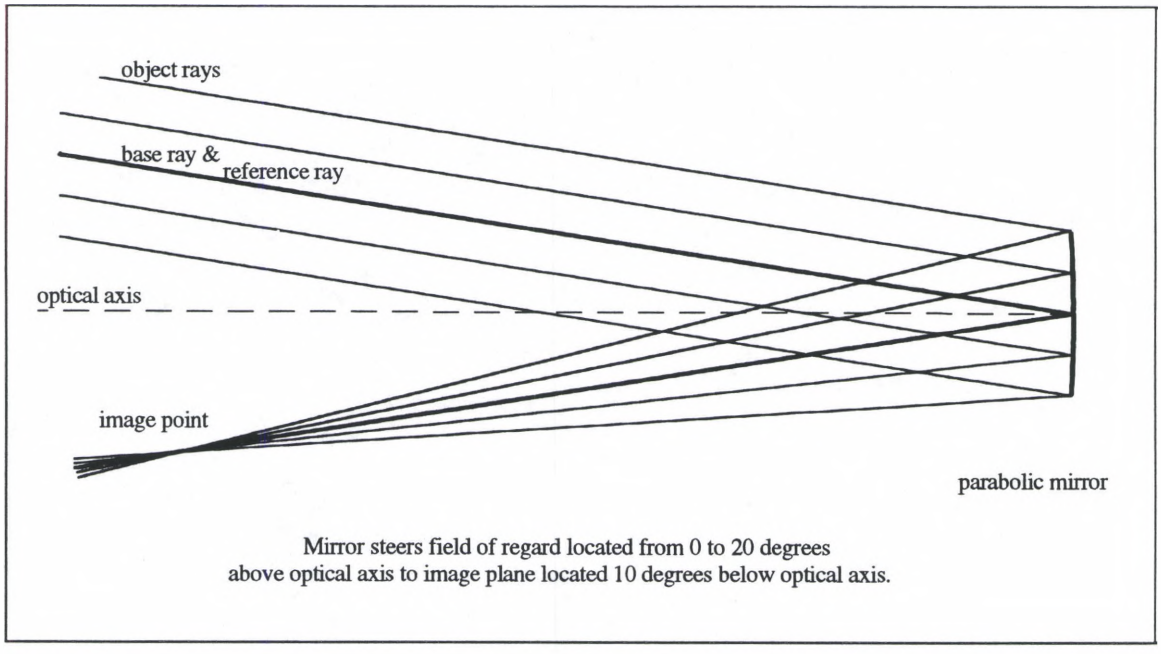

Figure 23 Optical Layout of Single Tilted Mirror System (STM)

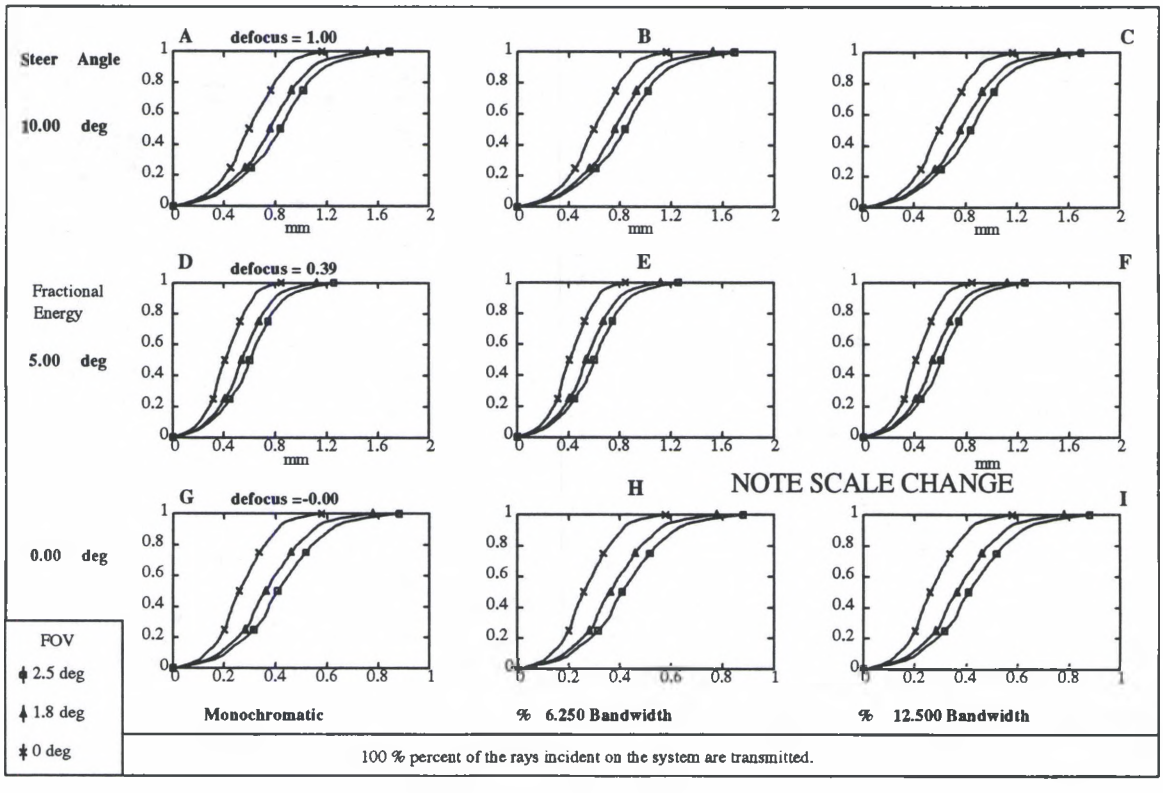

Figure 24 Radial Energy Plots for Single Tilted Mirror System (STM)

As shown in Fig. 24, this system is limited by the off-axis aberrations of the parabolic mirror, as is evident from the scale changes for increasing angles. No chromatic aberrations are evident as the plots are identical for any bandwidth of a steer angle. Because we do not want to obstruct rays traveling from the object to the entrance pupil, we desire an image location outside the angular extent of the field of regard. Therefore this reflective system is never operated on axis.

Parabolic surfaces possess field aberrations that severely limit the diffraction limited field of view. For a steering mirror system the object and image points are located at the same off axis angles from the normal to the reflective surface. This aberration is a minimum at a steered angle of -10 degrees and increases with increasing steer angle to a maximum at 10 degrees steer angle. This trend is evident, segments G, D, and A of Fig. 24, as the scale of the radial energy plots changes to accommodate the larger spot radius of the steered angles.

In telescopic systems field aberrations are usually corrected through the addition of a secondary convex hyperbolic mirror, but this approach would be difficult given the large field of regard for which the system would have to be corrected. An improvement to this system would be to insert a flat steering mirror in front of the parabolic imaging surface. This would allow the imaging system to be corrected for the 5 degree field of view as the flat mirror would steer this field of view about the 20 degree field of regard. Such a system is considered later.

4.3 : Single Concave Gratings

A grating on a concave reflective surface with a uniform period along the arc of the concave reflective surface introduces a monochromatic angular error due to the change of the angle of incidence along the *y* direction with respect to the normal to the concave surface. This can be corrected by writing the grating's constant period along the chord of the concave surface. Writing the constant period along the chord of the surface introduces complexity as the array period is no longer constant along the arc so a chirp will have to be written to the grating period along the surface as shown in Fig. 25. All of the concave gratings considered here will have a grating spacing constant along the chord length of the surface.

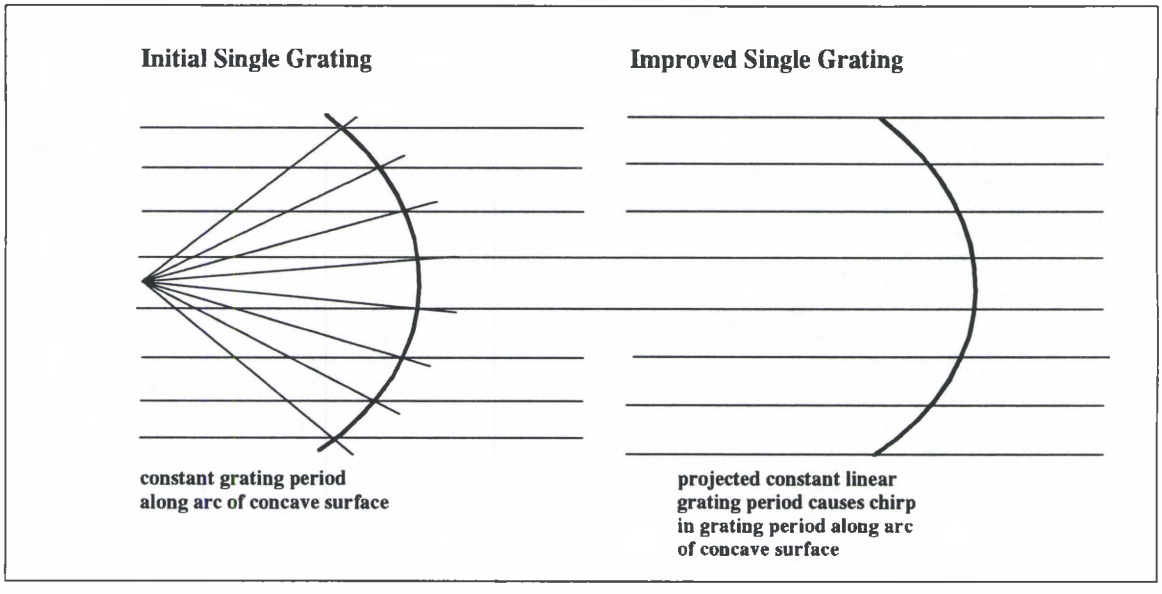

Figure 25 Grating Deformation Caused by Projecting a Linear Grating onto a Curved Surface

4.3.A : Basic Single Dynamic Grating System

A single element grating system (SGR20) similar to the single parabolic mirror system is shown in Fig. 26 and described in Appendix B.2. The grating steers the base ray located within the field of regard, which is centered about the optical axis, to an image point located 20 degrees below the optic axis. Because the field of regard is centered about the optical axis of the parabolic surface, the aperture of the system is as large as possible for a fixed aperture diameter yielding a minimum diffraction limited spot size as was shown in Chapter 2, Section 1. The diffractive deviation, $\theta_{diffraction}$, being performed by the grating is from -10 to -30 degrees and is given by

$$\theta_{diffraction} = \theta_{steer} - 20^{\circ}. \tag{60}$$

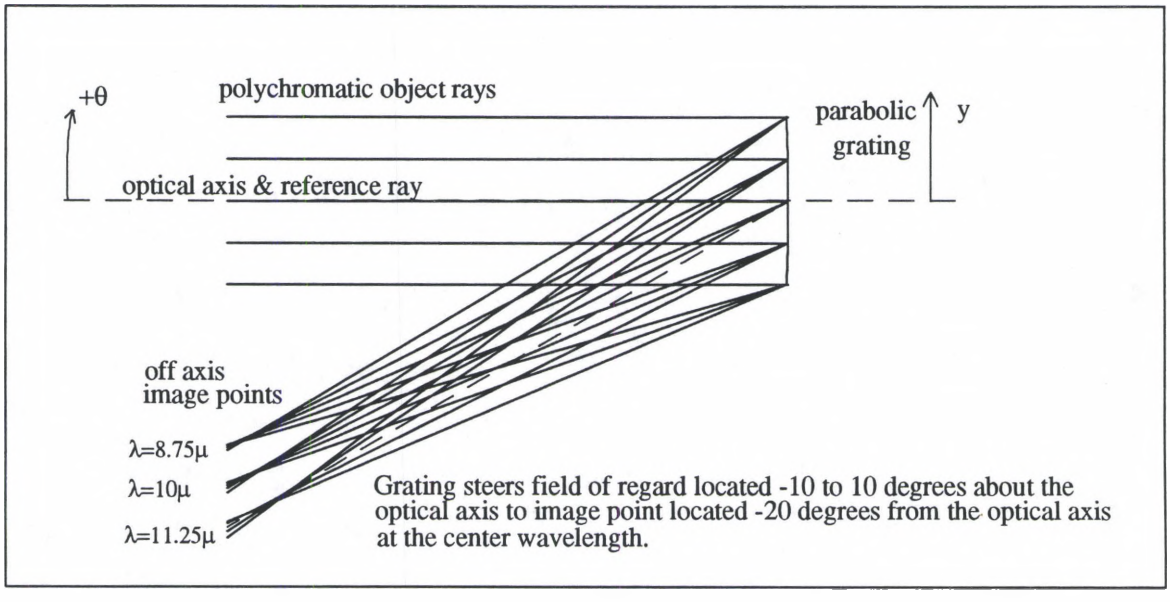

Figure 26 Optical Layout of Basic Single Dynamic Grating System (SGR20)

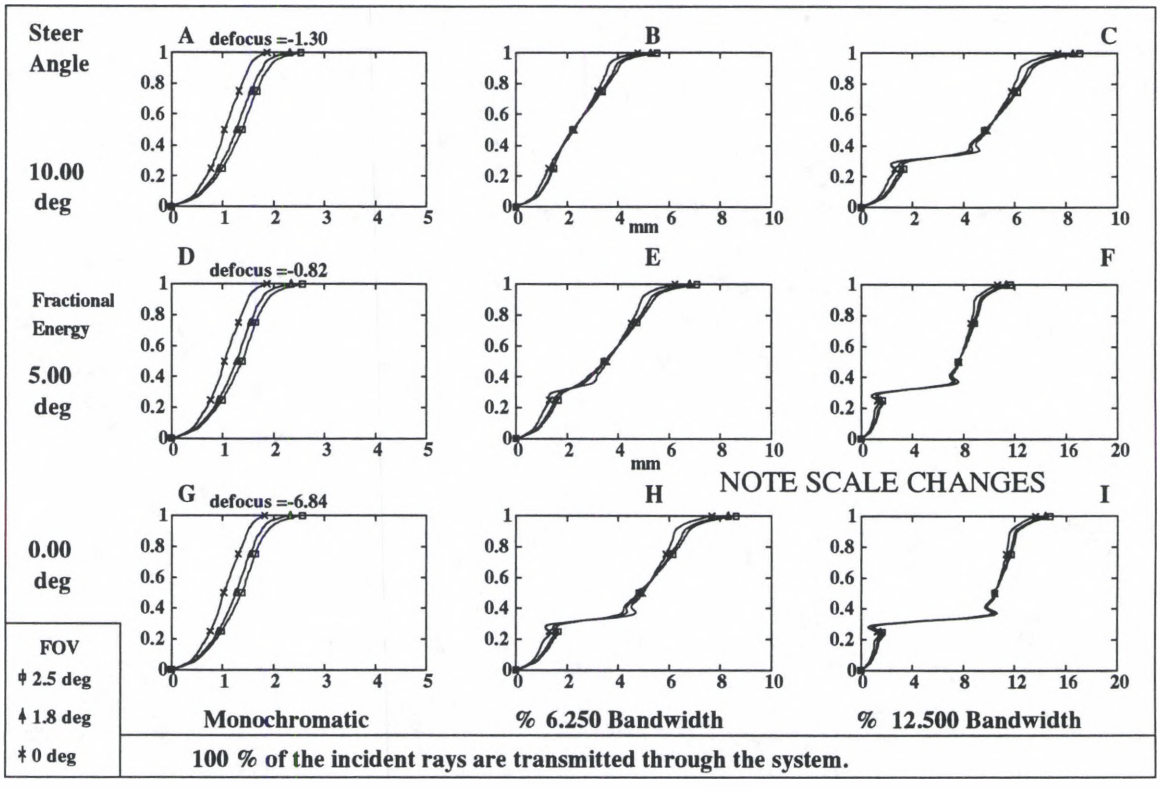

Figure 27 Basic Single Dynamic Grating System (SGR20) Radial Energy Plots

The radial energy distribution plots for this system are shown in Fig. 27. The wavelengths traced through the system for the spot diagram analysis were chosen to be the center wavelength and the maximum and minimum wavelengths of the band. The spline fitting graphics routine inherent to the optical design software causes the ringing in the curve when the radial energy is discontinuous, Fig. 27 (see segments C, E, F, H, and I). This discontinuity occurs because the three wavelengths of light traced through the system form non-overlapping images because of dispersion. Also, there are scale changes in the plots as the bandwidth increases caused by the domination of the chromatic aberration over the monochromatic aberrations. Large amounts of defocus (Δ focus = 6.02 mm) for the monochromatic spots are also documented on the plots as the system is allowed to defocus for the smallest monochromatic spot size at each angle..

The amount of diffractive deviation performed by the beamsteerer is never zero within the defined field of regard. The least magnitude of diffractive steering (10 degrees) performed by the grating occurs at the +10 degree steer angle and the most diffractive steering (30 degrees) occurs at the -10 degree steer angle. The series of plots, Fig. 27 segments B, E, and H, when compared to the plots, Fig. 27 segments C, F, and I, illustrate the effects of diffractive steering on the radial energy distributions for 6.25% and 12.5% bandwidths respectively. It is advantageous to have a point within the field of regard that has no diffractive deviation to reduce the chromatic dispersion caused by the diffractive steering for enhanced broadband performance. This is illustrated by the trend in Fig. 27 as the steer angle becomes larger for the non-monochromatic plots the radial energy distribution gets smaller. As the steer angles get larger the amount of diffractive deviation gets smaller. The system at a steer angle of +20 degrees consists simply of a concave mirror that possesses no chromatic aberrations, but field aberrations due to the large off-axis object and image location would cause degradation in the radial energy plots.

The monochromatic radial energy distributions for this single grating system exhibit spot sizes approximately 30 times the (0.062mm) size of the diffraction limited Airy disk for the same system (*f*/5;250 mm focal length) evaluated at the center wavelength (10 μm). The monochromatic performance can be improved by an on axis image location. Rowland circle theory[26] allows for on axis performance when the image is on axis regardless of the object location. This is due to the grating deviating the rays diffractively to strike the concave axis at an angle that determines the location of the image. For the proper period grating the image can be located on-axis.

4.3.B : Improved Monochromatic Grating System

An improvement to the single grating system for monochromatic imaging (SGR0) can be made by shifting the image plane to the optical axis of the parabolic surface and the field of regard to an off axis location, as shown in Fig. 28 and described in Appendix B.3. The reference ray chosen for this configuration is located 20 degrees above the optical axis of the parabolic surface.

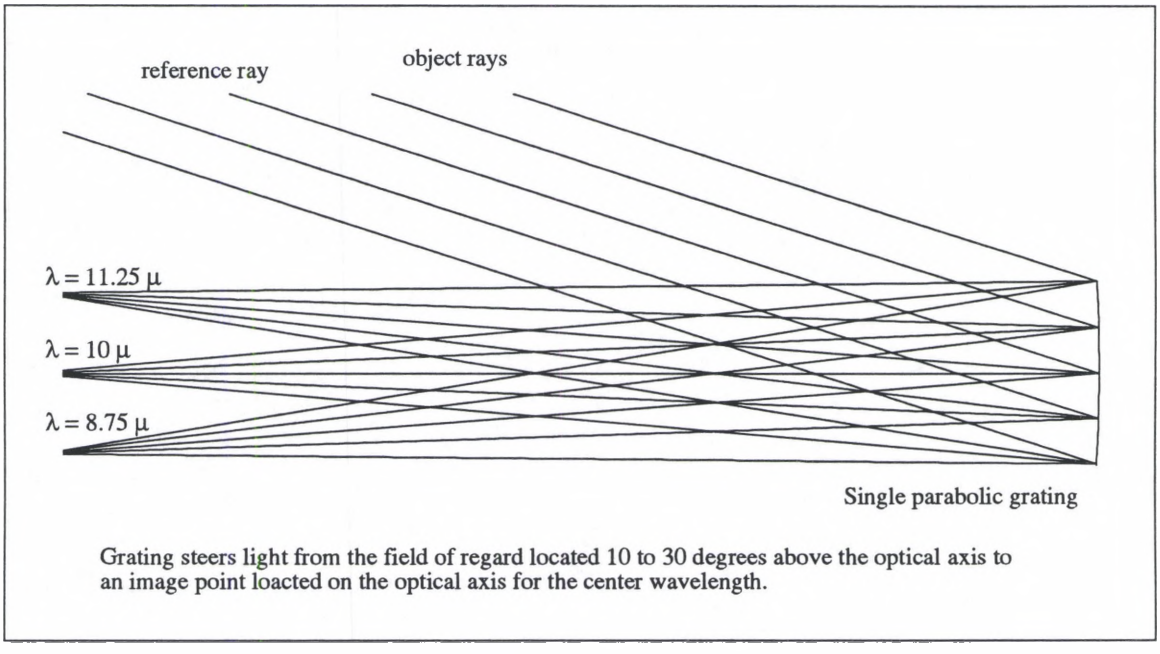

Figure 28 Optical Layout of Improved Monochromatic Grating System (SGR0)

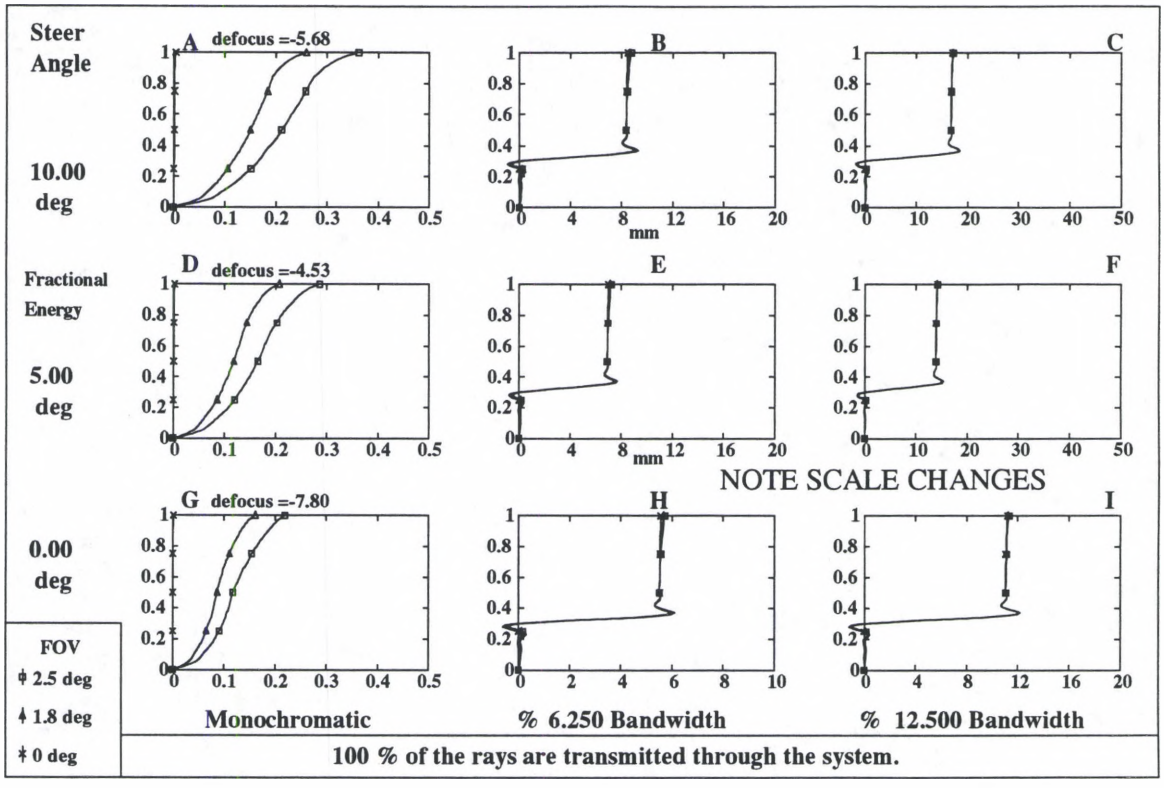

Figure 29 Improved Monochromatic Grating System (SGR0) Radial Energy Plots

The radial energy plots, segments A, D, and G of Fig. 29, show the improvement in the monochromatic imaging of the 0 degree field of view point over the same segments A, D, and G Fig. 24. The amount of diffractive steering, $\theta_{diffraction}$, for this system is between 10 and 30 degrees over the field of regard and is given by

$$\theta_{diffraction} = \theta_{steer} + 20^{\circ}. \tag{61}$$

The broadband performance of this system suffers from the comparatively large amount of diffractive deviation as shown in segments B, C, E, F, H, and I. of Fig. 29 when compared to the same segments of Fig. 27. This is due to the amount of diffractive steering being performed by the respective systems. The amount of diffractive deviation performed by

the systems given by Eq. 60 and Eq. 61. The initial single grating (SGR20) possesses a zero value for the diffractive deviation at a +20 degree steer angle where the improved monochromatic grating system (SGR0) possesses a zero value at a -20 degree steer angle. The plotted steer angles start at 0 degrees and increments in 5 degrees in the positive direction. The system with the minimum amount of diffractive deviation possesses the least amount of chromatic aberrations.

Again there are scale changes in the plots of Fig. 29. These large scale changes are caused by the good monochromatic performance of the system and the large amount of diffractive deviation being performed by the system at the angles evaluated, which dictates poor broadband performance. The amount of defocus (Δ focus = 3.27 mm) for this system is less than that required for the initial single grating system, SGR20, which is due to the good monochromatic performance of the system.

The steep slopes and large discontinuities of the radial energy plots in segments B, C, E, F, H and I of Fig. 29 show the good monochromatic performance of the system as the individual images for the three wavelengths traced possess small field aberrations and small spots. This is evidenced in the broadband segments of Fig. 29 as the slope of the radial energy plots excepting the region of the discontinuity is large. Thus small radial increments lead to large amounts of fractional energy which indicates small spot sizes for the individual monochromatic images. For a continuous broadband spectrum the curves in segments B, C, E, F, H, I of Fig. 29 would be smoother but bounded by the radius value of 1 for a broadband energy spot diagram with the same centroid location.

4.3.C : Improved Broadband Grating System

By changing the locations of the reference ray and image point as shown in Fig. 30, the amount of diffractive deviation can be reduced. This system, described in Appendix B.4 (SGR10), has a reference ray with no diffractive deviation and the amount of diffractive steering, $\theta_{diffraction}$, performed by the system is from -10 to 10 degrees. This is the minimum amount of diffractive deviation over the same field of regard as considered in the previous and following sections for a system with a single image plane location for the center wavelength and is given by

$$\theta_{diffraction} = \theta_{steer}. \tag{62}$$

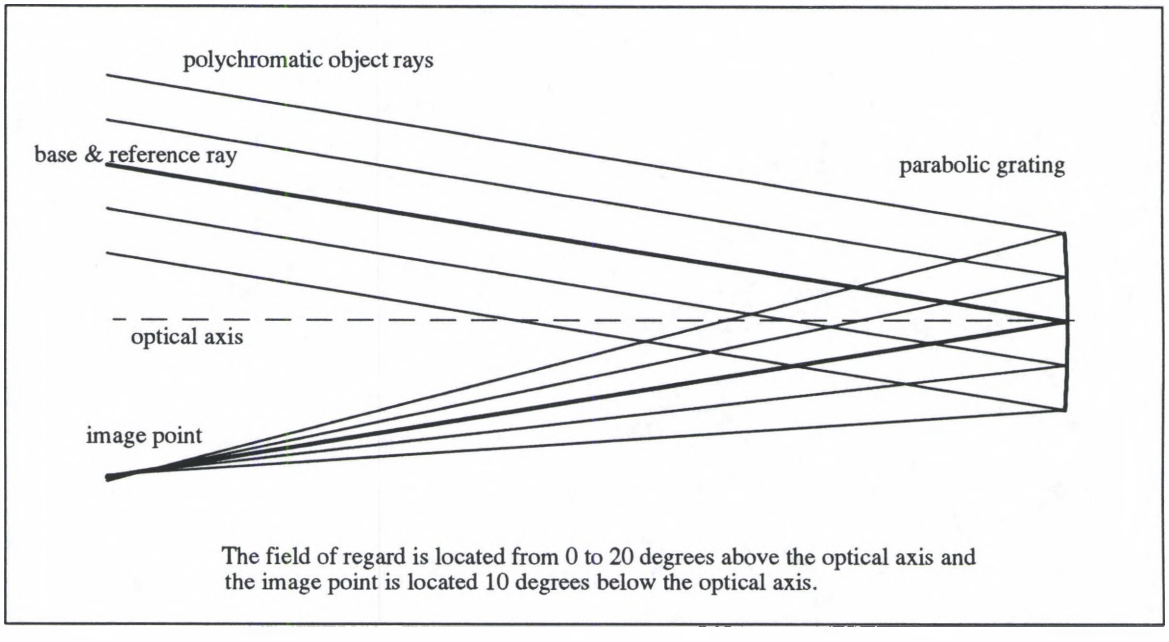

Figure 30 Optical Layout of Improved Broadband Grating System (SGR10)

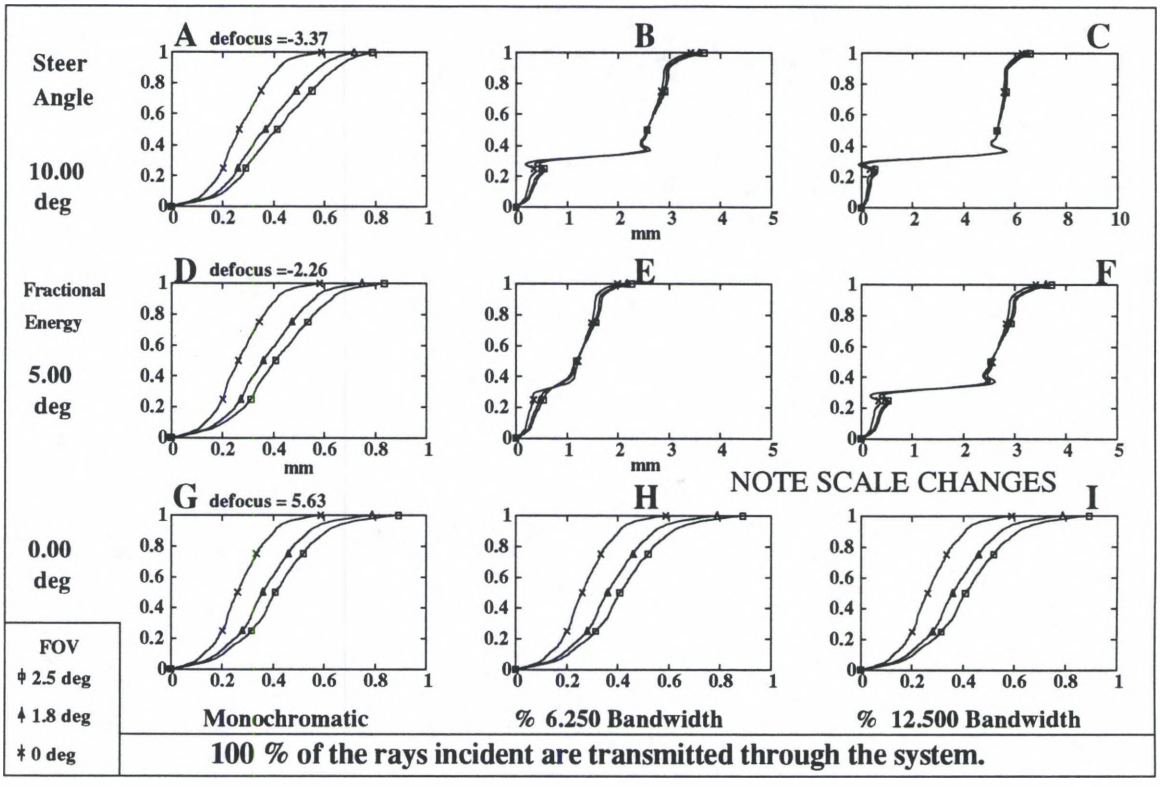

Figure 31 Radial Energy Plots of Improved Broadband Grating System (SGR10)

The broadband radial energy plots of Fig. 31, segments B, C, E, F, H and I show the improvement from the same segments in both Fig. 29 and Fig. 27. Segments B, C, E, F, H and I for Fig. 29 and Fig. 27 have spot sizes at least 1.5, 1.5, 2, 3, 10 and 20 times larger in radius than the respective radial energy plots in Fig. 31. This is due to having no diffractive deviation of the reference ray (0 degree steer angle). The 0 degree steer angle radial energy plots, segments G, H, and I of Fig. 31, show no degradation of performance for increasing bandwidth and are identical to the single tilted mirror for 0 degree steer angle, segments G, H, and I of Fig. 24,as the systems are identical, but the radial energy plots are approximately ten times the diffraction limit for an ideal system. This tradeoff of better broadband performance for worse monochromatic performance is illustrated in Figure 32.

This system also possess large amounts of defocus (Δ focus = 9.00 mm) for the monochromatic plots and scale changes. The monochromatic plots for all steer angles, Segments A, D, and G, and the unsteered plots for all bandwidths, Segments G, H, and I, all possess the same scale in Fig. 31. The remaining plots all possess a different scale dependent upon the steering-bandwidth product.

Figure 32 shows radial energy plots for the single tilted mirror system (STM), the initial single concave grating (SGR20), the improved monochromatic single grating system (SGR0), and the improved broadband single grating system (SGR10). These plots are for a 0 degree field of view angle at a 5 degree steer angle for 0 % (monochromatic) to 6.25 % bandwidths. The plots show the poor performance of a single tilted mirror for monochromatic imaging. The monochromatic imaging of the improved monochromatic grating system (SGR0) demonstrates its utility in a ladar transceiver as its 0 degree field of view performance is diffraction limited. It has the poor broadband performance over the entire field of regard, +10 degree to -10 degree steer angle, due to the large amount of diffractive deviation of the reference ray. The initial single grating system (SGR20) has poorer broadband performance with the same amount of diffractive deviation due to greater field aberrations than the other single grating systems. This limits the utility of both systems, (SGR20) and (SGR0), in a broadband passive acquisition channel.

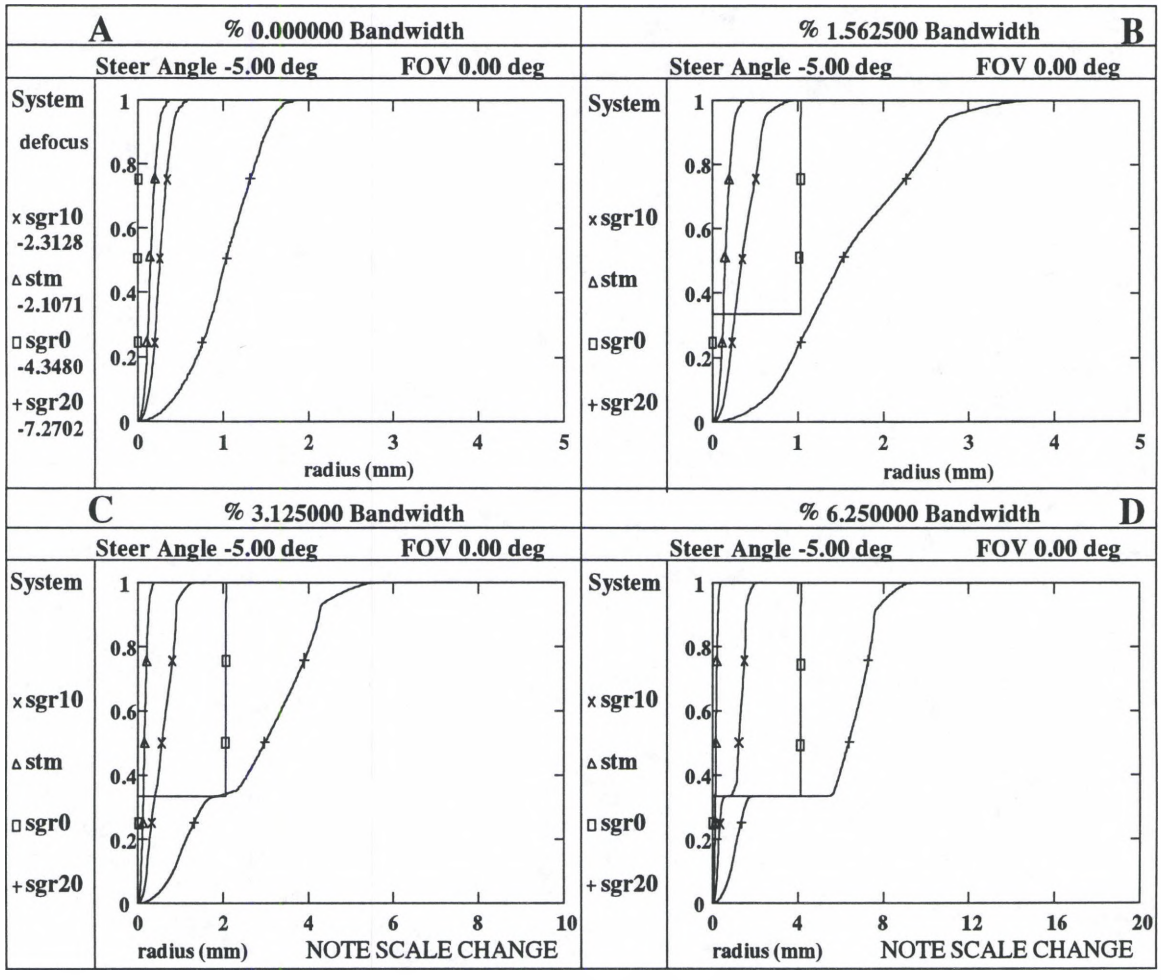

Figure 32 Single Element Radial Energy Plots

As shown in Fig. 32, the system with the best light gathering capacity (largest entrance pupil), initial single grating system (SGR20), possesses the largest amount of monochromatic aberrations due to the large amount of field aberrations caused by the 20 degree off axis image location. While the system with the best monochromatic performance, improved monochromatic single grating system (SGR0), has a reduced entrance pupil due to the off axis object location between 10 to 30 degrees. The best broadband performance of a single grating system is achieved by the system with no diffractive deviation of the reference ray, the improved broadband single grating system (SGR10), but it possesses field aberrations which limit its monochromatic performance or

its efficacy as a ladar transceiver. It is possible to exploit the attributes of each of these systems through the addition of another element. A dual grating system can possess no cumulative diffractive deviation of the reference ray, a field of regard centered about the axis of symmetry of the first element, and an on-axis location of the image point with respect to the imaging or powered element. A dual grating system will be considered in Section 4.5.

In summary, the single mirror system has performance unaffected by the bandwidth of the light as it is a tilted mirror steering system. The field aberrations of the system are such that is possesses 1.00 mm defocus. The spots sizes for the system are approximately 10 x the diffraction limited spot size for the *f*/5 system.

The initial single grating system, Figs. 26 and 27, steers light from off-axis object points located between -10 and 10 degrees with respect to the optical axis to an off axis image point located 20 degrees below the optical axis. The system has 20 degrees diffractive deviation of the reference ray and the largest possible entrance pupil for the field of regard. But the system possesses large amounts of defocus, 6.02 mm, and the best spot size for the system is 30 x the diffraction limited spot size.

The improved monochromatic single grating system, Figs. 28 and 29, steers light from 10 to 30 degrees above the optical axis to an image point located on the optical axis with 20 degrees diffractive deviation of the reference ray. The system possess the best monochromatic performance and has broadband system performance equivalent to the initial single grating system, SGR20. The defocus of the system is comparatively small, 3.27 mm, and the best spot size for the system is only 3 x the diffraction limited spot size.

The improved broadband single grating system, Figs. 30 and 31, steers light from 0 to 20 degrees above the optical axis to an image point located 10 degrees below the optical axis and the image plane has been tilted 10 degrees with respect to the optical axis.

The amount of diffractive steering over this field of regard is between -10 and 10 degrees and there is no diffractive steering of the reference ray (0 degree steer angle) as shown in Fig. 30. This reduces the amount of diffractive steering, which will increase the diffraction limited bandwidth, Fig. 5. The system does possess the largest amount of defocus of the single grating systems, 9.00 mm, and the best spot size is 10 x the diffraction limited spot size.

4.4 : Dual Mirror System

A system (BSO) consisting of a flat steering mirror and an off axis section of an imaging mirror is shown in Fig. 33 and described in Appendix B.5. This system steers light located between -10 and 10 degrees of the optical axis to an off axis parabolic section located 20 degrees below the optical axis. The off axis section is tilted 20 degrees with respect to the optical axis to reduce the field aberrations associated with the parabolic surface and focuses the light to a point located below the optical axis. The steered base ray from the second element to the image plane is parallel to the optical axis.

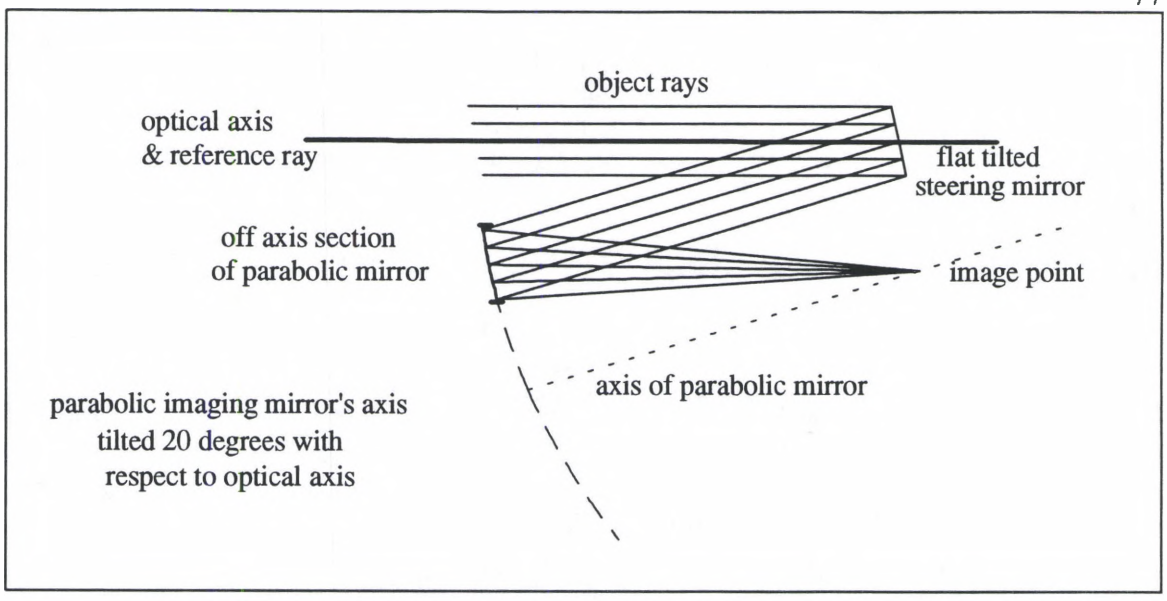

Figure 33 Optical Layout of Dual Mirror System (BSO)

The radial energy spots in Fig. 34 indicate excellent 0 degree field of view imaging over the entire field of regard for any bandwidth. The parabolic surface has poorer performance for non-zero fields of view, but this effect can be compensated by the addition of a hyperbolic surface as in a Cassegrainian configuration. Utilizing the hyperbolic surface will reduce the zero degree field of view performance and this tradeoff limits the diffraction limited field of view for a parabolic/hyperbolic system. Any commercial off-axis telescope could be used in this configuration in place of the parabola because the primary does not steer. The diffraction limited field of view for this type of system with a flat steering mirror is dependent only on the diffraction limited field of view of the telescope imaging system and the flat mirror quality.

The system as evaluated possesses no defocus and has diffraction limited spot sizes. The spot sizes are geometrically perfect for the 0 degree field of view rays for each steer angle. The flat tilted mirror will possess undesirable features of mechanical

beamsteering systems, i.e. reduced agility, jitter, and increased weight and power requirements.

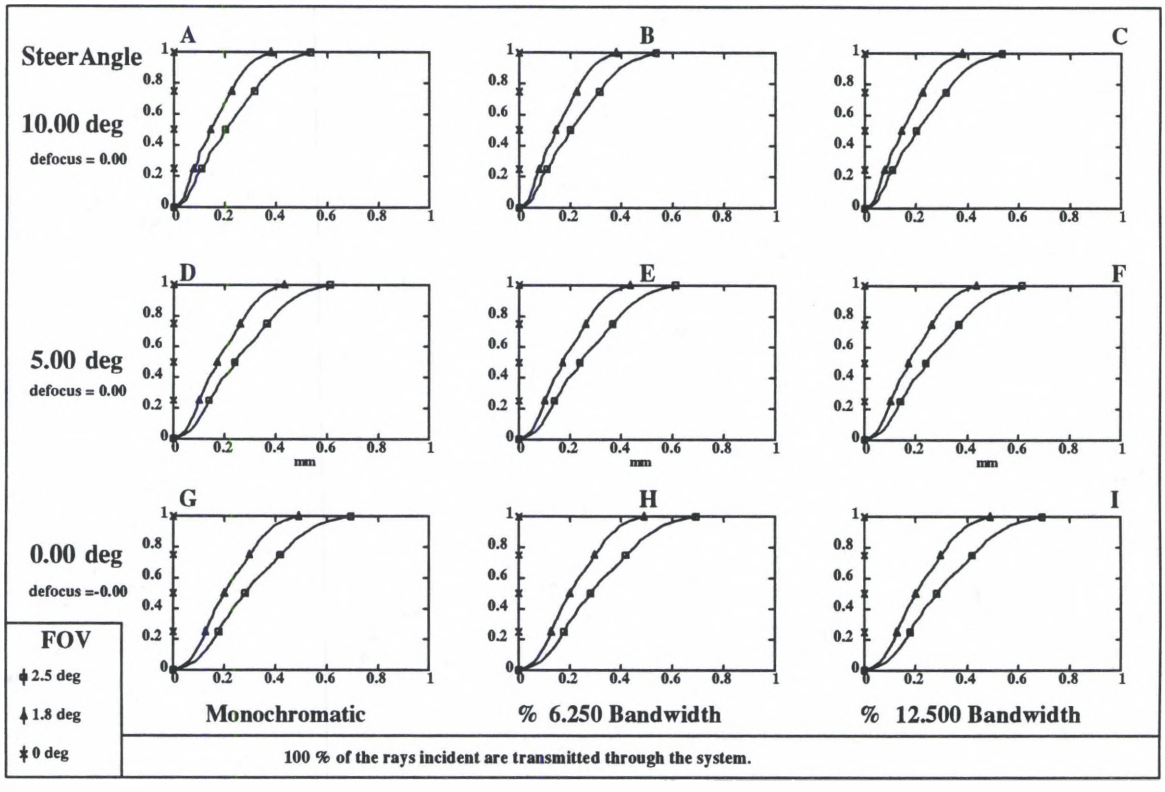

Figure 34 Radial Energy Plots for Dual Mirror System

4.5 : Dual Grating System

The grating equivalent to the dual mirror system is shown in Fig. 35 and described in Appendix B.6. This system (BBBS) consists of a flat steering grating directing the light to the parabolic grating element. The parabolic element is a linear grating written on the chord of the parabolic reflective surface. If both elements are dynamic (writeable gratings), then the system can eliminate the chromatic aberration by allowing the second

grating to null the effects of the first. This is accomplished by requiring that the second grating to have the same period and operate in the diffractive order of opposite sign as the first grating as is seen in Eq. 37 in Section 3.3, the dual grating paraxial analysis. Unfortunately, steering is also eliminated, which is shown in Eq. 40. The steered base ray will exit the second grating at the same angle it was incident on the first.

Fixing the period of the second grating and allowing the first grating to vary its period will allow the system to steer, but chromatic aberrations will be present. However, with a fixed image point and 20 degree diffractive deviation period written on the fixed grating, the reference ray will have zero chromatic aberration for an infinite object in a field of regard centered about the optical axis, which is normal to the first grating. This is due Eq. 37 as there is no position error in the rays at the image plane for all paraxial rays. This will allow the system to have the largest effective aperture and smallest diffraction limited spot size at the point of zero dispersion. Also, requiring no overall diffractive deviation of the reference ray, the system has the smallest amount of diffractive deviation of the beam over the entire field of regard where the deviation is given by Eq. 62,

$$\theta_{diffraction} = \theta_{steer}. \qquad 62.$$

It is noted that the base ray with zero chromatic aberration can be chosen anywhere in the object field by appropriate choice of the period of the fixed grating.

The amount of steering (diffractive deviation) is -10 to 10 degrees for the system shown in Fig. 35 and is symmetric in that the radial energy plot for +10 degrees steer angle is identical to that of -10 degrees if there is no vignetting of the rays by the second fixed period grating. The flat steering grating directs the light to a parabolic grating centered 20 degrees below the optical axis and the period of the second fixed grating is such that the steered base ray will be steered to an image point along a path parallel to the optical axis. The parabola is not tilted with respect to the optical axis, only decentered.

The image is centered about the normal ray to the parabola's center. Light not of the tuned wavelength will be partially vignetted by the second aperture causing a reduction of the number of rays transmitted as shown in broadband radial energy plots of Fig. 36. This is caused by the angular error of the light in the rays reflected and diffracted by the first surface leading to a positional error as they propagate to the second surface. For a fixed size of the second surface, the positional error of the rays at the second surface will cause some of the rays to miss the second surface. The second surface should not be made larger as it will then obstruct rays from negative steer angles propagating toward the entrance pupil. Decentering the second surface further off-axis and enlarging it will require the first surface to diffract the light to a larger angle causing greater angular error in the light. Thus simply enlarging and/or displacing the second grating will not solve the vignetting problem.

The ability of the grating to allow the parabola to operate on axis also will be degraded by the bandwidth of the light as light not at the center wavelength will be corrected only when the total amount of effective steering being done by the two gratings is zero. This occurs only at the on axis field of view object points, i.e. when the system doesn't diffractively deviate the angle of the base ray exiting the system from the angle of incidence for that ray with respect to the first element.

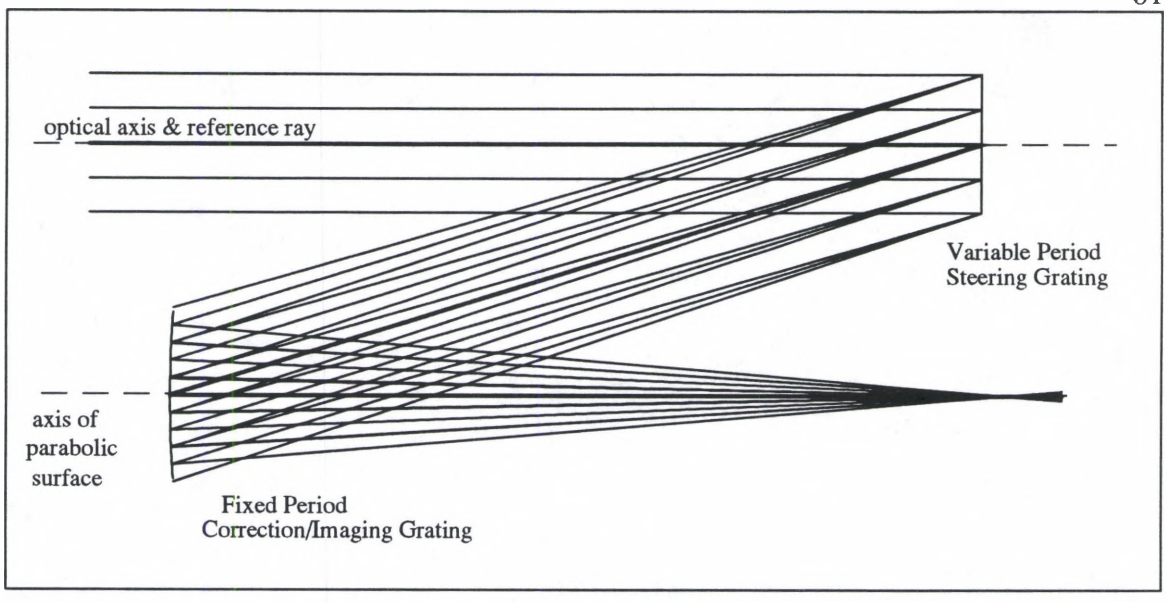

Figure 35 Optical Layout of the Dual Grating System (BBBS)

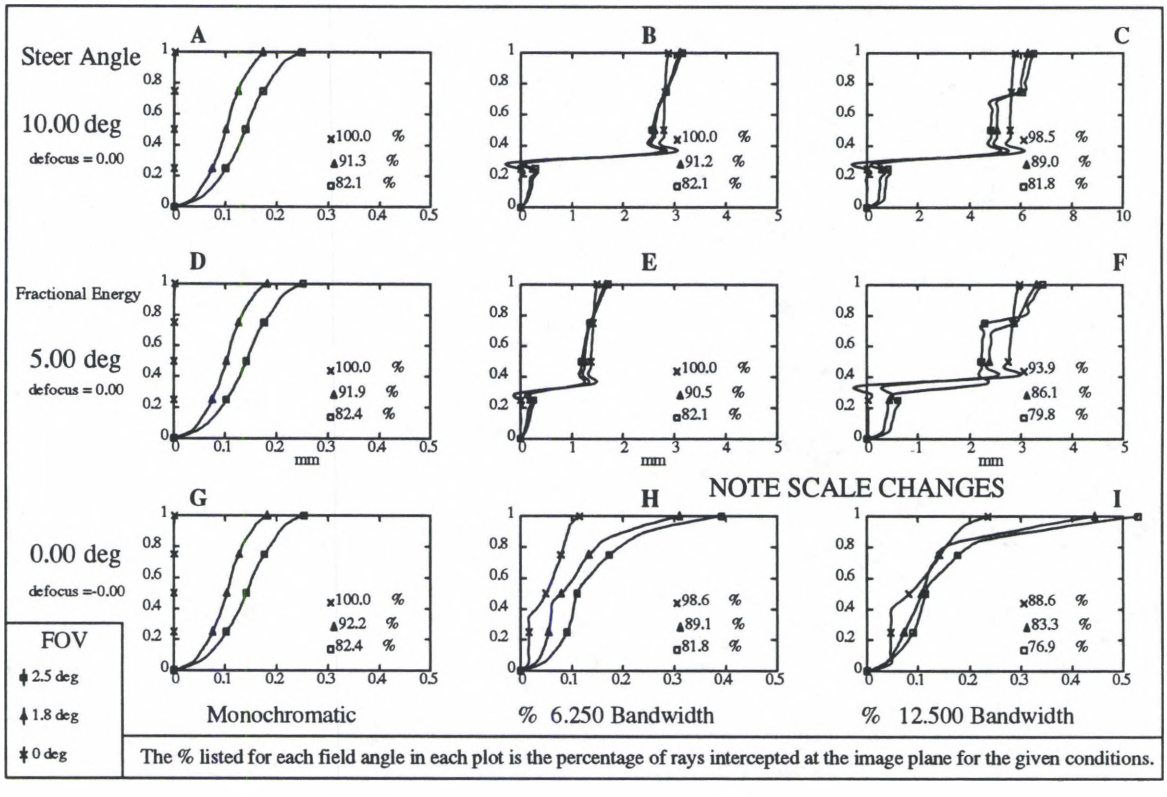

Figure 36 Radial Energy Plots for Dual Grating System (BBBS)

As can be seen from Fig. 36 (segments A, D, and G), the monochromatic radial energy plots for this system are better than the corresponding plots for the dual mirror system in Fig. 34 (segments A, D, and G) for non-zero field of view points. The unsteered plots , Fig. 36 (segments G, H, and I), are also better at non-zero field points than the corresponding dual mirror plots, Fig. 34 (segments G, H, and I). The dual mirror system, Fig. 34 (segments B, C, E, and F), out performs the dual grating system, Fig. 36 (segments B, C, E, and F) for the steered polychromatic plots due to the ability of the dual grating system to correct the dispersion for only one angle within the field of regard.

There is vignetting of the rays evident in the dual grating system given by the percentage of rays transmitted through the system in Fig. 36. This vignetting is a function of the bandwidth, the amount of diffractive deviation by the primary element, the spatial separation of the primary and secondary elements, and the ratio of the size of the secondary element to that of the primary elements. The system possesses no defocus as did the dual mirror system, BSO.

The improved monochromatic single grating (SGR0) with its dynamic chirped grating shown in Fig. 28 has approximately equivalent unsteered monochromatic performance as evidenced in Fig. 29 (segments A, D, G, H, and I) than the dual grating system Fig. 34 (segments A, D, G, H, and I). Because both the improved broadband single grating (SGR10) and dual grating (BBBS) systems have reference rays which are not diffractively deviated at 0 degree steer angle, the steered polychromatic plots have similar shapes. This is due to the domination of the dispersion over other aberrations and the fact that both systems have identical diffractive deviation for the same steer angle. The dual grating system has the advantage of writing the dynamic grating to a flat surface, which will not distort the grating, and that enables the dual grating system to have a dynamic grating of constant period with respect to the flat surface. The single grating

systems, SGR20, SGR0, and SGR10, have a chirped dynamic grating written to a concave parabolic surface, which involves greater complexity in the manufacturing of the devices. The parabolic correction/imaging grating of the dual grating also has a chirped grating with respect to the arc length of the surface, but as this is a fixed grating the increased complexity of writing the chirped grating to the parabolic surface is less than the fabricating dynamic chirped grating devices.

4.6 : Diffractive Lens System

An all diffractive imaging system, which is free of first order chromatic aberrations, was evaluated as a steering system. The diffractive lens system (DFY) consists of three diffractive lenses whose layout is shown (*f*/-1) in Fig. 37 and described (*f*/-5) in Appendix B.7. The design of the system was modified from Ref. 16 to allow it to steer by adding a dynamic phase grating to the diffractive lens. This is equivalent to shifting the first element off axis to accomplish steering. The system was also modified to make the system have *f*/-5. The other two diffractive lenses are fixed lenses (not dynamic). The system was evaluated at the virtual image plane because as noted earlier an all diffractive system cannot produce a real image if it is achromatic. The amount of diffractive deviation of a steered base ray is given by Eq. 62

$$\theta_{diffraction} = \theta_{steer}. \tag{62}$$

Individual rays may undergo greater diffractive deviation as the amount of diffractive deviation is now dependent on the position of the ray through each surface and differs for each ray by wavelength and input position because the power of the diffractive element is a function of wavelength.

The system in Reference 16 is a *f*/-1 system. For the system considered here, the first element (aperture stop) was reduced in size to make the system *f*/-5. The layout drawing shown in Fig. 37 is the original *f*/-1 system for clarity because the disproportionate size of the *f*/-5 system. The radial energy plots were obtained from the *f*/-5 system.

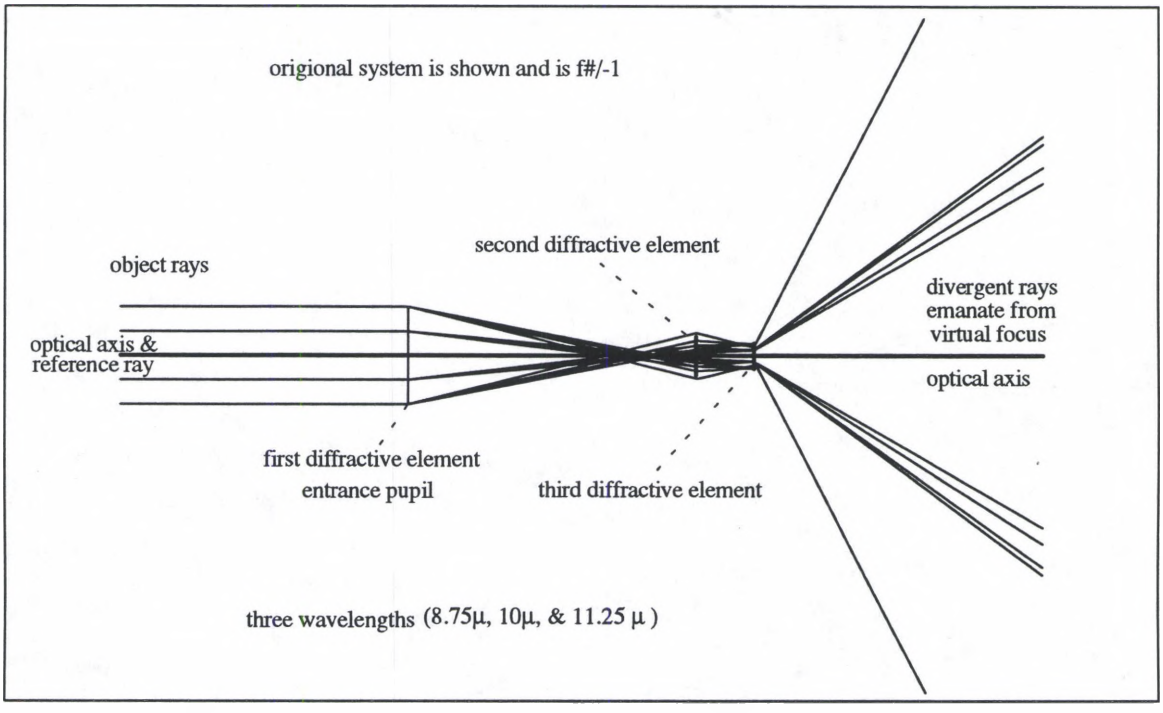

Figure 37 Optical Layout of Diffractive Lens System (DFY) at f/-1

The diffractive lens system is paraxially achromatic, i.e. the longitudinal and lateral color equal zero at the design wavelength because both the derivative of ray slope, $\partial u_3/\partial\lambda$, and the derivative of ray position, $\partial y_3/\partial\lambda$, at the last surface are zero when evaluated at the design wavelength, λ_0. As shown in Fig. 38, the derivatives with respect to wavelength of paraxial ray slope , $\partial u_3/\partial\lambda$, and position, $\partial y_3/\partial\lambda$, for the system shown in Fig. 37 are zero at the design wavelength, λ_0, but are not zero for wavelengths close to the design wavelength. The longitudinal color metric of the system is the derivative,

$\partial u_3/\partial\lambda$, evaluated for the marginal ray of the *f*#/-1 system and is shown in Fig. 38. The lateral color metric for the system is the derivative, $\partial y_4/\partial\lambda$, as shown in Fig. 38 and is evaluated for a chief ray with a 1 degree field angle. The system's performance degrades when evaluated away from the design wavelength as chromatic aberrations are evident in Fig. 38.

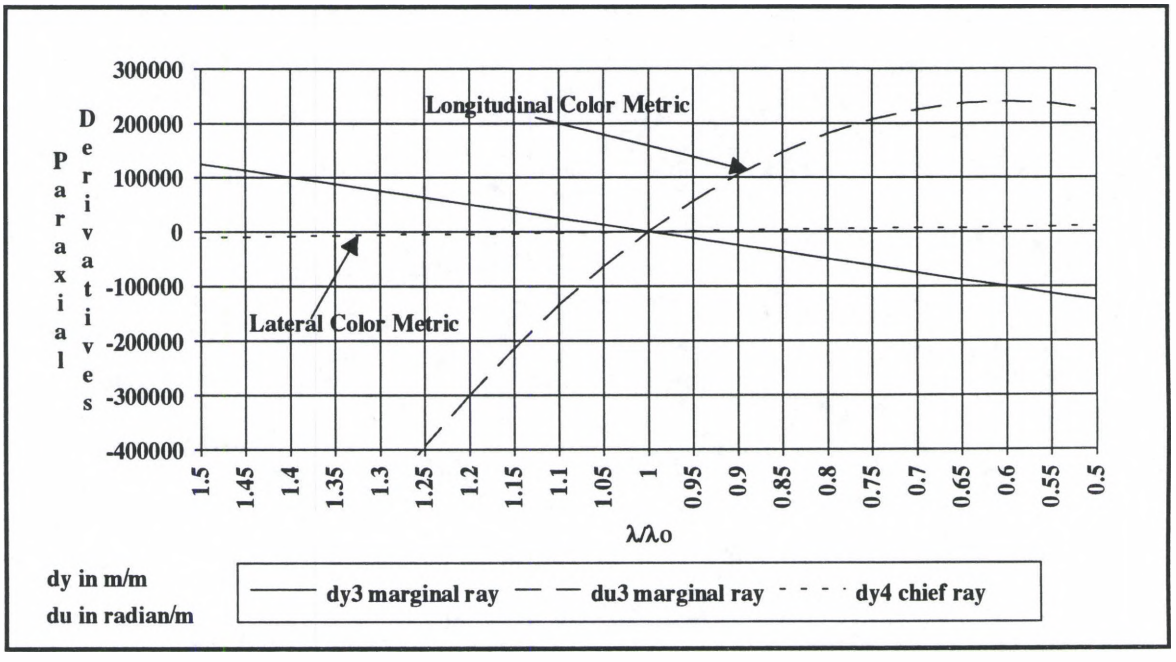

Figure 38 Paraxial Derivatives of System (DFY) Rays versus Ratio of Wavelength

The modified system will steer light from an object point located between -10 and +10 degrees of the optical axis to the second element at the tuned wavelength. The performance of the system will be degraded because the first element can now be modeled as an off-axis section of a diffractive lens and the other elements cannot correct for the angular errors introduced unless they are displaced off axis the same amount causing the system to be symmetric or the centers of the lenses are displaced to be colinear and the system is equivalent to a symmetric system with tilted elements. The radial energy plots in

Fig. 39 show the degradation caused by steering the bandwidths through the displacement of the first element.

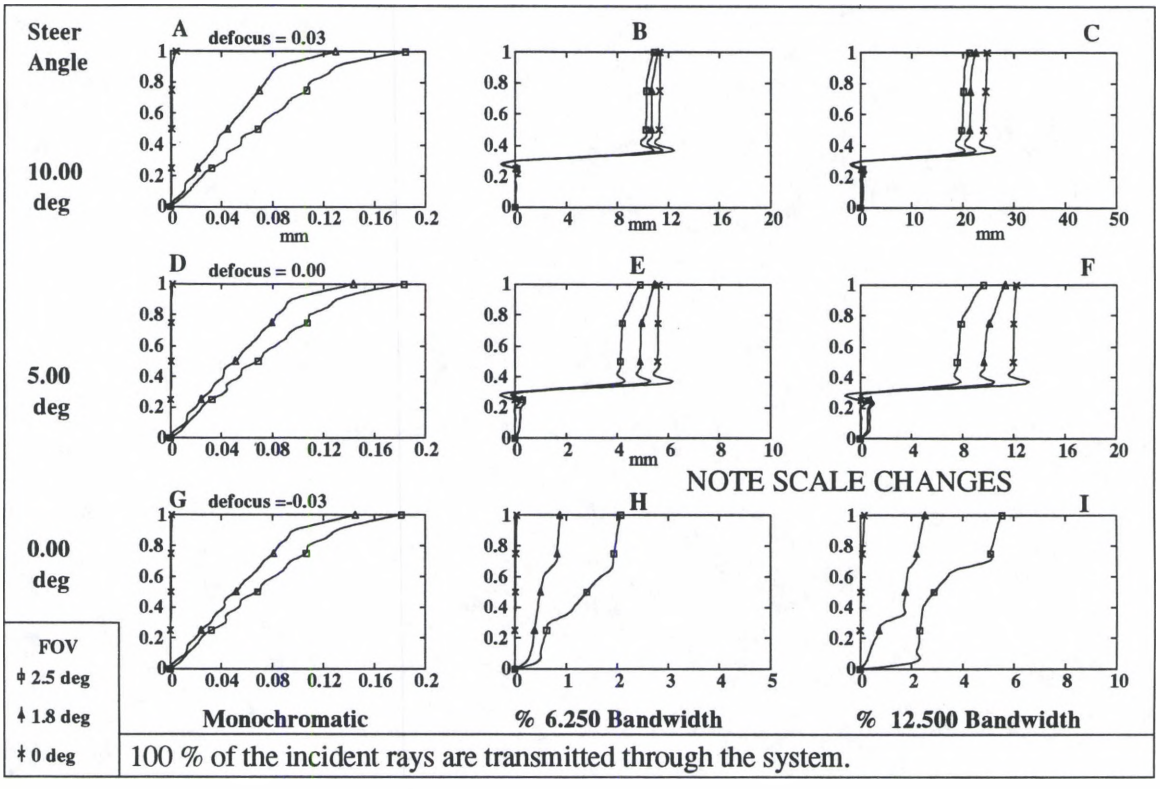

Figure 39 Radial Energy Plots for the Diffractive Lens System (DFY)

The radial energy plots in Fig. 39, segments A, D, and G demonstrate the good monochromatic performance of the diffractive lens system for all steered angles. Segments G, H, and I show the degradation of image quality for unsteered on axis broadband objects as the bandwidth is increased. The radial energy plot for 5 degree steering and 6.25% bandwidth, Fig. 39, segment E, shows a spot size approximately 4 times larger in radius than the corresponding spot sizes for the improved broadband single grating, Fig. 31, segment E, and dual grating systems, Fig. 36, segment E. This indicates increased diffractive deviations of the beam for the all diffractive element system

compared to diffractive/reflective systems. The system defocus is small at 0.06 mm and the best spot size is nearly geometrically perfect. Because the system possesses a virtual focus it requires additional optics for practical realization, which would affect the systems performance.

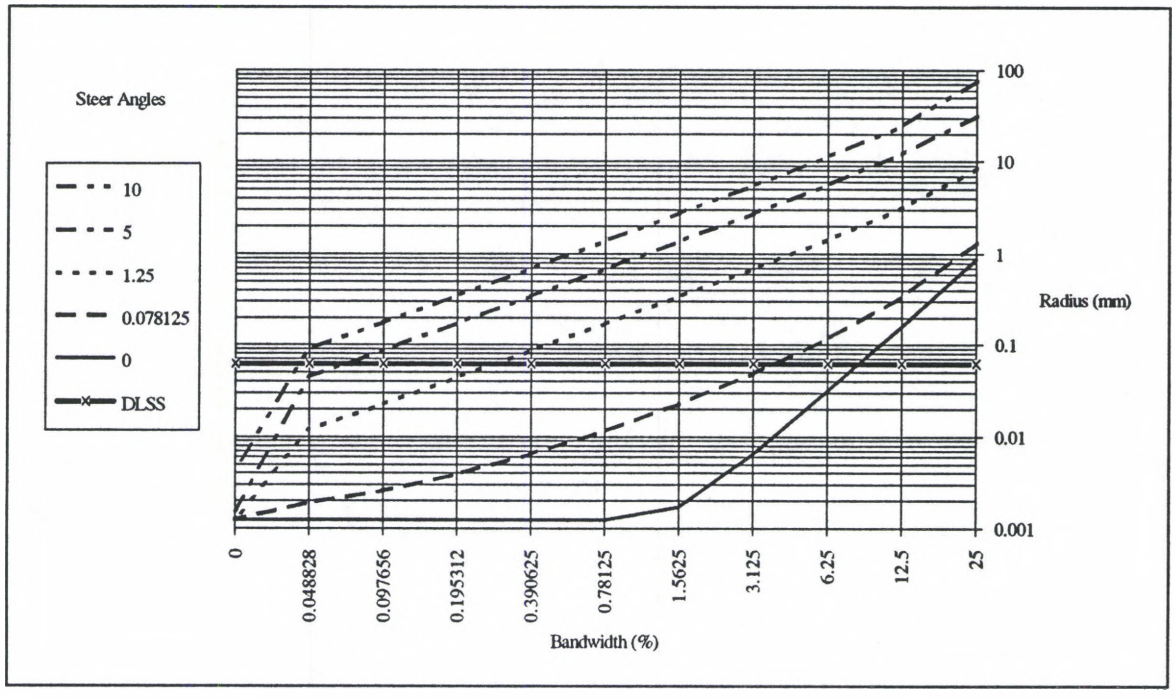

Figure 40 100 % Energy Radius Versus Bandwidth for Given Steer Angles for the Diffractive Lens System (DFY)

Fig. 40 illustrates how the image spot size increases with increasing bandwidth and steer angle. The plots in Fig. 40 summarize the information contained in the radial energy plots in Fig. 39; here we plot radius values encircling 100% of the energy. The plots are logarithmic in values of radius and the bandwidths and steer angle are in doubling increments except for the zero values. The zero values were added for reference. The diffraction limited spot size, DLSS in Fig. 40, for this system is 0.062mm and the diffraction limited range of operation for 100 % of the encircled energy is easily obtained from the graph.

4.7 : Discussion

The utility of the diffractive beamsteerers in LADAR systems is due to their excellent agility and monochromatic performance. Diffractive beamsteerers can have better optical performance than their reflective (mirror) counterparts. From the systems analyzed, I submit that the diffractive beamsteerers should deviate broadband beams diffractively as little as possible and the field of regard should be chosen such that the reference ray is not deviated diffractively and the diffraction limited spot size is a minimum for the reference ray field angle to enhance the performance of the diffractive beamsteerers for the passive channel application. Steering a beam with a flat mirror located before a traditional telescope design yields geometric image quality as good as that of the unsteered telescope. The dual mirror's imaging performance can be matched at a single wavelength (monochromatically or 0% bandwidth) by the single parabolic grating and the dual grating system's imaging performance, but both of the diffractive systems' performances degrade rapidly as the bandwidth-diffractive deviation product is increased.

The improved monochromatic single grating possesses the best monochromatic and unsteered performance for a single element system as indicated by the radial energy plots. The increased complexity of writing a grating of constant period with respect to the chord of the concave surface onto a concave surface. Its poor broadband performance may limit its utilization.

The dual grating system with its flat dynamic grating has slightly better broadband performance than the improved broadband single grating because it possesses better monochromatic performance and diffractively deviates the beam by the same amount. It has unsteered performance, normal incidence to the flat steerer, at all steer angles evaluated for monochromatic plots with the best diffraction limited spot size. Also, its

concave grating is fixed (non-dynamic) while the dynamic grating is written to a flat surface, thus is undistorted by curvature. It can vignette rays at the second element as only the 0 degree field of view rays at the center wavelength are not vignetted by the second element, which is the same size as the first element. A comparison of all the diffractive beamsteering systems illustrates these effects.

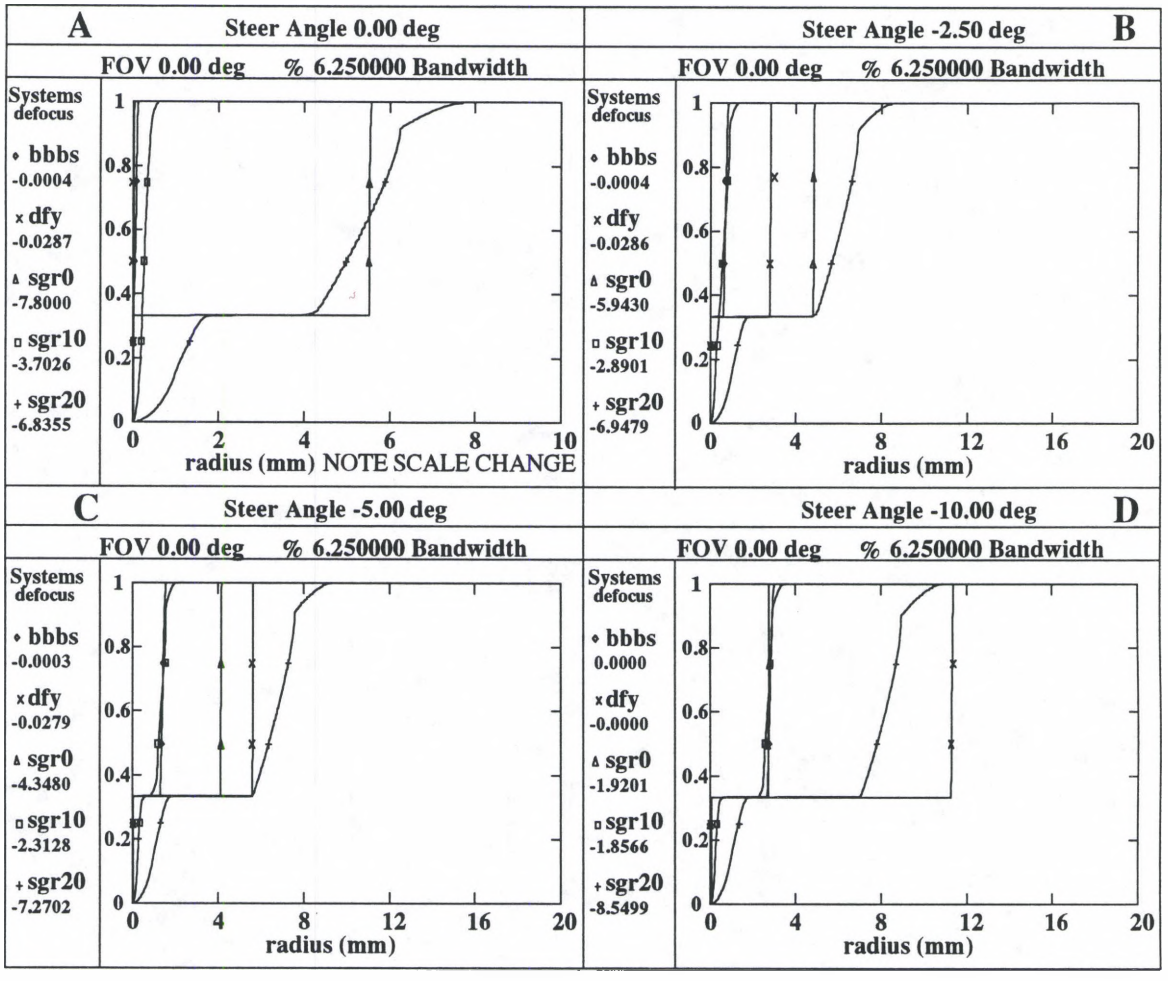

Figure 41 Diffractive Systems Radial Energy Plots for Negative Angles & 6.25% BW

The plots in Fig. 41 do not exhibit the overshoot observed in other radial energy plots of diffractively steered systems as the data was not spline fitted. Thus the discontinuity is accurately plotted, but the ray trace program only traces three

wavelengths. For continuous broadband light the radial energy plots would be smooth and bounded by the limit at a fractional energy value of 1.

The plot Fig. 41, segment A shows the radial energy plots for the diffractive systems unsteered. The initial single grating (SGR20) and improved monochromatic single grating (SGR0) both possess 20 degrees diffractive deviation and their spot sizes show the degradation caused by it. Because of the choice of their fields of regard and reference rays the amount of diffractive deviation for the improved monochromatic single grating (SGR0) becomes less for negative steered angles and more for positive steered angles. The effect is reversed for the initial single grating, which is evident comparing the plots in Fig. 41 with those in Fig. 42.

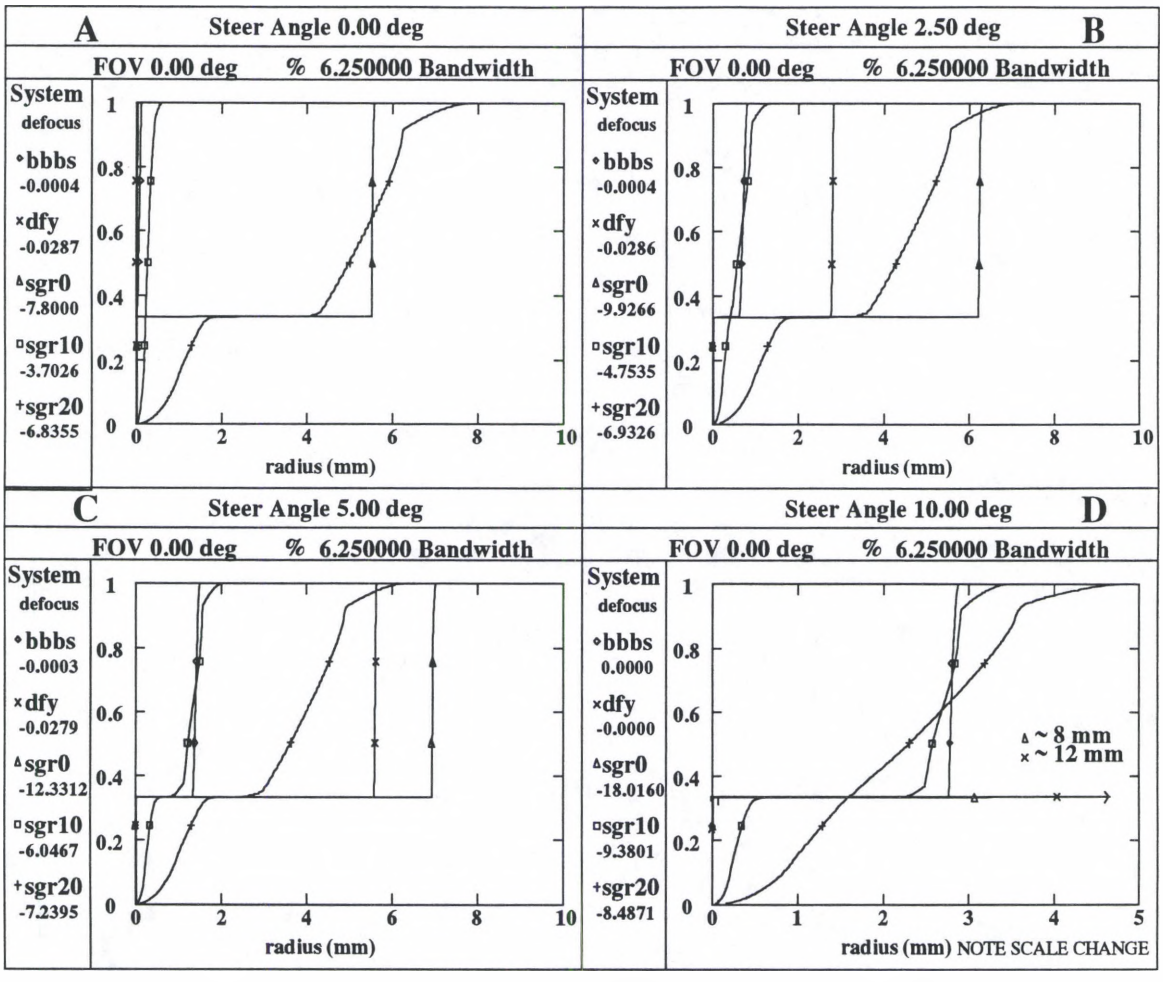

Figure 42 Diffractive Systems Radial Energy Plots for Positive Angles & 6.25% BW

For the diffractive concave grating systems the amount of aberration caused by diffractive deviation is constant, but the diffractive lens system (DFY) possesses a greater amount of diffractive chromatic aberration for the same amount of diffractive deviation of the base ray as shown analytically in Chapter 3 and demonstrated by the plots in Fig. 41 and Fig. 42. The dual grating system (BBBS) possesses the same amount of cumulative diffractive deviation as the diffractive lens system (DFY). Both systems diffractively deviate the base ray the amount of the steer angle. The radial energy plots show the advanced degradation in the spot sizes for the diffractive lens system (DFY) when compared to the dual grating system (BBBS).

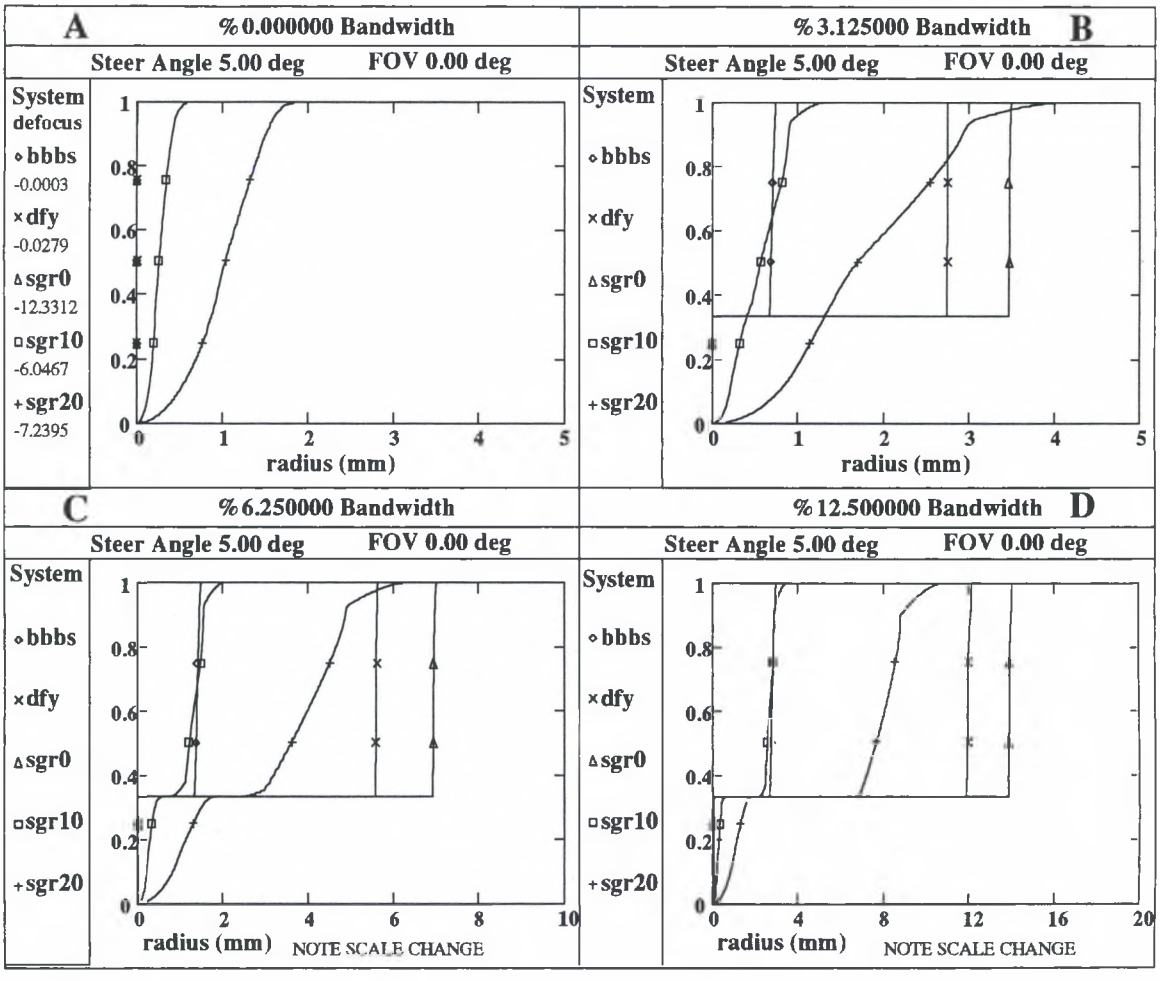

Figure 43 Diffractive Systems Radial Energy Plots for 5 degree Steer Angle

The increasing bandwidth plots in Fig. 43 and Fig. 44 show the effect of increasing the bandwidth for a single positive and negative steer angle respectively. Segment A of Fig. 43 and Fig. 44 show monochromatic, 0 % bandwidth, plots for the beamsteerers and are identical for positive and negative steer angles as the diffractive deviation of the beamsteerer steers monochromatically without error.

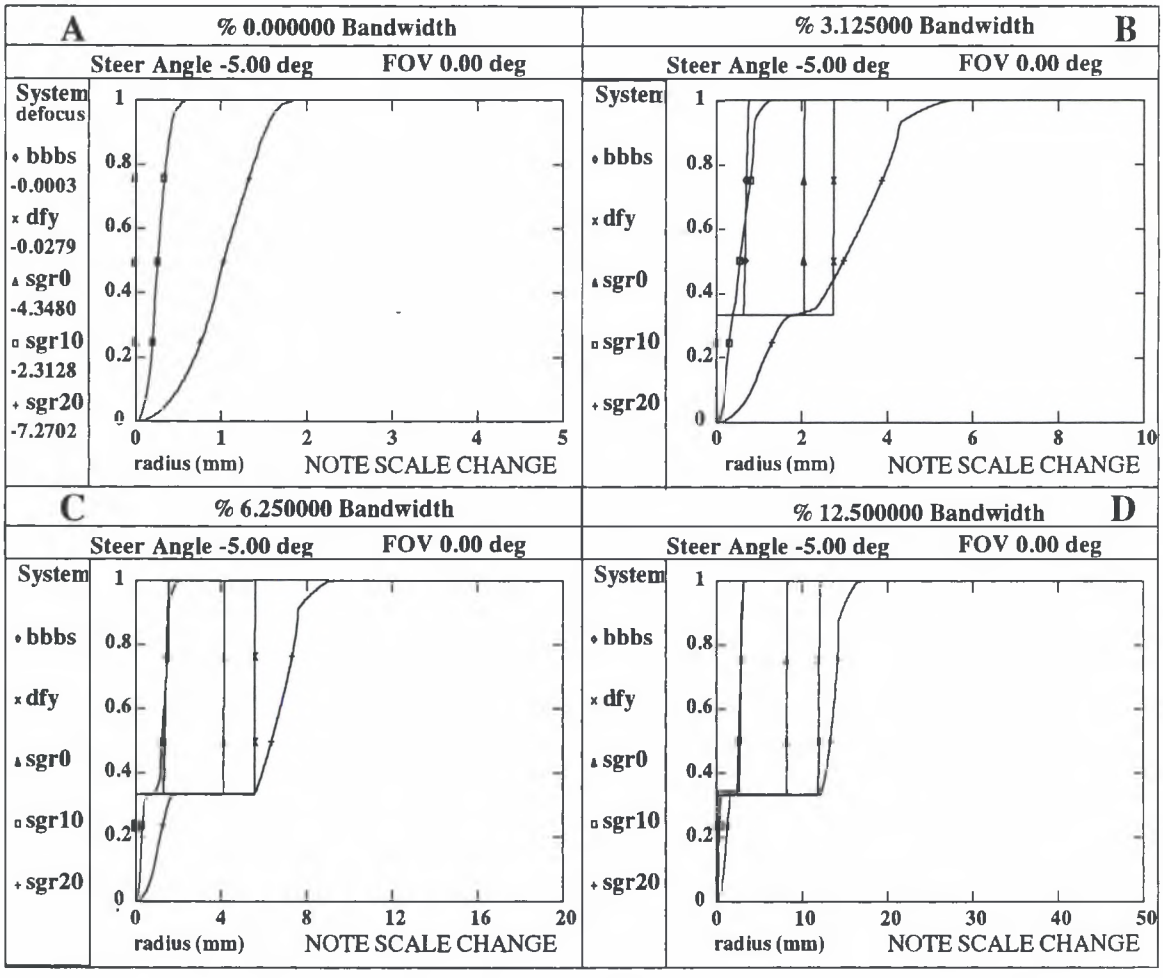

Figure 44 Diffractive Systems Radial Energy Plots for -5 degree Steer Angle

Chapter V

Conclusion

The utility of the non mechanical beamsteerer in a ladar transceiver with a passive acquisition channel is severely limited in bandwidth for a diffraction limited steering system with no correction of the chromatic aberrations. The amount of diffractive deviation of the passive channel of the system should be kept to a minimum to obtain the

largest possible bandwidth. Several configurations show the liquid crystal beamsteerer's utility in a ladar system as a monochromatic or narrow bandwidth beamsteerer for the active channel. Spot diagram analyses with radial energy plots show the improved monochromatic single grating and dual grating configurations of the liquid crystal beamsteerer have nearly identical geometric optical performance at 0% bandwidth to the dual mirror configuration, which has diffraction limited performance for a 0 degree field of view angle at any steered angle within the defined field of regard. This demonstrates the utility of this type of beamsteerer in a ladar system, but the passive systems performance was best for the dual grating configuration and the performance degraded rapidly with the steer angle bandwidth product for all of the diffractive systems.

Correcting for the dispersion caused by the diffractive elements is a non-trivial task. Because diffractive systems have the same dispersive properties, removing the angular errors in the broadband signal can occur only if the system performs equal and opposite diffractive deviation in a two element system. The use of diffractive elements to correct for the diffractive dispersion will only work if no cumulative steering is performed by the system.

One solution is to operate the device with few or no resets. This mode of operation is in the regime of multiple aperture telescopes not the many aperture regime of conventional grating theory. The drawback for operating the device in the few reset regime is that the thickness of each device would be required to be larger for steering to the same angles or each device would be required to steer to smaller angles. This would cause the speed in switching between steer angles to become larger for each device or the magnitude of the steer angles accessible to each device would become small. Using more beamsteering devices in the system could allow the system to steer to large angles with agility, but the complexity, size and expense of the system would increase.

The use of dispersive refractive elements could be used in a correction scheme as the sign of refractive dispersion is generally opposite that of diffractive dispersion for the same angle of deviation of the center wavelength. The use of diffractive elements in lens design for correction of dispersion is advantageous as the grating period can be large for correction of chromatic aberrations. The diffractive dispersion is orders of magnitude greater than the refractive dispersion for most refractive materials. This causes the utility of refractive components in a correction scheme of a diffractive steering system to be diminished due to the size, weight, and complexity of the refractive elements. It may be possible through multiple passes to reduce the size and weight of the refractive component, but the complexity of doing so for the number of different diffractive steering angles makes it a non trivial design problem.

The dual grating system is the best all diffractive combined broadband and monochromatic steering system. The complexity of the system is reduced over the single concave dynamic grating system as the concave parabolic grating has a fixed period and therefore is not a dynamic element. The fabrication of a dynamic grating element on a concave substrate with a chirped dynamic period is more difficult than fabricating a constant period dynamic grating on a plane substrate. The systems performance is dependent upon the object distance being infinite or approximately infinite. This allows the concave parabolic mirror to direct the rays to the image plane location dependent solely upon the input angle of incidence and independent of position. If the object is not infinitely far away i.e., rays emanating from a single object point will have different paraxial slopes at the entrance pupil, the positional ray errors at the imaging surface will be transformed into angular errors as shown in Chapter 3.3. The grating written on the imaging grating corrects the angular error in the rays for an object at infinity by nulling the

diffractive deviation of the rays. Thus the angle of incidence at the flat steering grating is equal to the angle of incidence at the concave reflective (imaging) surface.

A field of view selector system as discussed in Chapter 3.7 could be used if the field lens in Fig. 17 were replaced with optical elements which directed and reimaged the image at a single detector array. By subdividing the field of regard into a number of fields of view, the internal image plane could be separated into the finite number of fields of view and relayed to a single array detector. The selecting system could select one of the fields of view to be passed through the internal field stop and this field of view would be imaged at a common detector array. An approach using this method would be to use a array of fibers at the image plane to relay the image to the common detector array. This would present problems in that the fiber arrays would either be spliced together to present a single pixel a single fiber or the detector pixel would be required to accept signals from the finite numbers of fibers from the unique fields of view.

Finally as any system can be characterized for aberrations, it may be possible to deconvolve the information from a chromatically aberrated image, such as any of the diffractive systems considered in this thesis. The point response for the system could be deconvolved from the output image, but as the spectral content of the object could be position dependent the deconvolution may also be required to be position dependent. The problem here is similar to the problem of deconvolving motion blur from an image, but depending on the spectral content of the object, the image may possess a nonlinear blur and different spectral contents of different objects would possess different blurs in possibly the same image. The amount of dispersion and hence the blur would also be dependent upon the diffractive deviation or steering, thus each steer angle would also possess different blurs for the same object. This approach would require some apriori knowledge of the object field and bears further study.

Appendix A

Paraxial Proof of Conjugate Planes

A single lens or lens system, which relays a object plane to an image plane, cannot force an object point lying off-the optic axis to be imaged on the optic axis. This means that every unique location in the object plane is mapped to a unique location in the image plane. The paraxial proof follows with the variables as defined in the accompanying figure and the convention will be identical to that used in Chapter 3.

A single lens system with variables is shown in Figure A.1. The initial ray position for a ray in the object plane is y_0. The initial ray slope is u_0, as is shown in Figure A.1.

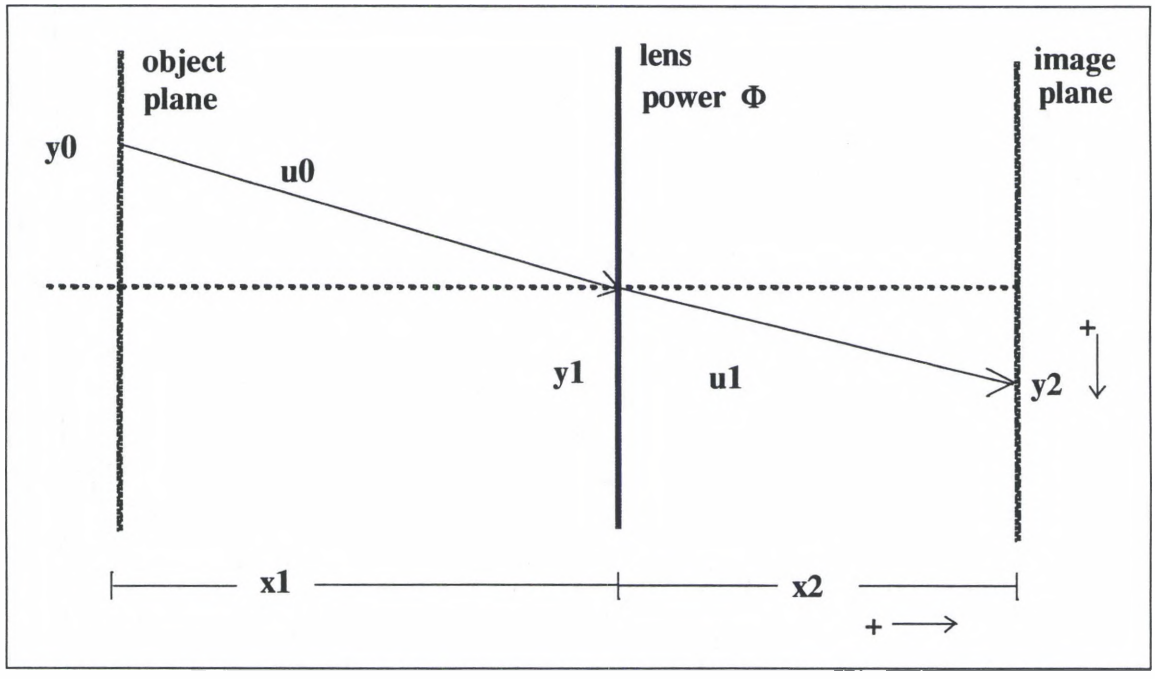

Figure A.1 Single Paraxial Lens Drawing

Appendix B

OSLO Lens Data and Steering Code

B.1 : Single Tilted Mirror System (STM)

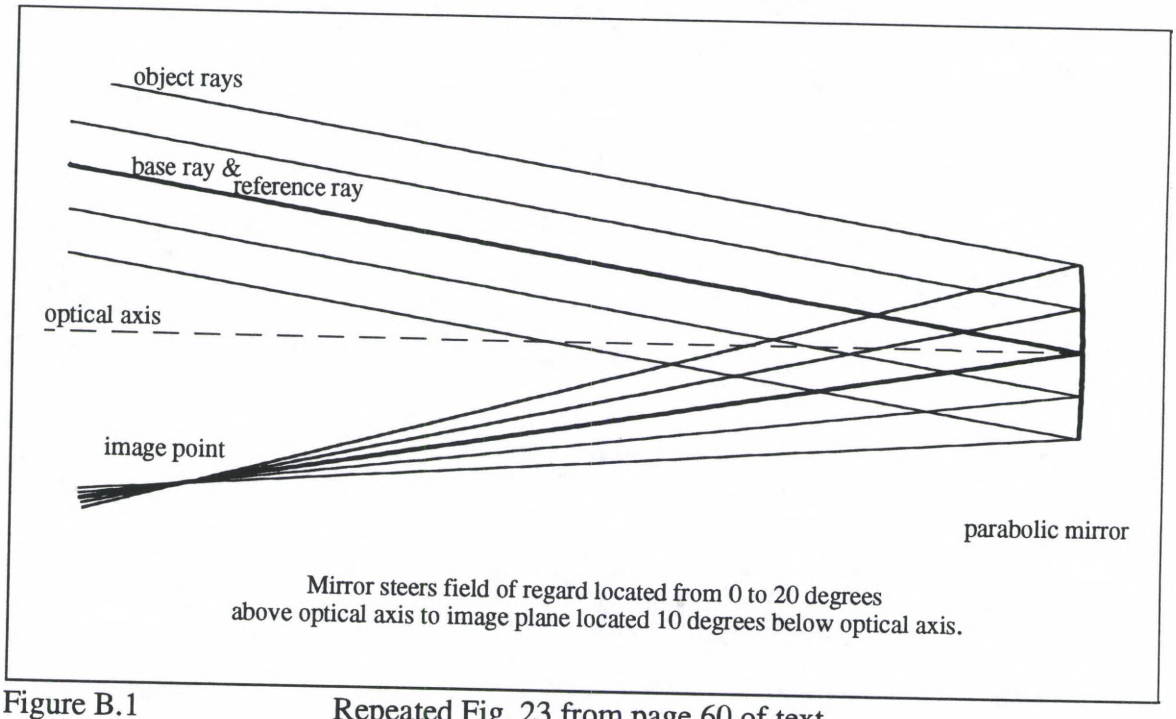

Figure B.1 Repeated Fig. 23 from page 60 of text
Optical Layout of Single Tilted Mirror (STM)

Table B.1 *OSLO LENS DATA Single Tilted Mirror STM

SRF	RADIUS	THICKNESS	APERTURE RADIUS	GLASS	SPE	NOTES
1	--	--	25.00000 A	AIR		
2	-500.00000	-250.00000	25.00000 S	REFLECT	*	
3	--	--	144.33757 S	AIR		

*GENERAL DATA
OSLO 3.2 SUN35927355

The ray propagates some distance x_1 and is deviated by the lens to an image point located some distance x_2 beyond the lens. The object (x_1) and image (x_2) distances are related to the power of the lens through the relation given by Eq. A.1

$$\Phi = \frac{1}{f} = \frac{1}{x_1} + \frac{1}{x_2} = \frac{x_1 + x_2}{x_1 x_2}. \tag{A.1}$$

Where f is the paraxial focal length of the lens and Φ is the paraxial power of the lens. The distances and can be written as

$$x_1 = a x_2 \tag{A.2}$$

where a is a constant bounded by $\pm\infty$. Thus Eq. A.1 becomes

$$\Phi = \frac{1}{f} = \frac{1}{x_1} + \frac{1}{a x_1} = \frac{x_1 + a x_1}{a x_1 x_1} = \frac{x_1(1+a)}{a x_1^2} = \frac{(1+a)}{a x_1}. \tag{A.3}$$

This proof will try to examine the conditions from which a non-zero input ray position can be mapped to a zero image position. The paraxial equation relating the image plane location y_2 to the input variables is

$$y_2 = 0 = y_0 - u_0 x_1 - \left[u_0 + (y_0 - u_0 x_1)\Phi\right] x_2. \tag{A.4}$$

Substituting Eq. A.3 and Eq. A.2 into Eq. A.4 yields

$$y_2 = 0 = y_0 - u_0 x_1 - \left[u_0 + (y_0 - u_0 x_1)\frac{(1+a)}{a x_1}\right] a x_1. \tag{A.5}$$

Simplifying Eq. A.5 gives

$$y_2 = 0 = y_0 - u_0 x_1 - u_0 a x_1 - y_0(1+a) + u_0 x_1 \frac{(1+a)}{a x_1} a x_1$$
$$= y_0 - u_0 x_1 (1+a) - y_0(1+a) + u_0 x_1 (1+a) = -a y_0 \quad . \tag{A.6}$$

The only solution for Eq. A.6 is a=0. The paraxial magnification is

$$m = \frac{i}{o} = \frac{x_2}{x_1} = -a. \tag{A.7}$$

This implies an infinite power paraxial lens, from Eq. A.1, Eq. A.2, and Eq. A.7. Therefore it is impossible for the symmetric paraxial lens to map a non-zero object point to an on-axis image point.

EPR	OBY	THO	CVO	CCO	UNITS	
25.00000	5.7735E+19	1.0000E+20	--	--	1.00000	
IMS	AST	RFS	AFO	AMO	DESIGNER	IDNBR
3	1	1	0	TRA	BARNES	285

*ASPHERIC DATA
2 CC -1.00000

*SPECIAL DATA
2 DT 1.00000 TLA 0.00000

*PARAXIAL CONSTANTS

EFL	FNB	GIH	PIV	PTZRAD	TMAG
-250.00000	5.00000	-144.33757	14.43376	-250.00000	-2.5000E-18

Steering code

```
*STEERSTM
!syntax steerstm [angle]
z3=#1
tla 2 (20-z3)/2
tla 3 +20-tla(2)
if (+z3<=0)
 oby -tho*tan(30)
els
 oby +tho*tan(30)
ife
if (#2==0)
 vwp
 clr
 color2 +z3 5 250 250
ife
```

B.2 : Initial Single Grating (**SGR20**)

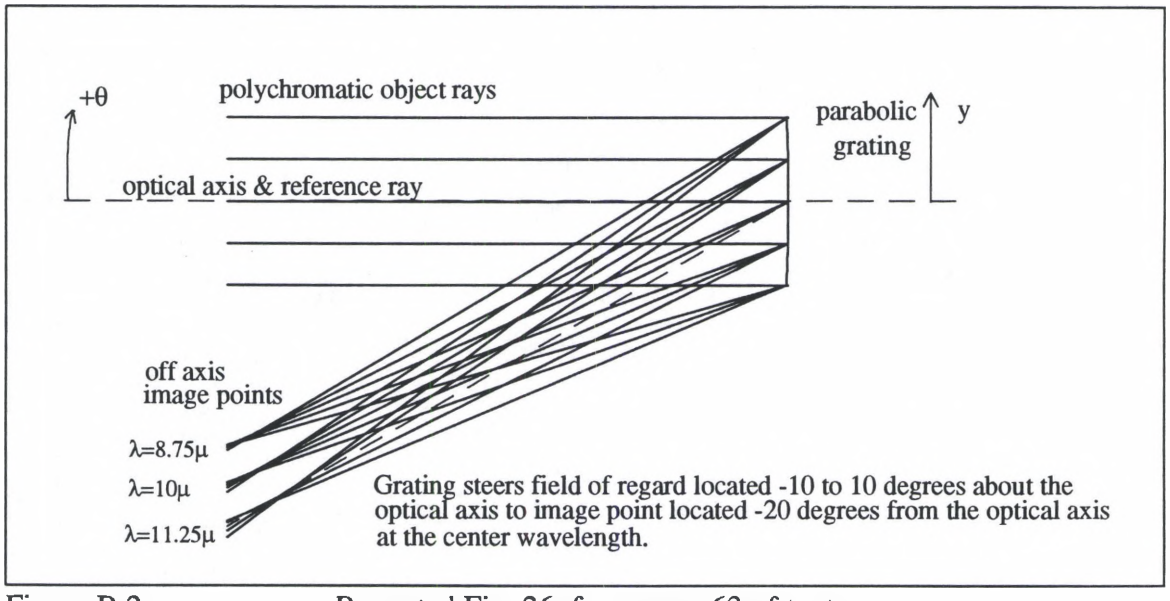

Figure B.2 Repeated Fig. 26. from page 63 of text
Optical Layout of Basic Single Dynamic Grating System (SGR20)

Table B.2 *OSLO LENS DATA Single Parabolic Grating SGR20:+-10;-20

SRF	RADIUS	THICKNESS	APERTURE RADIUS	GLASS	SPE	NOTES
1	--	--	25.00000 A	AIR		
2	-500.00000	-250.00000	25.00000 S	REFLECT	*	
3	--	--	144.33757 S	AIR	*	

*GENERAL DATA
OSLO 3.2 SUN35927355

EPR	OBY	THO	CVO	CCO	UNITS	
25.00000	5.7735E+19	1.0000E+20	--	--	1.00000	
IMS	AST	RFS	AFO	AMO	DESIGNER	IDNBR
3	1	1	0	TRA	BARNES	78

*ASPHERIC DATA
2 CC -1.00000

*SPECIAL DATA
2 GOR -1.00000
3 DT 1.00000 TLA 20.00000

*PARAXIAL CONSTANTS

EFL	FNB	GIH	PIV	PTZRAD	TMAG
-250.00000	5.00000	-144.33757	14.43376	-250.00000	-2.5000E-18

Steering code

```
*STEERSGR20
!syntax steersgr20 [angle][scale]  0=0inc for mirror mode,up pos
!steer the single grating system 30 deg max
pri off
z3=#1
if (#1>0)
  oby +(tan(30)*tho)
els
  oby -(tan(30)*tho)
ife
if (#2==0)
  z4=1
els
  z4=#2
ife
d=#3
z95=+z3
gor 2 -1
z4=+wv1/(+z4*1000)
gsp 2 +z4/(-sin(z3)+sin(20))
z3 = +z3/30
if (d==0)
  vwp
  clr
  *color2 +(z3) 5 250 250
ife
```

B.3 : Improved Monochromatic Grating (SGR0)

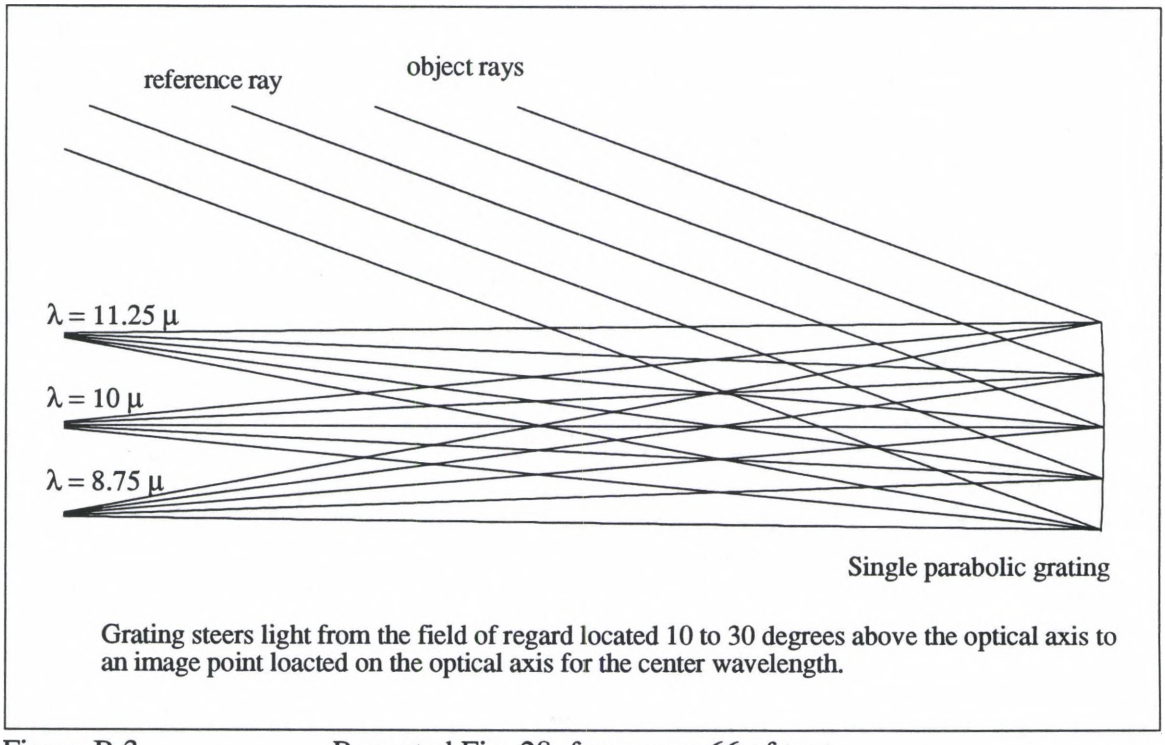

Figure B.3 Repeated Fig. 28. from page 66 of text
Optical Layout of Improved Monochromatic Grating System (SGR0)

Table B.3 *OSLO LENS DATA Single Parabolic Grating SGR0:10-30;0

SRF	RADIUS	THICKNESS	APERTURE RADIUS	GLASS	SPE	NOTES
1	--	--	25.00000 A	AIR		
2	-500.00000	-250.00000	25.00000 S	REFLECT	*	
3	--	--	144.33757 S	AIR		

*GENERAL DATA
OSLO 3.2 SUN35927355

EPR	OBY	THO	CVO	CCO	UNITS	
25.00000	5.7735E+19	1.0000E+20	--	--	1.00000	
IMS	AST	RFS	AFO	AMO	DESIGNER	IDNBR
3	1	1	0	TRA	BARNES	74

*ASPHERIC DATA
2 CC -1.00000

```
*SPECIAL DATA
2       GOR   -1.00000

*PARAXIAL CONSTANTS
EFL           FNB        GIH           PIV          PTZRAD       TMAG
-250.00000    5.00000    -144.33757    14.43376     -250.00000   -2.5000E-18

*CONFIGURATION DATA
TYPE  SN  CFG    VALUE
CC    2   2      --
```

Steering code

```
*STEERSGR0
!syntax steersgrm2 [angle][scale]  0=20 deg inc for mirror mode,up pos
!steer the single grating system 30 deg max
pri off
z3=#1
if (#2==0)
  z4=1
els
  z4=#2
ife
d=#3
z3=+z3+20
z95=+z3
gor 2 -1
oby +(tan(30)*tho)
z4=+wv1/(+z4*1000)
gsp 2 +z4/(-sin(+z3))
if (d==0)
  vwp
  clr
  *color2 +(z3) 5 250 250
ife
```

B.4 : Improved Broadband Grating (**SGR10**)

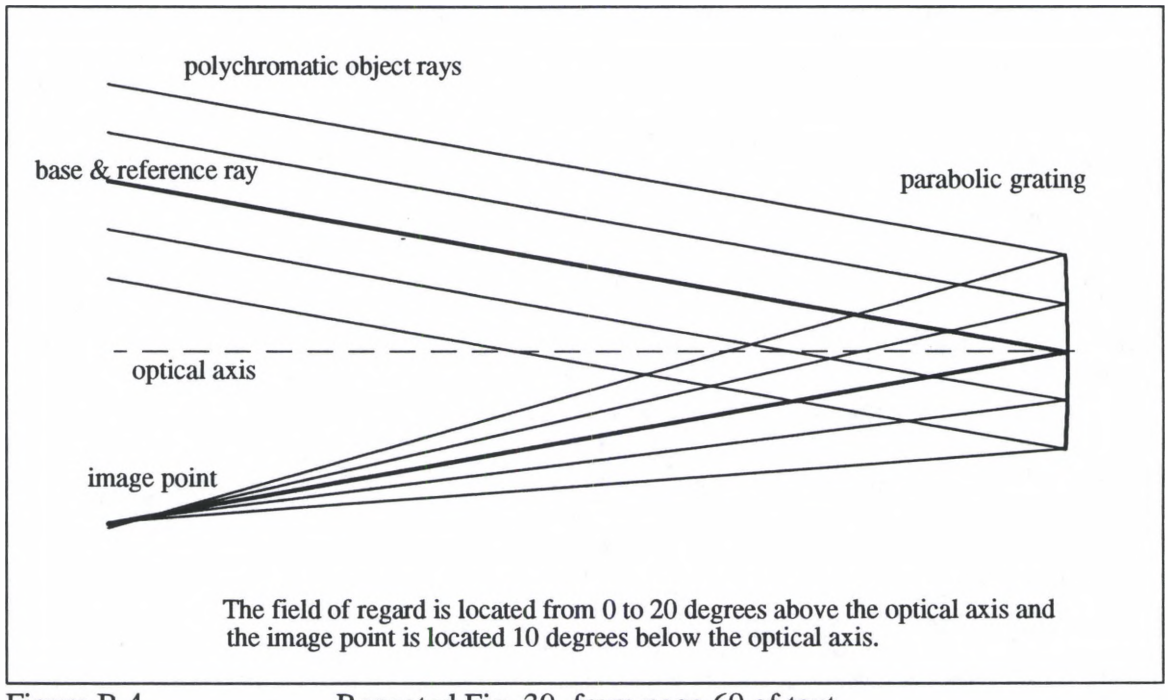

Figure B.4 Repeated Fig. 30. from page 69 of text
Optical Layout of Improved Broadband Grating System (SGR10)

Table B.4 *OSLO LENS DATA Single Parabolic Grating SGR10:0-20;-10

SRF	RADIUS	THICKNESS	APERTURE RADIUS	GLASS	SPE	NOTES
1	--	--	25.00000 A	AIR		
2	-500.00000	-250.00000	25.00000 S	REFLECT	*	
3	--	--	144.33757 S	AIR	*	

*GENERAL DATA
OSLO 3.2 SUN35927355

EPR	OBY	THO	CVO	CCO	UNITS	
25.00000	5.7735E+19	1.0000E+20	--	--	1.00000	
IMS	AST	RFS	AFO	AMO	DESIGNER	IDNBR
3	1	1	0	TRA	BARNES	76

*ASPHERIC DATA
2 CC -1.00000

*SPECIAL DATA
2 GOR -1.00000
3 DT 1.00000 TLA 10.00000

*PARAXIAL CONSTANTS

EFL	FNB	GIH	PIV	PTZRAD	TMAG
-250.00000	5.00000	-144.33757	14.43376	-250.00000	-2.5000E-18

Steering code

```
*STEERSGR10
!syntax steersgrx [angle][scale]  0=10 deg inc for mirror mode,up pos
!steer the single grating system 30 deg max
pri off
z3=#1+10
if (#2==0)
  z4=1
els
  z4=#2
ife
d=#3
z95=+z3
gor 2 -1
oby +(tan(30)*tho)
z4=+wv1/(+z4*1000)
gsp 2 +z4/(-sin(z3)+sin(10))
z3 = +z3/30
if (d==0)
  vwp
  clr
  *color2 +(z3) 5 250 250
ife
```

B.5 : Dual Mirror System (**BSO**)

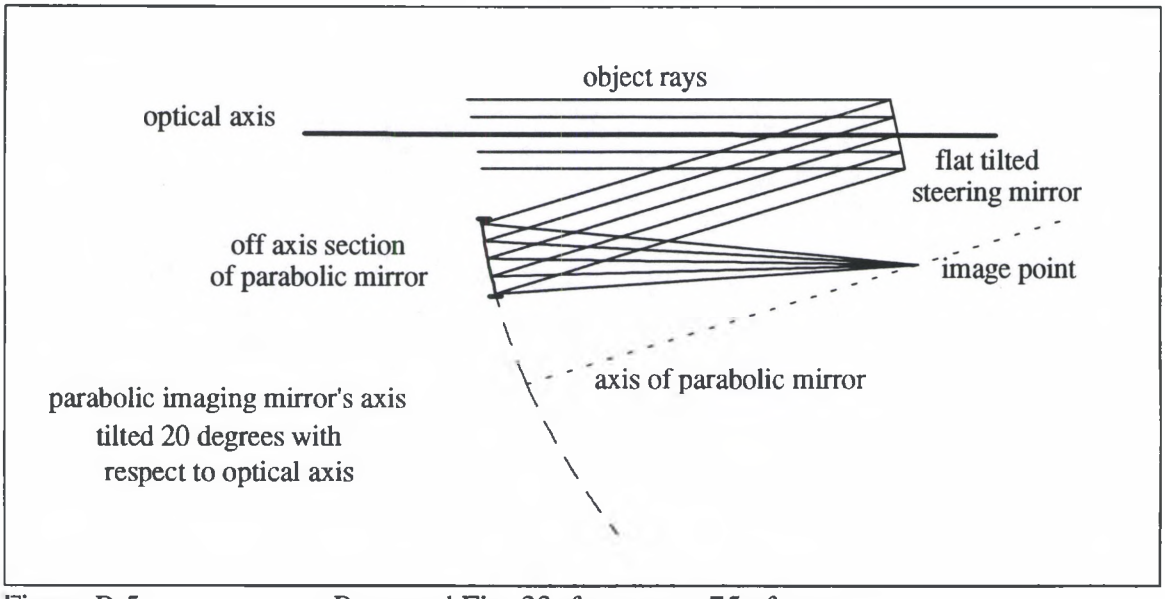

Figure B.5 Repeated Fig. 33. from page 75 of text
Optical Layout of Dual Mirror System (BSO)

Table B.5 *OSLO LENS DATA Dual Mirror System BSO

SRF	RADIUS	THICKNESS	APERTURE RADIUS	GLASS	SPE	NOTES
1	--	--	25.00000 A	AIR		
2	--	-250.00000	25.00000	REFLECT	*	
3	500.00000	250.00000	120.00000	REFLECT	*	
4	--	--	10.91524 S	AIR	*	

*GENERAL DATA
OSLO 3.2 SUN35927355

EPR	OBY	THO	CVO	CCO	UNITS	
25.00000	4.3661E+18	1.0000E+20	--	--	1.00000	
IMS	AST	RFS	AFO	AMO	DESIGNER	IDNBR
4	1	1	0	TRA	BARNES	1118

*ASPHERIC DATA

3	CC	-1.00000

*SPECIAL DATA

2	DT	1.00000	TLA	15.00000		
3	DT	1.00000	DCY	-160.11295	TLA	15.00000
4	DT	1.00000	TLA	-20.00000		

*PARAXIAL CONSTANTS

EFL	FNB	GIH	PIV	PTZRAD	TMAG
250.00000	5.00000	-10.91524	1.09152	250.00000	-2.5000E-18

Steering code

```
*STEERBSO
!syntax steerm [angle][plot flag]
!steers bsm to 30 degree max
z3=#1
if (z3<=0)
  oby -tho*tan(30)
els
  oby +tho*tan(30)
ife
pri off
tla 2 (20-z3)/2
dcy 3 250*(tan(tla(2))-2*tan(20))
tla 3 -tla(2)+20
!removes tla 2 and tilts 20
if (#2==0)
  vwp
  clr
  color2 +z3 5 250 250
ife
```

B.6 : Dual Grating System (**BBBS**)

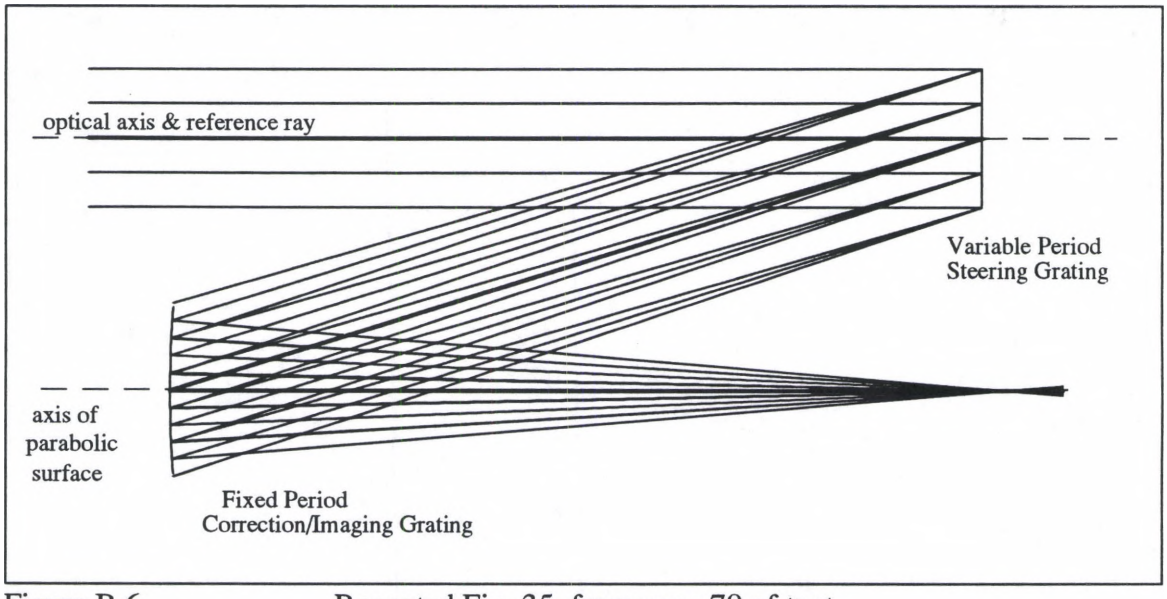

Figure B.6 Repeated Fig. 35. from page 79 of text
Optical Layout of Dual Grating System (BBBS)

Table B.6 *OSLO LENS DATA Dual Grating System (BBBS)

SRF	RADIUS	THICKNES S	APERTURE RADIUS	GLASS	SPE	NOTES
1	--	-651.30000	20.00000	AIR		
2	--	-250.00000	20.00000	REFLECT	*	
3	--	401.30000	30.00000	REFLECT	*	
4	85.21807	10.00000	40.00000 A	GERM C		
5	109.29678	88.70000	40.00000	AIR		
6	--	--	50.00000	AIR		

*GENERAL DATA
OSLO 3.2 SUN35927355

EPR	OBY	THO	CVO	CCO	UNITS	
20.00000	1.0000 0	1.0000E+14	--	--	1.00000	
IMS	AST	RFS	AFO	AMO	DESIGNER	IDNBR
6	4	2	0	TRA	BARNES	59

*SPECIAL DATA
2 GSP=0.02924 GOR=-1.00000
3 DCY=-90.99260 GSP=0.02924 GOR=1.00000

*PARAXIAL CONSTANTS

EFL	FNB	GIH	PIV	PTZRAD	TMAG
98.20558	2.45514	-9.8206E-13	2.0000E-13	-515.61986	-9.8206E-13

Steering code

```
*STEERBBBS
!syntax steer [angle] [scale]0=normal inc,up pos
!steer the dual grating system 30 deg max
z3=#1
if (z3>=0)
 oby +(tan(30)*tho)
els
 oby -(tan(30)*tho)
ife
z4=+wv1/(#2*1000)
pri off
z95=+z3
gsp 2 +abs(+z4/(sin(z3)-sin(20)))
gsp 3 +abs(+z4/sin(20))
if (#3==0)
 vwp
 clr
 *color2 +z3 5 275 275
ife
```

B.7 : Diffractive Lens System (**DFY**)

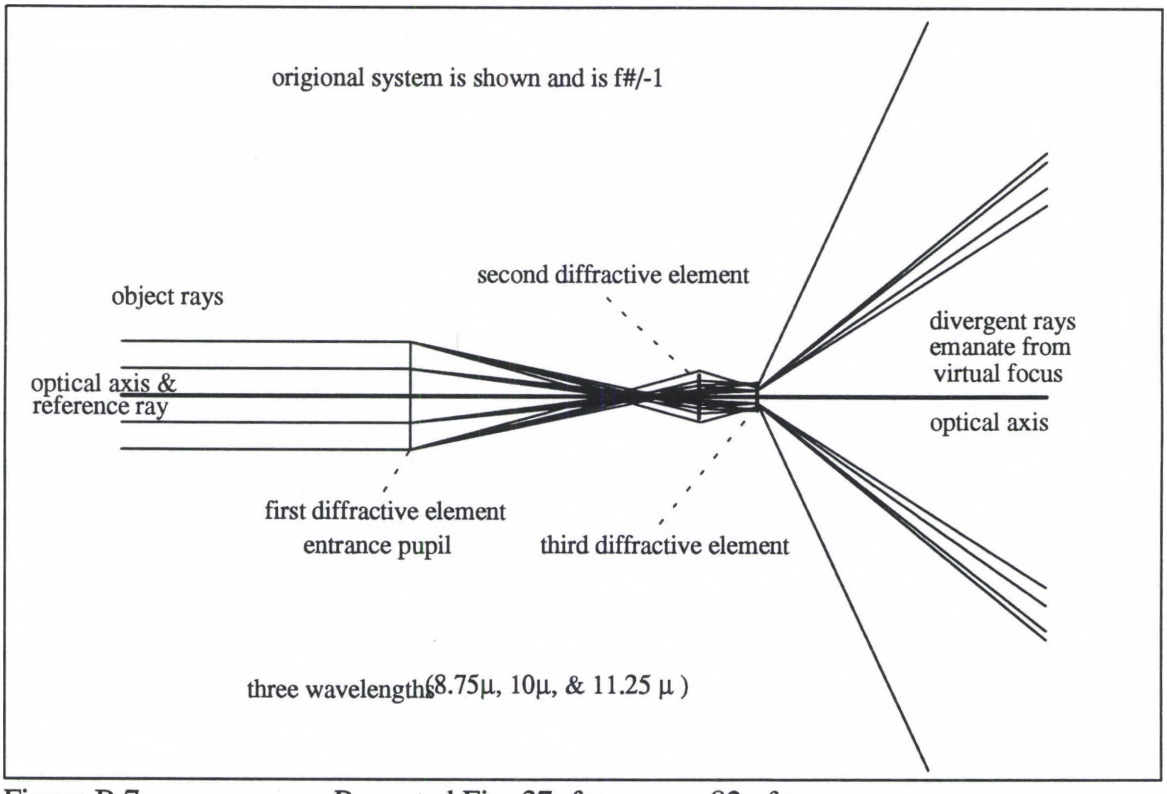

Figure B.7 Repeated Fig. 37. from page 82 of text
Optical Layout of Diffractive Lens System (DFY) at *f*/-1

Table B.7 *OSLO LENS DATA Sweat's Diffractive Spherical System DFY

SRF	RADIUS	THICKNESS	APERTURE RADIUS	GLASS	SPE	NOTES
1	--	--	25.00000 A	AIR		
2	--	--	25.00000	BK7 C	*	
3	--	6250.00000	25.00000 S	AIR	*	
4	--	--	300.00000 K	BK7 C		
5	--	1250.00000	300.00000 P	AIR	*	
6	--	--	300.00000 K	BK7 C		
7	--	-249.88273	300.00000 P	AIR	*	
8	--	--	341.54696 S	AIR		

*GENERAL DATA
OSLO 3.2 SUN35927355

EPR	OBY	THO	CVO	CCO	UNITS	
25.00000	4.3661E+18	1.0000E+20	--	--	1.00000	
IMS	AST	RFS	AFO	AMO	DESIGNER	IDNBR
8	1	1	0	TRA	BARNES	205

*SPECIAL DATA

2DT	1.00000	TLA=10.00000		
3	SDT=DFX 10	DOR=1.00000	S2=0.17633	S3=-0.00010
3	S5=-0.00010	S10 -1.0000E-12	S14 -1.0000E-12	S21 -2.0000E-20
3	S27=-2.0000E-20	S36=-5.0000E-28	S44=-5.0000E-28	S55=-1.4000E-35
3	S65=-1.4000E-35			
5	SDT DFX 10	DOR=1.00000	S3=-0.00040	S5=-0.00040
5	S10=-6.4000E-11	S14=-6.4000E-11	S21=-2.0480E-17	S27=-2.0480E-17
5	S36=-8.1920E-24	S44=-8.1920E-24	S55=-3.6700E-30	S65=-3.6700E-30
7	SDT DFX 10	DOR=1.00000	S3=0.00200	S5=0.00200
7	S10=8.0000E-09	S14=8.0000E-09	S21=6.4000E-14	S27=6.4000E-14
7	S36=6.4000E-19	S44=6.4000E-19	S55=7.1680E-24	S65=7.1680E-24

*PARAXIAL CONSTANTS

EFL	FNB	GIH	PIV	PTZRAD	TMAG
-2.4579E+35	-2.0000E+18	4.3661E+18	1.09152	1.0000E+40	1.00000

Steering code

```
*STEERDFY
!syntax steerdfy [angle] where 0 = normal inc,up pos
!steer the dfr system 30 deg max
!set apck on
z3=#1
if (z3>=0)
  oby +(tan(30)*tho)
els
  oby -(tan(30)*tho)
ife
s2 3 (tan(z3))
z95=+z3
if (#3==0)
  vwp
  clr
  *color2 +z3 5 20 10
ife
```

Bibliography

1. P.F. McManamon, E.A. Watson, T.A. Dorschner, and L.J. Barnes, "An Applications Look at the Use of Liquid Crystal Writable Gratings for Steering Passive Radiation," Optical Engineering, Vol 32, pp. 2657-2664, 1993.

2. J.A. Overbeck, S. McCracken, and B.D. Duncan, "Coherent Versus Incoherent Eyesafe Lidar Detection at 2.09 μm," Proceedings NAECON, Vol. 2, pp. 1142-1147, 1993.

3. M.A. Karim, *Electro-Optical Devices and Systems*, PWS-Kent Pub., Boston, Mass., pp. 64, 1990.

4. W.T. Kreiss, A. Tchoubineh, and W.A. Lanich, "Model for Infrared Sensor Performance Evaluation : Applications and Results," Optical Engineering, Vol. 30, No. 11, pp. 1797-1803, 1991.

5. L.E. Meyers, *Broadband Beam Steering with Liquid Crystal Optical Arrays*, MS Thesis, School of Engineering, University of Dayton, Dayton, Ohio:July 1990, p 47.

6. I.R. Abel, "Mirror Systems: Engineering Features, Benefits, Limitations and Applications", Proceedings of SPIE, Geometric Optics, Vol.531, Los Angeles Ca:1985, pp 121-134.

7. S.E. Forman, J.A. Sultana, and R.A. LeClair, "Laser radar beam steering mirrors", Optical Engineering, V. 29 No11, Nov 1990, pp 1342-1350.

8. E.A. Watson "Analysis of Beam Steering with Decentered Microlens Arrays", Optical Engineering, Nov. 1993 pp 2665-2670.

9. L.J. Hornbeck, "Deformable Mirror Spatial Light Modulators," Proceedings of SPIE, Spatial Light Modulators & Applications III, Vol. 1150, San Diego, Ca:1989, pp 86-102.

10. W.L.Wolfe and G.J. Zissis (Ed.), *The Infrared Handbook*, Washington,D.C.:Office of Naval Research, Department of Navy, 1978 pp 10.10-10.14.

11. D.B. Cook, *Digital Light Deflector Using Ferroelectric Liquid Crystals and Birefringent Wedges*, MS EO Thesis, University of Dayton, July 1989.

12. W.H. von Aulock, "Properties of Phased Arrays", Proceedings IRE, Vol. 48, Oct.1960, pp 1715-1727.

13. G.C. Loney, "Design of a Small-Aperture Steering Mirror for High-Bandwidth Acquisition and Tracking," Optical Engineering, Vol. 29, no. 11, 1360-1365, 1990.

14. T.A. Dorschner, R.C. Sharp, D.P. Resler, L.J. Freidman, D.C. Hobbs, R.L. Chandler, and A. Legere, *Basic Laser Beam Agility Techniques (BATS)*, Technical Report, WL-TR-93-1020, 1993.

15. A. Thevenon, J. Flamand, J.P. Laude, B. Touzet & J. Lerner "Aberration-corrected plane gratings", Proceedings of SPIE, Application and Theory of Periodic Structures, Diffraction Gratings, and Moire Phenomena III, Vol. 815, 1987, pp 136-145.

16. W. Sweat, "Achromatic Triplet Using Holographic Optical Elements", Applied Optics, 16(5):1390-1391 May 1977, pp 1390-1391.

17. F. Wyrowski, "Design theory of diffractive elements in the paraxial domain", J. Opt. Soc. Am.A,Vol 10, No 7, July 1993, pp 1553-1561.

18. OSLO Series 3, a product of Sinclair Optics, Inc., 6780 Palmyra Road, Fairport, New York, 4450

19. A.V. Jelalian, *Laser Radar Systems*, Boston:Artech House, 1992, pp 26.

20. J. Goodman, *Introduction to Fourier Optics*, San Francisco:McGraw Hill, 1968, pp 103-104.

21. M. Born and E. Wolf, *Principles of Optics 4^{th} Ed.*, London: Pergamon Press, 1970, p 403.

22. E. Champagne, "Nonparaxial Imaging, Magnification, and Aberration Properties in Holography", *Journal of the Optical Society of America*, Jan 1967, p 51-55.

23. W.J. Smith, *Modern Optical Engineering : The Design of Optical Systems 2nd Ed.*, McGraw-Hill Inc., New York, 1990, p 164-165.

24. D.A. Buralli and J.R. Rogers, "*Some fundamental limitations of achromatic holographic systems*", J. Opt. Soc. Am. A, Vol 6, Dec. 1989, pp 1863-1868.

25. M. Hutley, *Diffraction Gratings*, Academic Press, New York: 1982, p 41.

26. J.M. Lerner, "Direct Reading Spectrometer using Two Complementary Concave Holographic Gratings," Proc. SPIE, Vol 503, Application, Theory, and Fabrication of Periodic Structures, 1984, pp. 53-58.